ROBUST CONTROL OF A MICROGRID

BY

MEER ABDUL MATEEN KHAN

A Thesis Presented to the

DEANSHIP OF GRADUATE STUDIES

KING FAHD UNIVERSITY OF PETROLEUM & MINERALS

DHAHRAN, SAUDI ARABIA

In Partial Fulfillment of the

Requirements for the Degree of

MASTER OF SCIENCE

In

ELECTRICAL ENGINEERING

DECEMBER 2015

KING FAHD UNIVERSITY OF PETROLEUM & MINERALS

DHAHRAN- 31261, SAUDI ARABIA

DEANSHIP OF GRADUATE STUDIES

This thesis, written by **MEER ABDUL MATEEN KHAN** under the direction of his thesis advisor and approved by his thesis committee, has been presented to and accepted by the Dean of Graduate Studies, in partial fulfillment of the requirements for the degree of **MASTER OF SCIENCE IN ELECTRICAL ENGINEERING.**

Dr. Samir A. Al-Baiyat
(Advisor)

Dr. Ibrahim M. Elamin
(Member)

Dr Ali A. Al-Shaikhi
Department Chairman

Dr. Ibrahim O. Habiballah
(Member)

Dr. Salam A. Zummo
Dean of Graduate Studies

9/5/16

Date

Dedicated to

My Beloved Parents, Sisters

And

Azeemuddin, Aleemuddin, Abdul Qawi, Abdul Rahman

ACKNOWLEDGMENTS

Say (O Muhammad ﷺ): "This is my Way; I do invite unto Allah with a certain knowledge." I and whoever follows me (must also invite others to Allah, Oneness of Allah with sure knowledge). Glory to Allah! and I am not of the polytheists." (12: 108)

"O my Lord! Increase me in my knowledge!" (20:114) "O Allah I ask you for knowledge that is of benefit."

All praises and worship are for ALLAH alone, the most glorious and the most merciful; who has blessed us with Iman I always ask for his forgiveness as well as showing us right path. Peace and blessings be upon the most respected and high-status person, the last and the final Prophet, Muhammad ﷺ, upon his family, his companions, and all those who follow him until the day of judgment.

I owe to express a deep sense of gratitude to my thesis advisor Dr. Samir A. Al-Baiyat for this prompt inspiration, patience, timely guidance, valuable ideas throughout my thesis. I feel very great to say; he has successfully instilled in me a passion for scientific research, which will continue to guide me for many more years to come. His appreciation and words of encouragement gave a new life to my efforts in hard times. His immense knowledge and motivation helped me in writing my thesis in later stages.

I would like to appreciate my committee members Dr. Ibrahim M. Elamin and Dr. Ibrahim O. Habiballah for their thoughtful suggestions, insightful comments, and support during my thesis phase.

My sincere thanks to Dr. A. H. M. Abdur-Rahim for instilling and cultivating research interest in me. I am very grateful to him for providing me programming aids. He guided me the perfect direction so that I never get deviated.

I acknowledge King Fahd University of Petroleum & Minerals for providing me an opportunity to peruse my masters as a research assistant. I am thankful to Dr. Ali Ahmed Al-Shaikhi, Chairman Electrical Engineering Department, for providing an excellent environment for learning and research in the department. I also like to thank him for giving me a chance to teach various labs of undergraduate level.

I would like to appreciate and thank my parents, Mrs. & Mr. Meer Abdul Majeed Khan from the bottom my heart for their love, care, moral support and their patience when their only son wasn't around. I am grateful to my sisters for motivating me and their valuable efforts throughout my life. It's my family who made me live the most unique, magic and carefree childhood that has made me who I am now! O Allah grant them good in this world and good in the hereafter, Ameen!

I owe special thanks to my best friend, Abdul Nabi Qureshi, who was always with me even in my hard times. I have a profound respect and gratitude for my roommate Mohammed Abdul Raheem during my stay at KFUPM who helped me by his esteemed support. I would never forget the chats and beautiful moments that I shared with my friends here in KFUPM. Lastly, I would like to pass my gratitude to all my friends in my country who always supported whenever needed.

TABLE OF CONTENTS

LIST OF FIGURES

NOMENCLATURE

δ	:	Rotor angle of micro alternator
ω_0	:	Synchronous rotor speed
P_e, P_m	:	Output electrical and input mechanical power of the micro alternator
M, H	:	Coefficient of machine inertia and inertia constant
E_{fd}	:	Field voltage of micro-alternator along D-axis
V_t	:	Micro alternator's terminal Voltage
V_{tref}	:	Micro alternator's reference terminal Voltage
x_d	:	Synchronous reactance along D-axis
$x_d^{'}$	:	Transient reactance along D-axis
$T_{do}^{'}$	:	Open circuit field constant
K_A, T_A	:	Excitation system gain and time constant
P_{mw}, P_{ew}	:	input mechanical and output electrical power of the wind system
H_g	:	Wind generator's inertia constant
x_{dw}, x_{qw}	:	PMSG reactance along d and q axes
E_{fdw}	:	PMSG field voltage along D-axis
R_{pf}, L_{pf}, C_{pf}	:	PV output filter's resistance, inductance and capacitance

R_p, L_p	:	PV output coupling line resistance and inductance
R_{wf}, L_{wf}, C_{wf}	:	Wind output filter's resistance, inductance and capacitance
R_w, L_w	:	Wind output coupling line resistance and inductance.
R_s, L_s	:	VSC transmission line resistance and inductance
r_t, x_t	:	Interconnected resistance and reactance between a line connected to micro alternator and Microgrid common bus
r_b, x_b	:	Interconnected resistance and reactance between a line connected to microgrid common bus and main grid
g, b	:	Conductance and susceptance of the load
V_s, θ	:	Microgrid's voltage magnitude and phase angle
i_{gwd}, i_{gwq}	:	PMSG currents along D-q axis
m_{pv}, ψ_{pv}	:	PV inverter's modulation index and phase angle
m_{wr}	:	Wind generator side converter's modulation index
m_{wi}, ψ_{wi}	:	Wind inverter's Modulation index and phase angle

LIST OF ABBREVIATIONS

DG	:	Distributed generation
PV	:	Photovoltaic system
WT	:	Wind turbine
DER	:	Distributed Energy Resources
DS	:	Distributed Storage
VSC	:	Voltage source converter
FACTS	:	Flexible AC Transmission System
STATCOM	:	Static Compensator
PLL	:	Phase Locked Loop
SMR	:	Switched Reluctance Motor
SVC	:	Static VAR Compensator
PMSG	:	Permanent magnet synchronous generator
SMIB	:	Single Machine Infinite Bust
PSO	:	Particle Swam Optimization
ANN	:	Artificial Neural Network
PCC	:	Point of common coupling

THESIS ABSTRACT

Full Name : [Meer Abdul Mateen Khan]

Thesis Title : [Robust Control of a Microgrid]

Major Field : [Electrical Engineering]

Date of Degree : [December 2015]

The introduction of renewable energy sources directed us to integrate the clean sources to the power grid, thereby forming a microgrid. This thesis describes a detailed nonlinear modeling and robust control technique for a microgrid system that includes different DG sources such as PV, Wind Energy, and conventional micro-alternator along with STATCOM. Proper interfacing of power electronics devices was carried out in the modeling of the microgrid. Power generation of micro-alternator, PV and wind system is considered so that proper power sharing is done in a microgrid system.

For the purpose of understanding the interaction of DG sources, two different configurations are considered in this work. The first comprises of a micro-alternator, PV system along with STATCOM. Both nonlinear model and linear model of the system was obtained to estimate the plant transfer function for the purpose of designing controller. A robust central supervisory controller was obtained, where the controller design is proposed by satisfying the performance and stability criteria. An open loop transfer function was obtained by employing loop-shaping algorithm. This controller was found to perform excellently on a linear system of the microgrid. The robust controller obtained was tested for a nonlinear system of microgrid subjected to torque disturbance and even three phase fault.

While, a second test system of a microgrid is formed by integrating micro-alternator, wind system along with STATCOM. A loop-shape controller was designed for such a system and was tested under the environment of various torque disturbance and even three phase fault. The proposed controller was reliable for the system performing at different operating points and for various disturbance scenarios.

ملخص الرسالة

الاسم الكامل : مير عبد المتين خان .

عنوان الرسالة : التحكم الفعال في شبكات القوى الكهربية الصغيرة .

التخصص : الهندسة الكهربية .

تاريخ الرسالة : ديسمبر 2015

إن وجود مصادر الطاقة المتجددة تقودنا إلى تقديم مصادر الطاقة النظيفة ، من هنا جاءت شبكات القوى الكهربية الصغيرة. هذه الرسالة تقدم وصفا تفصيليا للتحكم الفعال لطرق التحكم غير الخطي لشبكات القوى الكهربية الصغيرة والتي تشمل مصادر التوليد الكهربي المتنوع مثل وحدات الطاقة الشمسية ، طاقة الرياح ، والمولدات التقليدية الصغيرة مع الموجهات الثابتة . إن التفاعل المناسب لأجهزة القوى الالكترونية تم أخذه في الاعتبار. مولدات الطاقة الكهربية الصغيرة ، الوحدات الشمسية ، مع طاقة الرياح تم اعتبارها ايضا ولذا فإن المشاركة الفعالة للشبكة الكهربية الصغيرة في الشبكة كان مناسبا.

لكي يتم فهم التداخل في الادوار بين عناصر مولدات الطاقة المختلفة ، تم اعتبار نموذجين مختلفين في هذه الرسالة . الأول ، تم اعتبار تداخل المولدات الصغيرة مع الوحدات الشمسية جنبا إلى جنب مع المعادلات الثابتة . تم دراسة ذلك في ضوء نموذجي التحكم الخطي وغير الخطي وذلك لتقدير الدالة الوظيفية للشبكة من أجل التصميم الامثل للمتحكم . تم تصميم متحكم مشرف فعال ، حيث روعي في تصميم المتحكم الأداء الفعال والاتزان . في الدراسة تم الحصول على نظام دائري متوالي عن طريق توظيف دالة التشكيل الدائري. هذا المتحكم قدم أداءا متميزا في حالة التحكم الخطي للشبكة ، تم اختبار أداء المتحكم في الشبكة في وجود عدة عوامل مثلا العزم المتغير ، والخطأ ثلاثي الأوجه.

بينما، النموذج الثاني للشبكة الكهربية الصغيرة تم دارسته في وجود المولدات الصغيرة مع طاقة الرياح في وجود المعادلات الثابتة . تم تصميم متحكم التشكيل الدائري لهذا الغرض وتم اختباره في ظروف بيئية مختلفة من العزم المتغير وايضا الخطأ ثلاثي الأوجه. وقد أثبت المتحكم المقترح في الدارسة أداءا ثابتا عند نقاط تشغيل مختلفة وتحت نماذج بيئية متنوعة .

CHAPTER 1

INTRODUCTION

In today's world, generation of electricity is going to be a challenging task for the power system operators to meet the requirement of consumers, as there is a rapid increase in demand of global energy consumption. Since most of the power generation is done by traditional methods, these methods have an adverse effect on the environment in terms of carbon dioxide emissions and nuclear waste problems. Because of traditional power generation, there is also a decline in fossil fuels and adverse effect on global climate. Transmissions networks have their associated problems of real power losses and reactive power consumption. The conventional power generation is liable to various stability as well as energy security issues.

Most of the conventional generation by combustion engines, micro-alternator, etc., have a hazardous effect on the environment. For this reason, non-conventional renewable energy sources such as solar energy, wind energy, hydropower, etc. along with conventional generation are being used for the production of electricity in order to overcome this problem. In a power system, generation can be can be done on a large scale as well as small scale. In small scale, generation can take place at the distribution level. Such type of power system which involves generation of power at distribution level is termed as Distributed Generation (DG) system. Micro-alternators, combustion engines, Photovoltaics (PV) system, wind power corresponds to the different form of DG, which may or may not be connected to the utility grid. Based on their connection to utility, DG's can be broadly classified into two types. The first category of DGs includes inertial

machines such as internal combustion engines and microturbines, which involves rotating machinery. The second category of DG's direct us towards interfacing of electronic devices such as inverters, filters, and coupling elements, etc. in PV and wind system [1]. Inverters are employed by interfacing the renewable sources are meant for flexibility in operation and control.

1.1 Microgrid

The clean resources have directed to a new direction for generation of power without any hazardous effect on the environment. They led us to the new era of smart grids. Smart grid is a partially automated, centralized network which maximizes performance and reliability and reduces environmental impact. Smart Grids are a network which can deploy a new innovative and intelligent control, better communication between distributors to consumers and provides better reliability of power system [2]. This gave rise to a study named 'Microgrid'.

Microgrid has a dominant role in the power system, as it is formed by a cluster of distribution network connected to distributed generation (DG) for maintaining the system reliability when grid supply in not available. They can improve the utilization of renewable energy and important load supply reliability. Microgrid in generally a network which is an assembly of distributed generators, storage devices and local loads operating individually or interconnected to main grid [3].Thus, micro-grid facilitates many consumers, e.g. commercial buildings, residential buildings and industrial areas. They comprise of Distributed energy resources (DER), intermediate switches, and basic control systems [4]. DER units include both distributed storage (DS) units and distributed generation (DG) with

different capacities and characteristics. Distributed generation (DG) connected to microgrid system is a conventional micro-alternator, photovoltaic system or wind system.

Microgrids are powered by micro sources such as a photovoltaic cell, fuel cells, and micro-turbines and can function in both grids connected and islanded mode [5]. In the grid-connected or non-autonomous mode, so as to feed continuous power into the network at a certain voltage. A microgrid consists of a low or medium voltage distribution system; distributed generations, such as wind turbine generators and photovoltaic arrays. In the islanded or autonomous mode, a group of DG units is designed to maintain the reliability of various critical loads, even though when there is no availability of utility supply [6]. It is also called standalone mode.

An electrical microgrid consists of micro-alternator as well as a renewable energy source, due to which problems arises such as uncertainty in the behavior of power, inefficient power sharing, etc., can be overcome by designing a central controller which supervises various power flow in DG's. The various components of a microgrid can be interfaced to the power system in either of the two ways: direct connection or connection through power electronic devices. Small micro alternators have synchronous machines operating at synchronous speed when connected with the utility. They are used mostly with reciprocating engines and gas turbines. The power electronics technology allows extracting power from renewable sources and converting electric power to fixed frequency AC power. The flexibility and adaptability of the system have increased due to the advent of power electronics. Most renewable sources generate either in the form of DC or other forms, which requires some power electronics devices for their interconnection with the grid.

A microgrid is a vast topic in research. Hence, it is extremely important to highlight some of its benefits

- Decrease in emission of hazardous gasses in environment
- Low capital cost and reduced the time for construction of the plant.
- Increase in reliability of power supply when disconnected from main grid
- Deregulation in market levels, allows one individual to participate in power generation thereby producing employment opportunity.
- Reduction in energy loss due to a decrease in the reduction of line flow losses.
- Provides flexibility in setting a power system.
- Promotes the growth of renewable energy sources.

1.2 Microgrid Challenges

In general, there are two important issues regarding the protection of microgrid. The first one is related to many generation units installed in a microgrid and second is any disturbance or faults in the system which takes the system towards the unstable environment. A microgrid configuration can be formed by the combination of various DG sources; it is extremely important to monitor the power sharing of individual DG's in an integrated microgrid. Another important requirement is the proper loading conditions as well as to observe whether the system is connected to the grid or not. When microgrid is not connected to utility or it is in grid autonomous mode, total active and reactive power requirement of load shall be met.

The integration of renewable energy sources such as photovoltaic, fuel cells and wind generation systems, with the utility distribution systems, require power electronics

devices and converters. Hence, proper operations of this converters and inverters are going to be a challenging task. There is a need for selection of best coupling, and filtering elements shall also be considered. Power electronics interface introduce new issues for control aspect. It is very necessary to create a power electronics interface for the microgrid, which allows many combinations of micro generators to function in both island mode and as a satellite to the power grid while providing a better power quality at minimum equipment cost.

Basic requirement of the power electronics interface are:

- To provide fixed power and local voltage regulation.
- Using storage that helps DG fast load tracking

1.3 Problem Statement

In a system of a microgrid, formed by both micro-alternator and renewable energy such as PV system or wind energy system which require power electronic devices resulting in problems related to stability and operational issues. As a result, it is extremely important to maintain system stability during normal conditions as well as during contingencies. Other problems that arise due to the integration of renewables include generation of harmonics, voltage and frequency variations in the microgrid which may deteriorate the stable operation. Power electronic devices such as inverters, filters, coupling elements require proper tuning of capacitors, inductors, etc. Proper switching of inverter parameters is also essential in a system of the microgrid.

Moreover, the power-sharing contribution of both conventional and renewable source also corresponds to certain problems. In some cases, microgrids may be subjected to some disturbances such as load variation or faults at any bus terminals.

1.4 Methodology

In view of the problems stated in the previous section, there is a need for a robust controller which can stabilize the system in the event of any faults or disturbance. Microgrids are non-linear power systems in their nature, which comprises of the micro-alternator, PV system, Wind System. Designing a controller for this nonlinear system is much more complicated than the linear systems. Therefore, the system is linearized by selecting an operating point and based on this model; the controller is designed. As a result, the challenging task is to implement this controller on a non-linear model. The performance of the controller can be investigated by subjecting the system to various contingencies.

1.5 Thesis Objectives

This research presents a microgrid system which can be expressed as a nonlinear model as well as a small signal model. An efficient, robust controller shall be developed which guarantee stable and proper operation of microgrid system which is formed by the integration of micro-alternator, PV system, STATCOM, etc.

The following are the main objectives of this research

1. To obtain a non-linear mathematical model for individual as well as integrated DG sources namely micro-alternator, PV system and wind system along with STATCOM, connected to the utility grid.
2. To develop a small signal model from the nonlinear model about a certain operating point for the purpose of designing controller.
3. To design a robust controller for a linear system of microgrid and test the performance of the non-linear system.
4. Test the controller robustness by subjecting the system to various torque disturbance and even for three phase fault.

1.6 Thesis Organization

The thesis is organized in a total of 5 chapters, and their brief contents are illustrated below:

Chapter 2 addresses a detailed literature review on the configuration of microgrids. Recent studies on PV system and STATCOM is also presented. Various control techniques adopted to overcome stability issues related to microgrid system.

Chapter 3 gives detailed nonlinear modeling of the micro-alternator, PV system, Wind system and STATCOM individually. The models of various power electronic devices that are to be used for integration of renewables have also been established Dynamic nonlinear and small-signal linearized model of an integrated microgrid system with PV-STATCOM and wind -STATCOM is also presented.

Chapter 4 deals with designing a robust loop-shape controller for models described in chapter 3 based on a loop-shape algorithm. The efficient controller obtained is implemented on nonlinear system subjected to various torque disturbances and even for severe three phase fault. Lastly, the performance of the loop-shape controller was compared with PID controller

Chapter 5 concludes the research work and highlights some scope of future work in this area.

CHAPTER 2

LITERATURE REVIEW

This section highlights on some of the recent work on electrical microgrid system in the present modern power industry. Modeling of various DG whether it is a simple alternator, PV or wind system was enhanced over the period of time depending upon requirement by the power system. Hence, huge literature can be found on modeling of microgrid and various issues related to the operation, performance, stability, and control. A variety of control algorithms is proposed to maintain the stability of the system. As the primary requirement of a power system plant is to operate in a stable mode. Hence, it is extremely important to design the best controller.

2.1 Microgrid Overview

Distributed generators involve the use of various micro-sources like a micro turbine, photovoltaic cell, batteries for their operation. In a certain local area, the microgrid is formed by a cluster of parallel distributed generation system and loads. Hence, for better operation of a microgrid, a good power control system, and voltage regulation algorithm should be implemented [7]. A microgrid in general, has two main types of DG units, rotational or inertial type, and stationary type. In either type, they require devices such as power electronic inverters converters that would connect them to main grid [8].To understand the importance of distributed generation a microgrid system was proposed which is a combination of loads associated and generation as a subsystem. Thus, a local controller is needed. In the account of any disturbances, persist in generation and load gets

isolated from the system of microgrid as a result preventing transmission gird's integrity. This ability provides better reliability to entire electrical power system [9].

The concept of a microgrid is considered as the best solution for the problem of integrating a huge amount of micro-generation without disconnecting from utility network. On account of any disturbance, the grids power falls below certain standard requirement. Hence, microgrid gets disconnected from the main network and operates independently facilitating in improving the quality of power to consumers [10]. Microgrid could be a small as well as a large power system, integration of renewable energy sources forms a complex system. A large number of DER's connected to microgrid which makes the system critical. As a result, many problems arise concerning control of DER's in a best reliable manner [11].

2.2 Photovoltaic System

The method of harvesting solar energy came into light several decades ago. Today humans have learned many methods to extract and make use of solar radiations in many applications. In 1839, a French scientist Edmund Becquerel proposed photoelectric effect. Some materials have a tendency to produce electric current when exposed to sunlight. Based on the photoelectric effect, incident radiation of solar energy can be directly converted into electricity by a method called photovoltaic. Electrical charges are produced in a solar cell when the incident photon energy is sufficient enough to break the covalent bond of the semiconductor material [12]. Solar cells can be connected in large number in a pattern of the series-parallel package which constitutes a solar array or solar module. Therefore, the power output of solar module depends on a number of cells and their arrangements.

PV cell exhibits nonlinear characteristics; its equivalent circuit can be considered as a current source in parallel with a diode [12]. A practical PV cell is the one that incorporates series and parallel resistances to account for voltage drop in the device and shunt current loss. Determination of various parameters of a solar cell is an important task in order to understand the behavior of the device and also to model the system with high accuracy.

Extraction of maximum power from PV array is a tedious task as it requires a lot of calculation. As there is a nonlinearity in V-I characteristics which results in variation of terminal voltage. These characteristics can manipulate by certain factors such as

- Temperature
- Insulation
- Fully/Partially shaded conditions
- Solar Radiation intensity

Keeping these environmental factors in mind, a strategy should be developed to extract maximum output from the solar array. Some of those methods were expressed in [13]

1. Constant voltage method
2. Constant current method
3. Pilot cell method
4. Curve fitting method
5. Look up table method
6. (P&O) Perturb and observe method

Apart from this methodology some other methods were also expressed such as Artificial neural network (ANN) based method, Fuzzy logic control method [13]. An another approach for driving maximum output wherein a control design for PV system supplied by the Switched Reluctance Motor (SMR) based on proportional and integral (PI) controller. This controller can obtain MPPT by supervising current and voltage of PV array and adjust the duty cycle of DC/DC converter [14]. A sub-program was designed to estimate maximum power for photovoltaic modules. The process requires a 32 microprocessor a TMS320F28335 and in the program, incremental conductance method is employed for maximum power point tracking [15].

PV model can be designed by employing power electronics components such as inverters, convertor, etc.; and are grabbing the attention of most researcher in this particular field. Detailed dynamic model of a PV system explains the behavior and associated control circuitry very well, but they are seldom employed for microgrid studies due to their computational complexity. Description of a PV module either as constant real power generation or constant negative real power loads has also been noticed. Such simplifications of PV model are not applicable for transient stability studies and are mostly employed in the steady-state analysis. PV module designed with a source converter controlled through modulation technique. A simplified model as current controlled source by depicting phase angle and magnitude by National Renewable Energy Laboratory (NREL) [16].

A test model for PV inverter is formed by a DC source, load bank, and a simulator. The task of this model is to simulate frequency, voltage deviation of the grid under steady state condition. The DC source was considered as acting PV array operating at maximum

power. The load bank is a general resistive and reactive load which can dissipate both real and reactive power. A number of tests were performed over this setup namely under voltage transients, islanding of inverter from the grid, short circuits inverter test, etc. [17]. It is well-known fact that control configuration for grid-connected PV inverter is traditional current source inverter. As a result, it is not an easy task to regulate AC voltage and frequency. In one of the proposed methodology, a CERTS PV micro source controller is constructed that guides the PV to behave as a voltage source, thus facilitating in maintaining voltage stability in the account of any load transients [18] .

An experimental setup of grid-connected PV system acting as DG source is formed by using LabVIEW for monitoring purposes. This setup was simulated under Simulink test bench. Phase locked loop (PLL) is employed to track inverter voltages which match the output during the simulation time [19]. Moreover in a microgrid due to fluctuation due to resistive load have an adverse effect on the supply voltage. An inverter control double loop principle is adopted to maintain a stable voltage even when the system is subjected to various fluctuations [20].

2.3 Wind System

Owing to abundance availability of winds all over the globe, the wind power generation market has developed into a highly competitive environment. Wind machines generally fall into two categories the fixed speed type and the variable speed turbines. Fixed speed machines are usually composed of self-excited induction generators with either two pole pairs or rotor resistance controlled type. They operate at a constant speed irrespective of variations in wind energy. On the other hand, the variable speed wind systems include grid-connected wind turbines and generator coupled through modern power electronic

circuitry extracting maximum output from the wind. They can be either wound rotor machines or permanent magnet synchronous generator or externally magnetized synchronous generator[21].

The Fixed speed wind turbine concept

Most of the wind turbines operating during 1990's were found to be fixed rotor speed with no influence from wind speed variations[22]. Induction generators of wound rotor type operating in the asynchronous mode have very little variation in rotor speed and hence can be considered fixed speed machines. Wind generators connected to power grids operate at a speed defined by the nominal frequency of the utility grid. For varying wind speeds, constant rotor speed operation is established through a gear ratio and special design of the generator[23].

The Variable speed wind turbine concept

Optimal tip-speed ratio or blade pitch angle control defines the operation strategy of a variable speed wind turbine, which make it to run at a certain speed relative to the current wind speed, to extract maximum power from wind energy[22]. Use of variable speed turbines in wind energy generation systems has inherent benefits such as reduced mechanical stresses, diminished torque oscillations, efficient operation and highest aerodynamic efficiency.

2.4 STATCOM

In present day's Flexible AC Transmission System (FACTS) devices has gained their place in power system with the advancements in the field of power electronics devices. The primary function of FACTS devices is to provide compensation and support

to control voltage of a system. With the help of FACTS devices, reactive power compensation is achieved by thyristor-based Static VAR Compensator (SVC) [24]. The compensation can be provided in both shunt and series connection. A device which is capable of compensating reactive power and provides voltage support to an AC power system is termed as STATCOM (Static Synchronous compensator). Modern STATCOM devices are based on power electronics devices such as Insulated Gate Bipolar Transistor (IGBT) or insulated Gate commutated thyristor (IGCT).

A direct-current vector control mechanism employing VSC based STATCOM for grid voltage support and reactive power enhancement was proposed, where an optimal control strategy through integrated PID, fuzzy and adaptive control mechanism was found to exhibit weak performance in extreme situations [25]. In VSC based STATCOM control scheme, where the operation of the converter is within the mode of linear modulation, such a scheme is capable of maintaining STATCOM capacitor DC voltage within the reference value [25]. In one of the study, bifurcation analysis was implemented on a twelve pulse two-level voltage source converter (VSC) based STATCOM, where the impact of the DC capacitor on the stability is studied[26]. The entire STATCOM model is formed in the d-q frame, and a small reactance is considered which represents the coupling leakage reactance of a transformer. A feedback nonlinear controller is designed to control the bifurcation of the STATCOM in the region of inductive and thus eliminating Hopf bifurcation and limiting point cycles[26].

For active power enhancement of a network, a Battery Energy Storage System (BESS) is integrated to dc side of the converter, so as to allocate active power between various storage energy modules. As a result, a control technique for an STATCOM/BESS

is implemented by tuning variable proportional coefficient [27]. Frequency control for a weak electrical power supply network was carried by use of STATCOM employing Supercapacitor Energy Storage (SES) [28].

Research based on renewable energy sources where Wind Energy Conversion System (WECS) as DG. STATCOM is integrated along with induction generators, facilitates to regulate the terminal voltage of induction generator. In this proposed design STATCOM and power system stabilizer (PSS) parameters are optimized by using Generic Algorithm (GA) [29]. Another approach of a similar kind where Single Machine Infinite Bus (SMIB) with STATCOM, an AC and DC controller, PSS is designed whose parameters are optimized by particle Swarm optimization technique [30].

2.5 Control of Microgrid

Stability is the primary issue in a microgrid system, as it comprises of non-conventional Renewable sources. Microgrid power system is subjected to various load as well as generation disturbances. For this reason, a central controller is designed for the proper functioning of the system. Even though rotating parts are minimized by employing power electronics devices, it is extremely important to control the operation by proper interfacing of the inverter.

Considering a mode where the grid is connected, the stability can be attained by selecting parameters for controller, filter capacitance and inductance. In order to estimate the filter parameters a trial and error method is incorporated for analyzing system characteristics. But, trial and error method cannot forecast all operational scenarios of microgrid and would lead to low power quality and voltage/angle stability [31]. A control

technique to implement islanding mode of operation in microgrid is introduced in "Intelligent control for intentional islanding operation of microgrid"[32]

The robustness of microgrid operation is mainly dictated by the robustness and effectiveness of the Control functions that yield regulated power operation. Various control techniques are reported to enhance the robustness of the control system in grid-connected converters and isolated microgrid[33][34]. Voltage and power sharing controllers were implemented to provide high disturbance rejection performance against voltage disturbances and power angle swings, respectively[35].

In order to reject harmonic disturbance from the public utility grid or nonlinear loads, a repetitive control $H\infty$ method which ensures that a designed controller is performing effectively[36]. $H\infty$ robust control scheme for DC-AC interfaced micro source, a double loop current-regulated voltage control a control scheme is developed [36]. A well-known control strategy for voltage and frequency control of an islanded microgrid is based on the droop control technique[37]. In the droop control strategy, load dynamics are not directly included in the control loop and load changes results in a large disturbance in terms of voltage/frequency instability. So, this issue drawbacks of conventional droop control can be overcome by the proposed modified droop control strategy [35].

To improve the coordinated control effect and robustness against system uncertainties of the microturbine and energy storage (ES), the particle swarm optimization (PSO) based fixed-structure $H\infty$ loop shaping control is applied[38]. As the load is uncertain and unknown and hence it is a source on unmolded dynamics, to regulate the load voltage a controller is designed which will be characterized by two degree of freedom

feedback feed forward controller (2DOF), finally the control design problem is reduced to non-convex optimization[39].

A system of microgrid supplying local electrical loads was considered, and a control strategy was developed which ensures power sharing for a generation unit. DG's operating in islanded mode, a robust control method is developed by employing H-infinity (H∞) loop-shaping design (HLSD) for Inverters which are parallel connected to DG's. The aim of this controller is to duty cycles thus changing the output current delivered by the individual inverters [40]. In another proposed research for wind power applications hybrid excitation synchronous generator (HESB) who's output voltage is controlled by excitation DC field. A cascade control scheme where the excitation current inner loop is controlled by PI controller and for outer speed loop H∞ controller is designed [41].

For a four-machine power system, a robust STATCOM damping controller is designed by a graphical loop shape technique. After proposing the desired controller, the system order is reduced by using model reduction technique. The estimation of this robust controller is done by incorporating PSO algorithm [42]. Another loop-shaping technique for a system with a single DG and STATCOM is implemented. The system is linearized, and open loop transfer function was estimated then a robust controller is designed. This power system was subjected to various torque disturbance and even three phase fault, but the proposed controller was found to be robust. The performance of this controller was compared by PID controller whose gains are calculated by pole placement technique [43].

CHAPTER 3

MODELING OF MICROGRID SYSTEM

This section describes the designing of the electrical microgrid dynamic system and its mathematical representation of components associated with it. Both nonlinear and linear model of the individual DG sources, as well as combined integrated microgrid model, will be given. Detailed model for STATCOM is also described in this chapter. In this research combined microgrid integrated model is formed by the combination of synchronous generator, STATCOM and photovoltaic system and wind system connected to the utility grid is given. These sources incorporate power electronic device for integration of renewable sources.

3.1 Microgrid Design

A microgrid can be designed by connecting various DG units to the power grid along with combined load. The system is designed by considering the first DG as micro-alternator which is modeled as a gas turbine or diesel engine. Second DG is considered as PV module or Wind System, which is integrated to the grid by means of voltage source converter, filtering circuit and coupling inductance. STATCOM module along with energy storage device is also connected to the grid. All units including loads are connected to a common point termed as a point of common coupling (PCC). A simple single line diagram for a complete integrated microgrid model can be shown in Figure 3. 1

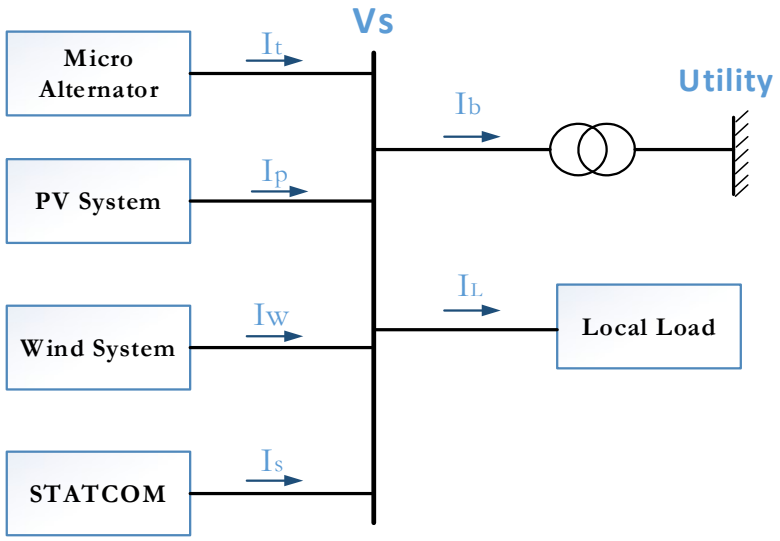

Figure 3. 1 Configuration of microgrid

3.1.1 Micro-Alternator Model

Micro-Alternator is basically modeled as a conventional generator. This generator can be used directly for connection to the utility grid. This micro-alternator is provided with excitation control. The dynamic model of the synchronous generator is best described by 4th order model. The swing equation represented as 2nd order model as:

$$\frac{2H}{\omega_b}\frac{d^2\delta}{dt^2} = P_m - P_e - D(\omega - \omega_0) \tag{3.1}$$

Splitting 2nd order swing equation in two first-order non-linear differential equation as:

$$\frac{d\delta}{dt} = \omega_0(\omega - 1) \tag{3.2}$$

$$\frac{d\omega}{dt} = \frac{1}{2H}[P_m - P_e - D(\omega - \omega_0)] \tag{3.3}$$

Where δ is load angle, ω is rotor speed, P_m is mechanical input power, P_e is an electrical power of generator, ω_0 is rated angular speed and D is damping expressed

in above equation. Due to the excitation applied on dc windings of micro alternator there develops an EMF as a result the internal voltage is given as:

$$\frac{de_q{}'}{dt} = \frac{1}{T_{d0}{}'}\left[E_{fd} - e_q{}' - (X_d - X_d{}')i_{td}\right] \tag{3.4}$$

In the equation (3.4) x_d, T'_{do} and x'_d are the synchronous reactance, open circuit field constants and transient reactance along d-axis and $\mathrm{e_q}'$ is voltage behind the transient reactance along q axis.

For synchronous generator or alternator voltage regulator excitation used, which is IEEE type-1.

$$\frac{dE_{fd}}{dt} = \frac{1}{T_A}\{K_A\langle V_{tref} - V_t\rangle - \langle E_{fd} - E_{fd0}\rangle\} \tag{3.5}$$

Field voltage along d axis given by E_{fd}, K_A is the exciter gain constant and T_A is the time constant of exciter. As the synchronous generator it-self is a conventional one, so there is no need of any power electronics devices. Since this is a 4th order system its state variables can be chosen as

$$X_{DG1} = \left[\delta, \omega, e_q{}', E_{fd}\right]$$

3.1.2 Micro-Alternator Connected to Grid

In this section, a single synchronous generator is connected to a bus via transmission line considering resistance R_t and inductance L_t, let V_t is the terminal voltage, i_t is the transmission current and V_s is the bus voltage.

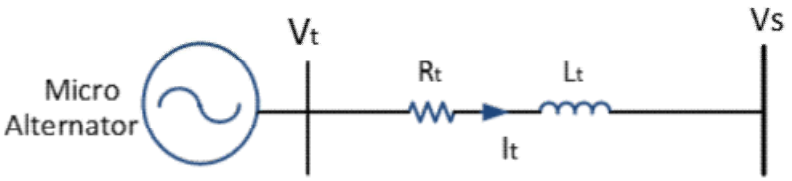

Figure 3. 2 Micro-Alternator connected to grid

Terminal voltage for this grid-connected micro-alternator is given as

$$V_t = V_s + (R_t + jX_t)i_t \tag{3.6}$$

Expressing terminal voltage equation into d-q terms as shown below

$$V_{td} + jV_{tq} = V_{sd} + jV_{sq} + (R_a + jX_a)\left(i_{td} + ji_{tq}\right) \tag{3.7}$$

$$X_q i_{tq} + j\left(e_q{}' - X_d{}' i_{td}\right) = \left(V_{sd} + R_t\, i_{td} - X_t i_{tq}\right) + j\left(V_{sq} + R_t i_{tq} + X_t i_{td}\right)$$

Separating real and imaginary parts, we can get current in d-q components

$$i_{td} = \frac{-R_t V_{sd} + \left(e_q{}' - V_{sq}\right)X_2}{R_t{}^2 + X_1 X_2} \tag{3.8}$$

$$i_{tq} = \frac{V_{sd} X_1 X_2 + R_t\left(e_q{}' - V_{sq}\right)X_2}{X_2(R_t^2 + X_1 X_2)} \tag{3.9}$$

Where, $X_1 = \left(X_d{}' + X_a\right)$ & $X_2 = \left(X_q + X_a\right)$.

Now after driving the equation of current, terminal voltage can be expressed in terms of these currents

$$V_t = \sqrt{V_{td}{}^2 + V_{tq}{}^2} = \sqrt{\left(X_q i_{tq}\right)^2 + \left(e_q{}' - X_d{}' i_{td}\right)^2}$$

Also, the electrical generator power output can be expressed as:

$$P_e = V_{td} i_{td} + V_{tq} i_{tq} = e_q{}' i_{tq} + \left(X_q - X_d{}'\right) i_{td} i_{tq}$$

Thus, utilizing the above equations, power output of the micro-generator and the terminal voltage can be expressed in terms of V_{sd} and V_{sq} which are voltage components of the microgrid.

3.1.3 The Photovoltaic System

The solar cell is the fundamental block in a photovoltaic system. The semiconductor device present in solar cell behaves as a current source when solar radiation is incident on it. Working principle is based on photoelectric effect in which due to absorption of sunlight an electron gets ejected from the conduction band. Nonlinear P-V and I-V characteristics can be exhibited by the system which varies with cell temperature as well as radiation intensity. PV cell is modeled by considering a current source in parallel with a diode as shown Figure 3. 3 [44]

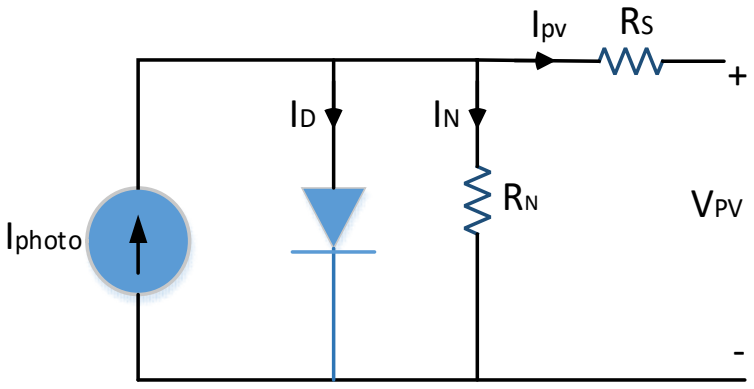

Figure 3. 3 Equivalent circuit for PV cell

By applying Kirchhoff's current law, (KCL) output current is given by

$$i_{pv} = I_{photo} - I_D - \frac{(V_{pv} + i_{pv}R_s)}{R_N} \tag{3.10}$$

The diode p-n junction current can be given as:

$$I_D = I_{RSC}\left(e^{\frac{(V_{pv}+R_s i_{pv})}{\eta v_T}} - 1\right) \tag{3.11}$$

The reverse saturation current I_{RSC} , the PV cell current i_{pv} and cell voltage V_{pv} , the diode ideality factor η, and the thermal voltage v_T determines the terms associated with the PV module. Where R_N is shunt resistance and v_T thermal voltage given by $v_T = \left(\frac{k\,T}{q}\right)$.

The current generated by the photodiode at cell working temperature of 25^0C and solar irradiation 11kW/m^2 is given as:

$$I_{photo} = \left[I_{SC} + a(T - T_{ref})\right]$$

Now the reverse saturation current dependent on temperature can be obtained in the form

$$I_{RSC} = I_{RSCref}\left(\frac{T}{T_{ref}}\right)^{\frac{3}{n}} e^{\frac{-qE_g}{nk}\left(\frac{1}{T}-\frac{1}{T_{ref}}\right)}$$

From all the above equations we get the final PV cell current as given below:

$$i_{pv} = I_{SC} - I_{RSC}\left[e^{q\left(\frac{V_{pv}+i_{pv}R_s}{nv_T}\right)} - 1\right]$$

A typical solar cell can generate power in the range of 2W at 0.5V. As the power obtained by the solar cell is very low, hence there is a need for connection of these solar cells either in series or in parallel in order to meet the power range of watts. The approximate photovoltaic array model comprises of series models N_s and parallel modules N_p, can be described by a characteristic equation.

$$i_{pv} = N_p I_{photo} - N_p I_{RSC}\left[e^{\left(\frac{V_{pv}}{N_s}+\frac{i_{pv}R_s}{N_p}\right)/nv_T} - 1\right] \quad (3.12)$$

By utilizing Newton-Raphson method, the nonlinear relation between cell current and voltage can solve by an iterative process. As a result, we get voltage relation as

$$V_{pv}=N_s\left[ln\left(\frac{N_p I_{photo}-i_{pv}}{N_p I_s}+1\right)nv_T - \frac{i_{pv}R_s}{N_p}\right] \quad (3.13)$$

3.1.4 Interfacing of PV System with Power Electronics

Photovoltaic system before connecting to the utility grid, require the use of various power electronics devices. The DC/DC converter, DC link capacitor, DC/AC inverter and filter circuit constitutes the major components of a power conditioning unit (PCU). The task for DC/DC is to transform or boost the voltage level of PV array. The harmonics and power quality problems arise due to the presence of the power electronics devices and the need for LC filters at inverter output terminal. Finally, inverter serves as a primary requirement for converting DC to AC and thereby injecting it to the grid. The basic system can be represented as shown in Figure 3. 4 [45].

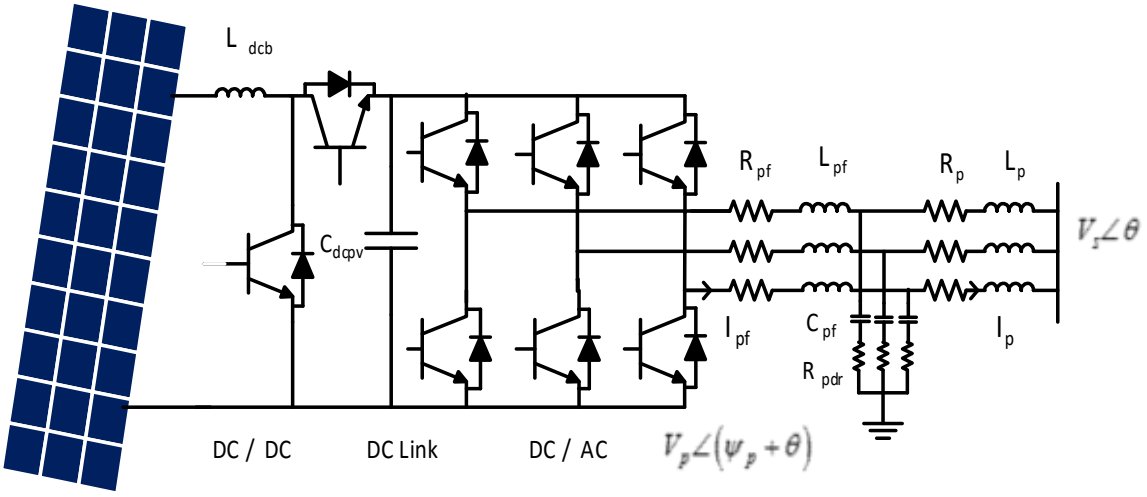

Figure 3. 4 Microgrid connected with PV System

3.1.4.1 Boost Converter DC/DC

A DC converter is designed by a circuitry of power electronics switches such as IGBT, thyristor and storage elements such as inductors and capacitors. The voltage obtained from the PV array is stepped up to a reasonable value before being applied for inversion. Since a lot of DC/DC converter topologies are available in power electronics industry but boost converter and buck converters are widely used. In this research for stepping up the output of PV voltage, the boost converter is utilized. The DC output voltage of boost converter is governed by the duty cycle of the converter, which is defined as the ratio of ON period to the switching period Application of KVL to the boost converter circuit in Figure 3. 5 yields the dynamical relations involved in the converter model.

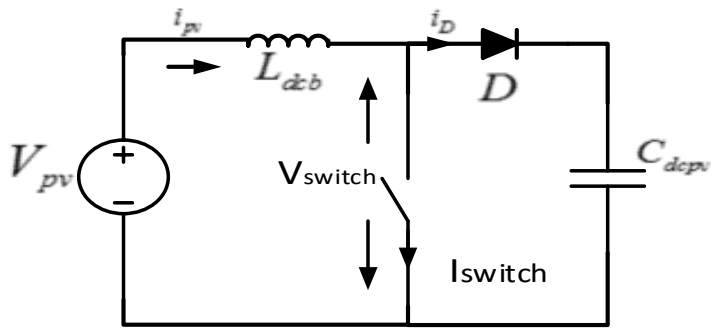

Figure 3. 5 Configuration for DC/DC converter

The differential equation describing the DC boost converter model is obtained as:

$$V_{pv} = L_{dcb}\frac{di_{pv}}{dt} + V_{switch}$$

The voltage obtained across the switch can be written in terms of the converter duty ratio dr_{pv} and output capacitor voltageV_{dcpv} as:

$$V_{switch} = (1 - dr_{pv})V_{dcpv}$$

Incorporation of above two equations transient equation pertaining to DC boost converter can be expressed as:

$$\frac{di_{pv}}{dt} = \frac{1}{L_{dcb}}[V_{pv} - V_{switch}] = V_{pv} - \left(1 - \mathrm{dr_{pv}}\right)V_{dcpv}] \tag{3.14}$$

3.1.4.2 Capacitor DC-link Model

The main purpose of the capacitor DC link of the (PWM) pulse width modulated inverter is to behave as an energy storage element and filter for the DC voltage from boost converter. The DC-link capacitor acts as a connecting link between the DC boost converter and DC/AC inverter. Irrespective of the inverter operation, DC/DC converter regulates the capacitor voltage. By taking KCL at the DC-link node dynamics of DC-link capacitor shall be obtained as.

$$\frac{dV_{dcpv}}{dt} = \frac{1}{C_{dcpv}}(I_{dcin} - I_{dcout}) \tag{3.15}$$

The output current of converter is $\mathrm{I_{dcin}} = \left(1 - \mathrm{dr_{pv}}\right)\mathrm{i_{pv}}$, while the inverter input current $\mathrm{I_{dcout}}$ could be written in terms of output inverter current.

3.1.4.3 Inverter Model (DC/AC)

The purpose of introducing DC/AC inverter is to get a stabilized output AC voltage from PV system. The voltage source inverter (VSI) being modeled through a voltage gain model is used in this research.

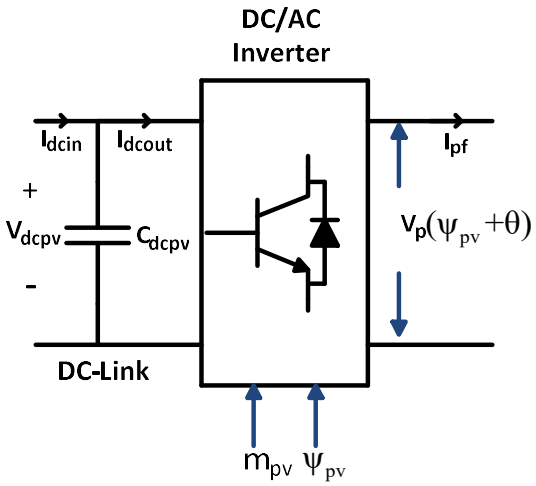

Figure 3. 6 Inverter Model

From the figure the input DC power through the capacitor for the inverter is given by:

$$P_{DC} = V_{dcpv}\mathrm{I}_{\mathrm{dcout}}$$

The instantaneous power output towards AC side of inverter is expressed as:

$$P_{AC} = Re[V_p I_{pf}^*]$$

The above equation can be expressed in d-q terms

$$P_{AC} = V_{pd} i_{pfd} + V_{pq} i_{pfq}$$

For a lossless inverter, both DC and AC power can be equated

$$P_{DC} = P_{AC}$$

$$V_{dcpv} I_{dcout} = V_{pd} i_{pfd} + V_{pq} i_{pfq}$$

Considering the inverter to be operated in the PWM mode, with a modulation index $\mathrm{m_{pv}}$ and phase angle of the inverter ψ_{pv}, an expression can be derived as

$$V_p = m_{pv} * V_{dcpv} \llcorner \psi_{pv}$$

The d-q components of the inverter output voltage are given by

$$V_{pd} = m_{pv} * V_{dcpv} * \cos(\psi_{pv} + \theta)$$

$$V_{pq} = m_{pv} * V_{dcpv} * \sin(\psi_{pv} + \theta)$$

From above to equation we have

$$I_{dc\text{out}} = \left(i_{pfd} m_{pv} \cos(\psi_{pv} + \theta) + i_{pfq} m_{pv} \sin(\psi_{pv} + \theta\right)$$

3.1.4.4 LC Filter and the Coupling Inductance Model

A low pass filter is used in order to attenuate switching frequency ripple of the output voltage of the inverter. The filter comprises a T-section RL circuit which is shunted by a capacitor. High-frequency harmonics are attenuated by inductor block and thus allows only low frequencies to pass, on the other hand, capacitor allows high frequencies and attenuates low frequencies in this way ripples are reduced and block harmonics. Apply KVL around the loop of PV, inverter and filter we get the nonlinear differential equation as:

$$V_p = i_{pf} R_{pf} + L_{pf} \frac{di_{pf}}{dt} + V_{cp} + (i_{pf} - i_p) R_{pdr}$$

Where R_{pf} Corresponds to filter resistance, L_{pf} depicts the filter inductance, V_{cp} is the filter capacitor voltage, and R_{pdr} is the damping resistor. Splitting the above equation in d-q terms:

$$\frac{di_{pfd}}{dt} = \frac{-\omega_0 R_{pf}}{L_{pf}} i_{pfd} + \omega_0 \omega i_{pfq} + \frac{\omega_0 m_{pv} V_{dcpv} \cos(\psi_{Pv} + \theta)}{L_{pf}} - \frac{\omega_0 V_{cpd}}{L_{pf}} - \omega_0 R_{Pdr}\left(i_{pfd} - i_{pd}\right) \quad (3.16)$$

$$\frac{di_{pfq}}{dt} = \frac{-\omega_0 R_{pf}}{L_{pf}} i_{pfq} - \omega_0 \omega i_{pfd} + \frac{\omega_0 m_{pv} V_{dcpv} \sin(\psi_{Pv} + \theta)}{L_{pf}} - \frac{\omega_0 V_{cpq}}{L_{pf}} - \omega_0 R_{Pdr}(i_{pfq} - i_{pq}) \quad (3.17)$$

Writing KVL for the loop formed by the filter capacitor, coupling transmission line, and microgrid bus will produce the dynamic relations pertaining to coupling inductance as:

$$V_{cp} = i_p R_p + L_p \frac{di_p}{dt} + V_s - (i_{pf} - i_p) R_{pdr}$$

In d-q components, the above equation can be expressed as,

$$\frac{di_{pd}}{dt} = \frac{-\omega_0 R_p}{L_p} i_{pd} + \omega_0 \omega i_{pq} + \frac{\omega_0}{L_p}(V_{cpd} - V_{sd}) + \omega_0 R_{Pdr}(i_{pfd} - i_{pd}) \quad (3.18)$$

$$\frac{di_{pq}}{dt} = \frac{-\omega_0 R_p}{L_p} i_{pq} - \omega_0 \omega i_{pd} + \frac{\omega_0}{L_p}(V_{cpq} - V_{sq}) + \omega_0 R_{Pdr}(i_{pfq} - i_{pq}) \quad (3.19)$$

Now for the filter capacitor, the use of KCL produces,

$$C_{pf} \frac{dV_{cp}}{dt} = (i_{pf} - i_p)$$

Expressing the above equation into d-q reference frame, gives two nonlinear ordinary differential equations explaining the dynamics involved with the filter capacitor as,

$$\frac{dV_{cpd}}{dt} = \frac{1}{C_{pf}}(i_{pfd} - i_{pd}) + \omega_0 \omega V_{cpq} \quad (3.20)$$

$$\frac{dV_{cpq}}{dt} = \frac{1}{C_{pf}}(i_{pfq} - i_{pq}) + \omega_0 \omega V_{cpd} \quad (3.21)$$

Thus, the connection of photovoltaic system with the utility grid employs the use of power electronic converters and associated filter circuitry. This can be represented by eight nonlinear ordinary differential equations, each equation denoting a state variable used in the process.

The state variables selected for the PV system when interfaced to the utility grid are,

$$X_{PV} = [i_{pv}, V_{dcpv}, i_{pfd}, i_{pfq}, i_{pd}, i_{pq}, V_{cpd}, V_{cpq}]$$

3.1.5 Wind Energy Model

In the last few decades, there has been extensive research reported in the domain of wind systems. The behavior of wind turbines along with the corresponding power generation devices is very well understood by researchers, and comprehensive models have been developed which depict the performance of wind systems to a larger extent. This section describes the mathematical representation of a permanent magnet synchronous generator (PMSG) which is driven by a wind turbine; the PMSG is connected to PCC via power electronic converter circuits.

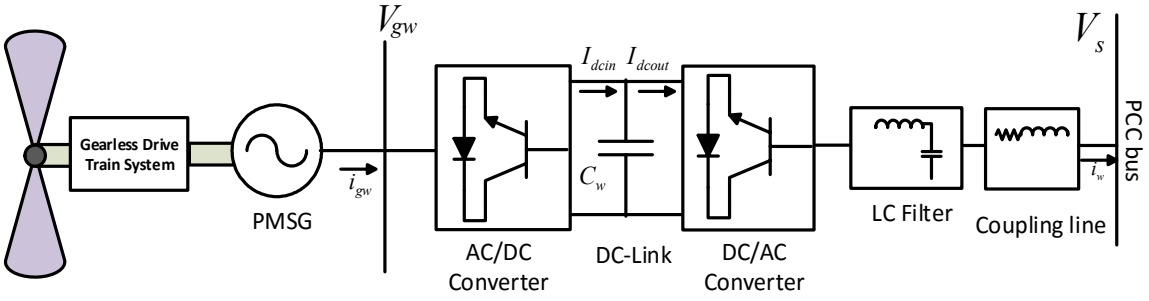

Figure 3. 7 Schematic of variable speed WT-PMSG connected to grid

From the Figure 3. 7 the permanent magnet synchronous generator is driven by a horizontal axis wind turbine by means of the gearless drive train. Permanent magnets mounted on the generator rotor are sufficient enough to generate field excitation to the generator. AC voltage with constant grid frequency can be achieved by means of power electronic converters connected between the stator of PMSG and the grid.

The dynamic model of wind system comprises of a wind turbine, the gearless drive train, the PMSG, transmission line and converter circuits connected at grid side. The IGBT switch, controlled through PWM a method, forming an important component of power electronic converter system, connects directly with the stator of PMSG system and receives an AC power at a variable frequency. Two voltage source converters (VSC) connected as a back-to-back converter system through a DC-link constitutes the power electronic circuitry. Generator side converter acts as a rectifier while the grid side converter acting as an inverter maximizes the power injected into the DC-link. The dynamic model of each of the component involved with the generation system is dealt in the following section.

3.1.6 The wind Turbine Model

Extraction of energy from wind and conversion into mechanical power is the main function of a wind turbine employed in a wind generation system. There are various configurations of a wind turbine being around the globe, and the choice of a particular wind turbine depends on several factors. Wind speed, the turbine rotor size, and the blade area affect the power output of a wind turbine. The cubic relation between the wind speed and the mechanical power output is exciting, as a small increase in speed will amount to a greater increase in the wind power. Owing to economic and technical challenges, there has been a limitation on the size of the wind turbine blades. The amount of power P_m extracted from the wind turbine is related to the wind speed V_w by [46]

$$P_m = \frac{1}{2}\rho\pi R^2 V_w^3 C_P(\beta, \lambda)$$

Here, R is the radius of the rotor blades and C_P is a power coefficient, which is a function of the tip speed ratio λ and the blade pitch angle β. The parameter λ may be

defined as the ratio of linear speed at the tip of the blades to the speed of the wind, given as:

$$\lambda = \frac{\omega_t R}{V_w}$$

The power coefficient C_P being a nonlinear function of the tip speed ratio and blade pitch angle. The drive train system of wind energy conversion system to be used in this study includes a two-mass model as shown in Figure 3. 8. The wind turbine constituting a greater mass having inertia of H_t connects the PMSG rotor with the inertia of H_g. A mechanical shaft with a stiffness coefficient of K_s is used to couple the two masses. The damping coefficients for the turbine and generator are taken as D_t and D_g respectively.

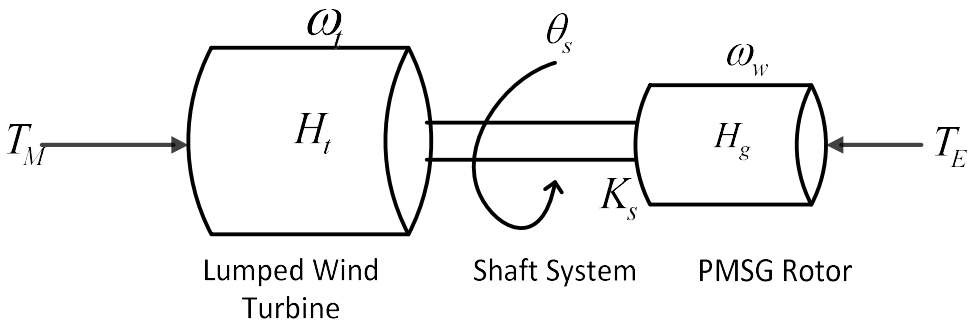

Figure 3. 8 Two mass model of drive train

Four first-order nonlinear ordinary differential equations describe the electromechanical dynamics of the drive train system in terms of the torsional angle θ_s , the turbine speed ω_t, the PMSG rotor angle δ_w and the PMSG rotor speed ω_w as

$$\frac{d\theta_s}{dt} = \omega_0(\omega_t - \omega_w) \tag{3.22}$$

$$\frac{d\omega_t}{dt} = \frac{1}{2H_t}(P_{mw} - K_s\theta_s - D_t(\omega_t - 1)) \tag{3.23}$$

$$\frac{d\delta_w}{dt} = \omega_0(\omega_w - 1) \tag{3.24}$$

$$\frac{d\omega_w}{dt} = \frac{1}{2H_g}\left(K_s\theta_s - P_{ew} - D_g(\omega_w - 1)\right) \tag{3.25}$$

3.1.7 The Variable Speed PMSG Model

The transient nonlinear model of a variable speed permanent magnet synchronous generator (PMSG) will be developed in this section. The voltage-current-flux relationships for a PMSG system can be expressed as,

$$\psi_d = -X_{dw}i_{gd} + X_{afdw}i_{fdw}$$

$$\psi_q = -X_{qw}i_{gwq}$$

$$\psi_{fdw} = -X_{afdw}i_{gd} + X_{ffdwi_{fdw}}$$

$$V_{gwd} = -R_a i_{gd} - \omega_w\psi_q + \frac{1}{\omega_0}\frac{d\psi_d}{dt}$$

$$V_{gwq} = -R_a i_{gq} + \omega_w\psi_d + \frac{1}{\omega_0}\frac{d\psi_q}{dt}$$

Due to the use of permanent magnets in the field circuit of the PMSG machine, the field flux pertaining to the term $X_{afdw}i_{fdw}=\psi_0$ is assumed to be constant. The PMSG system can be assumed as a source of emf e_{gw} driving current to the circuit through its own resistance and reactance. Considering sinusoidal flux distribution, the equivalent circuit for a PMSG can be shown as in

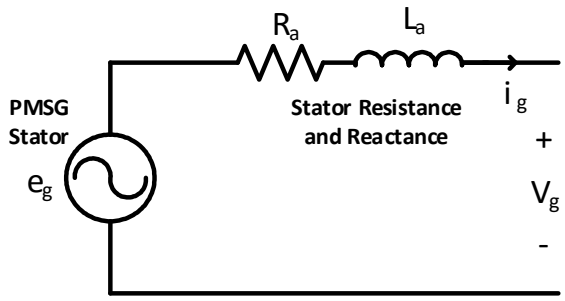

Figure 3. 9 Electrical equivalent circuit of PMSG

Considering the flux produced by the permanent magnets in the field circuit of PMSG to be constant, we can write the voltage relations as,

$$V_{gd} = -R_a i_{gwd} + \omega_w X_{qw} i_{gwq} - \frac{X_{dw}}{\omega_0}\frac{di_{gwd}}{dt} \tag{3.26}$$

$$V_{gq} = -R_a i_{gwq} - \omega_w X_{dw} i_{gwd} + \omega_w \psi_0 - \frac{X_{qw}}{\omega_0}\frac{di_{gwq}}{dt} \tag{3.27}$$

Hence, the dynamical relations for the PMSG system can be finally written as,

$$\frac{di_{gd}}{dt} = \frac{\omega_0}{x_{dw}}[-r_a i_{gd} + \omega_w\, x_{qw} i_{gq} - V_{gd}] \tag{3.28}$$

$$\frac{di_{gq}}{dt} = \frac{\omega_0}{x_{qw}}\left[-r_a i_{gq} - \omega_w x_{dw} i_{gd} + \omega_w E_{fdw} - V_{gq}\right] \tag{3.29}$$

Here, i_{gd} and i_{gq} are the d-q axes PMSG currents, $X_{dw}$and X_{qw} are the stator reactance along d-q axes, E_{fdw} is the field voltage along d-axis, ω_w is the generator rotor speed.

3.1.8 The Wind System Converter Model

In order to feed, the electrical power obtained from the permanent magnet synchronous generator driven by a wind turbine to the utility grid, two back-to-back converters, one on the grid side and the other at the stator side coupled through a common DC-link are

necessary. Due to the use of DC-link capacitor, there exists a decoupling between the two converters and hence separate control algorithms could be employed.

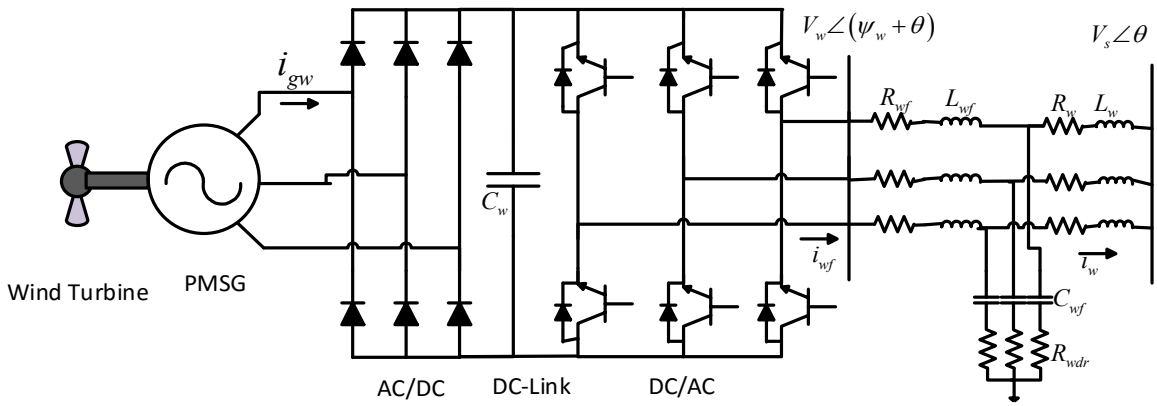

Figure 3. 10 Converter configuration for variable speed PMSG wind system

As shown in Figure 3. ***10***, the rectification operation is obtained through the converter working near the PMSG side while the other converter performs the inversion operation converting the DC voltage obtainable from the output of rectifier into fixed frequency AC voltage. The use of DC-link capacitor provides an intermediate storage, isolating the generator side synchronous system and grid side synchronous system. Keeping the voltage across the DC-link capacitor as constant, the transfer of real power from the generator into the grid can be achieved.

As shown in Figure 3. 10, the stator of PMSG directly feeds power into the rectifier; there exists a relation between the terminal voltage of PMSG and the rectifier output voltage as indicated,

$$V_g = m_{wr} V_{dcw} \angle \alpha_1$$

Here, m_{wr} is the modulation index of the PMSG side converter system, V_{dcw} is the DC-link capacitor voltage and α_1 is the firing angle. Replacing the firing angle with the generator rotor angle using relation $\alpha_1 = 90 - \delta_w$ and decomposing into d-q components will give,

$$V_{gd} = m_{wr} V_{dcw} \sin\delta_w$$

$$V_{gq} = m_{wr} V_{dcw} cos\delta_w$$

The power output from the PMSG system, which is same as the power on the AC side of the rectifier is given by,

$$P_{gw} = V_{gwd} i_{gwd} + V_{gwq} i_{gwq}$$

Now referring to the grid-side converter system, the modulation index m_{wi} and its phase angle ψ_{wi} dictates the output voltage given as,

$$V_w = m_{wi} V_{dcw} \llcorner(\psi_{wi} + \theta)$$

$$V_{wd} = m_{wi} V_{dcw} \cos(\psi_{wi} + \theta)$$

$$V_{wq} = m_{wi} V_{dcw} \sin(\psi_{wi} + \theta)$$

The d-q components of inverter output voltage are V_{wd} and V_{wq} respectively and θ is the phase angle of the microgrid voltage V_s.

The voltage V_w drives a current i_{wf} towards the grid, hence, the power output of the inverter can be written as,

$$P_w = V_{wd} i_{wfd} + V_{wq} i_{wfq}$$

3.1.9 The DC Link Capacitor Model

Application of KCL at the DC-link node will produce the dynamic relation describing the behavior of the DC-link capacitor. It can be seen that the dc power through the capacitor is given as,

$$P_{DC} = V_{dcw} * C_w * \frac{dV_{dcw}}{dt}$$

Assuming the capacitor to be lossless the net power change will be $P_g - P_w$, hence

$$V_{dcw} C_w \frac{dV_{dcw}}{dt} = P_g - P_w$$

Finally, the transient of the DC-link voltage can be written as,

$$\frac{dV_{dcw}}{dt} = \frac{1}{C_w}[m_{wr}\sin\delta_w i_{gd} + \cos\delta_w i_{gq} - m_{wi}\cos(\psi_{wi} + \theta)\, i_{wd} - m_{wi}\sin(\psi_{wi} + \theta) i_{wq}] \quad (3.30)$$

3.1.10 The LC Filter and Coupling Transmission Line Model

The purpose of filtering circuit in the PMSG system is to attenuate the harmonics encountered in the output current of the inverter before being fed to the utility grid. An LC filter is employed in order to achieve the smoothening of output current. The dynamic relations would be derived by applying KVL and KCL to the filter section shown in Figure 3. 10. Consider the filter circuit to be included with a resistance of R_{wf}, an inductance of L_{wf} and a damping rheostat R_{wdr}, the voltage equation can be written as,

$$V_w = i_{wf} R_{wf} + L_{wf} \frac{di_{wf}}{dt} + V_{cw} + (i_{wf} - i_w) R_{wdr}$$

Similar to the dynamical equations obtained for PV system, the splitting of above equation will produce two nonlinear differential equations describing the dynamics of the filter inductance as given by,

$$\frac{di_{wfd}}{dt} = \frac{-\omega_0 R_{wf}}{L_{pf}} i_{wfd} - \frac{\omega_0 V_{0wd}}{L_{wf}} - \omega_0 R_{wdr}\left(i_{wfd} - i_{wd}\right) + \omega_0 \omega i_{wfq} + \frac{\omega_0 m_{wi} V_{dcw} \cos(\psi_{wi} + \theta)}{L_{wf}} \tag{3.31}$$

$$\frac{di_{wfq}}{dt} = \frac{-\omega_0 R_{wf}}{L_{pf}} i_{wfq} - \frac{\omega_0 V_{0wq}}{L_{wf}} - \omega_0 R_{wdr}\left(i_{wfq} - i_{wq}\right) - \omega_0 \omega i_{wfd} + \frac{\omega_0 m_{wi} V_{dcw} \sin(\psi_{wi} + \theta)}{L_{wf}} \tag{3.32}$$

Now applying KVL to the loop formed by the filter capacitor and the coupling line will produce the following equations,

$$V_{cw} = i_w R_w + L_w \frac{di_w}{dt} + V_s - \left(i_{wf} - i_w\right) R_{wdr}$$

Thus, the d-q components of the coupling line current can be expressed by nonlinear differential equations of the first order as

$$\frac{di_{wd}}{dt} = \frac{-\omega_0 R_w}{L_w} i_{wd} + \omega_0 \omega i_{wq} + \frac{\omega_0}{L_w}\left(V_{owd} - V_{sd}\right) + \omega_0 R_{wdr}\left(i_{wfd} - i_{wd}\right) \tag{3.33}$$

$$\frac{di_{wq}}{dt} = \frac{-\omega_0 R_w}{L_w} i_{wq} - \omega_0 \omega i_{wd} + \frac{\omega_0}{L_w}\left(V_{owq} - V_{sq}\right) + \omega_0 R_{wdr}\left(i_{wfq} - i_{wq}\right) \tag{3.34}$$

To obtain the dynamics of the filter capacitor C_{wf} we write KCL at the node producing the following,

$$C_{wf} \frac{dV_{cw}}{dt} = \left(i_{wf} - i_w\right)$$

$$\frac{dV_{cwd}}{dt} = \frac{1}{C_{wf}}\left(i_{wfd} - i_{wd}\right) + \omega_0 \omega V_{cwq} \tag{3.35}$$

$$\frac{dV_{cwq}}{dt} = \frac{1}{C_{wf}}\left(i_{wfq} - i_{wq}\right) - \omega_0 \omega V_{cwd} \tag{3.36}$$

The state variables chosen for the wind system are expressed as,

$$X_{wind} = [\theta_s, \omega_t, \delta_w, \omega_w, i_{gwd}, i_{gwq}, V_{dcw}, i_{wfd}, i_{wfq}, i_{wd}, i_{wq}, V_{cwd}, V_{cwq}]$$

3.2 Controller Model

STATCOM with an energy capacitor storage unit is used for supervisory control. In this work an energy storage capacitor is interfaced by means of STATCOM along with DC- DC buck-boost converter. Duty ratio can be varied through S_1, Charging and discharging of capacitor module is regulated by S_2, in this manner, the operation of the buck-boost converter is controlled. The configuration of the source voltage controller (STATCOM) is shown in Figure 3. 11. By varying the modulation index (m_{st}) of VSC STATCOM will compensate for reactive power unbalance in the system, while the variation of the phase angle (ψ_{st}) caters in providing real power supplement as demanded. As a result, it has the ability to serve for active and reactive power need for the system.

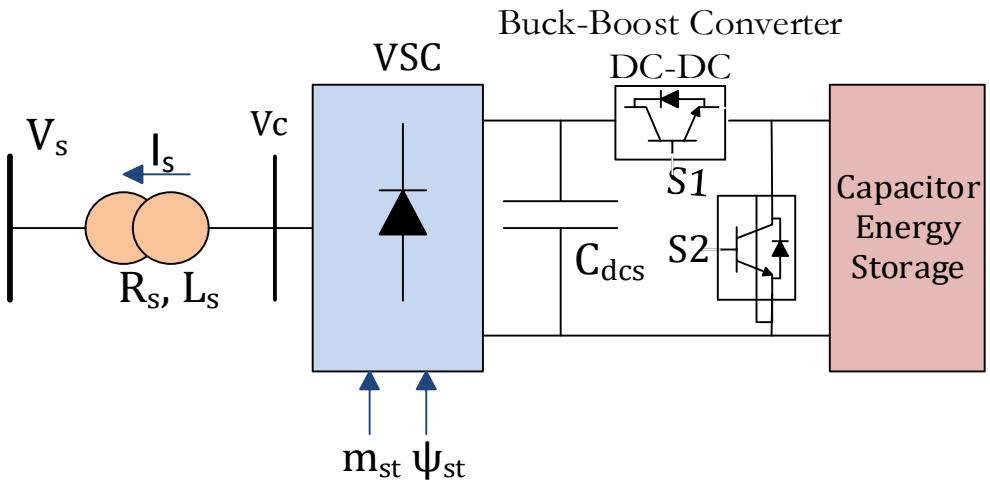

Figure 3. 11 Configuration for STATCOM Controller

At the output node of STATCOM, apply KCL to get

$$L_s \frac{di_s}{dt} + R_s i_s = V_c - V_s$$

Here, R_s and L_s are the impedances of STATCOM, where V_c and I_S are output voltage and current of STATCOM.

$$V_c = m_{st} V_{dcs}(\psi_{st} + \theta)$$

Expressing the equation for V_c in d-q frame:

$$V_{cd} = m_{st} V_{dcs}\ Cos(\psi_{st} + \theta)$$

$$V_{cq} = m_{st} V_{dcs}\ Sin(\psi_{st} + \theta)$$

The dynamic relationships of the current and dc capacitor voltage of the STATCOM are:

$$\frac{di_{sd}}{dt} = -\frac{\omega_o R_s}{L_s} i_{sd} + \omega_o \omega i_{sq} + \frac{\omega_o m_{st} \cos(\psi_{st} + \theta)}{L_s} - \frac{\omega_o V_{sd}}{L_s} \quad (3.37)$$

$$\frac{di_{sq}}{dt} = -\frac{\omega_o R_s}{L_s} i_{sq} - \omega_o \omega i_{sd} + \frac{\omega_o m_{st} \sin(\psi_{st} + \theta)}{L_s} - \frac{\omega_o V_{sq}}{L_s} \quad (3.38)$$

By taking KCL at DC-link, we get, where C_{dcs} is STATCOM capacitor, i_{dcs} is input current to the inverter and V_{dcs} is DC-link voltage.

$$C_{dcs}\frac{dV_{dcs}}{dt} = -i_{dcs} + i_{dsc}$$

Finally, we can get capacitor current i_{dcs} as,

$$i_{dcs} = i_{sd}m_{st}\cos(\psi_{st} + \theta) + i_{sq}m_{st}\,sin(\psi_{st} + \theta)$$

From energy balance, the DC-link capacitor voltage equation can be written as,

$$\frac{dV_{dcs}}{dt} = \frac{-1}{C_{dcs}}\left(i_{sd}m_{st}\cos\psi_{st} + i_{sq}m_{st}\sin\psi_{st}\right) + \frac{I_{dcs}}{C_{dcs}} \tag{3.39}$$

The state vector for STATCOM model is given as

$$X = [i_{sd}, i_{sq}, V_{dcs}]$$

$$U = [m_{st}, \psi_{st}]$$

3.3 Linear Model of Microgrid

This section is focused on getting a small signal model for individual as well as grid connected DG's. As designing a controller for a nonlinear system is going to be a tedious task, we first get a small signal model of the microgrid. After the linear model is developed one can determine the frequency response of the system and also perform Eigenvalue analysis in order to design a controller. Then the controller can be designed and implemented on the system.

3.3.1 Small Signal Model of Micro-Alternator

The nonlinear model of a micro-alternator corresponds to 4th order system. A linearized model is obtained by linearizing the nonlinear differential equation about an operating point we get

$$\frac{d\Delta\dot{\delta}}{dt} = \omega_0 \Delta\omega \tag{3.40}$$

$$\frac{d\Delta\dot{\omega}}{dt} = \frac{1}{2H}\{-\Delta P_e - D\Delta\omega\} \tag{3.41}$$

$$\frac{d\Delta\dot{e_q^{'}}}{dt} = \frac{1}{T_{do}^{'}}\left[\Delta E_{fd} - \Delta e_q^{'} - (X_d - X_d^{'})\Delta i_{td}\right] \tag{3.42}$$

$$\frac{d\Delta\dot{E}_{fd}}{dt} = \frac{-K_A}{T_A}\Delta V_t - \frac{1}{T_E}\Delta E_{fd} \tag{3.43}$$

Electrical current output of the generator is obtained as,

$$\Delta i_t = \Delta i_{td} + j\Delta i_{tq}$$

Generator output current along d axis q axis are expressed as

$$\Delta i_{td} = \frac{-R_t}{{R_t}^2 + X_1 X_2}\Delta V_{sd} + \frac{X_2}{{R_t}^2 + X_1 X_2}(\Delta {e_q}' - \Delta V_{sq})$$

$$\Delta i_{tq} = \frac{\Delta V_{sd}}{X_1} + \frac{R_t}{X_d' + X_t}(\Delta {e_q}' - \Delta V_{sq})$$

The terminal voltage expressed in terms of the above currents as below

$$V_t^2 = V_{td}^2 + V_{tq}^2$$

$$\Delta V_t = \frac{V_{td0}}{V_{t0}}\left(X_q \Delta i_{tq}\right) + \frac{V_{tq}}{V_{t0}}\left(\Delta e_q^{'} - X_d^{'}\Delta i_{td}\right) \tag{3.44}$$

At last micro-alternator power output can be written as

$$P_e = \left(e_q{}'i_{tq}\right) + \left(X_q - X_d{}'\right)i_{td}i_{tq}$$

$$\Delta P_e = e_{qo}{}'\Delta i_{tq} + i_{tq0}\Delta e_q{}' + \left(X_q - X_d{}'\right)\left[i_{td0}\Delta i_{tq} + i_{tq0}\Delta i_{td}\right] \quad (3.45)$$

Substituting $\Delta P_e, \Delta \mathrm{i_{tq}}, \Delta \mathrm{i_{td}}$ linearized model of generator state equation to get state variables in terms of $\Delta \mathrm{V_{sd}}$ and $\Delta \mathrm{V_{sq}}$.

3.3.2 Small-Signal Model of Photovoltaic System

Small signal perturbed model is obtained from the nonlinear model taken at an operating point.

$$\frac{\mathrm{d}\Delta v_{pv}}{\mathrm{dt}} = -N_s\left[\frac{nv_T}{N_{prll}I_{photo} - i_{pv0} + N_{prll}I_s} + \frac{R_s}{N_{prll}}\right]\Delta i_{pv}$$

Each of the components involved in the power conditioning unit of the PV system such as the DC-boost converter, the DC-link capacitor, the DC/AC inverter, the LC output filter and coupling transmission line when linearized around an operating point will give the complete small-signal model. For the DC-boost converter relation, the perturbed relation is given as,

$$\frac{d\Delta i_{pv}}{dt} = \frac{1}{L_{dc}}\left[\Delta V_{pv} - \left(1 - d_{rpv}\right)\Delta V_{dcpv}\right] \quad (3.46)$$

For the DC-link capacitor dynamic voltage equation described in perturbation would give the following

$$\begin{aligned}\frac{d\Delta \dot{V}_{dcpv}}{dt} = \frac{-1}{C_{dcpv}}[&-i_{pfd0}m_{pv}\,sin\left(\psi_{pv} + \theta\right)\Delta\psi_{pv} + m_{pv}cos\left(\psi_{pv} + \theta\right)\Delta i_{pfd} \\ &+ i_{pfd0}\,cos\left(\psi_{pv} + \theta\right)\Delta m_{pv} + \; i_{pfq0}m_{pv}\,cos\left(\psi_{pv} + \theta\right)\Delta\psi_{pv} + \\ &m_{pv}sin\left(\psi_{pv} + \theta\right)\Delta i_{pfq} + i_{pfq0}\,sin\left(\psi_{pv} + \theta\right)\Delta m_{pv} - \left(1 - d_{rpv}\right)\Delta i_{pv}\end{aligned} \quad (3.47)$$

The LC filter output current Δi_{pfd} and Δi_{pfq}along d-q axis is given by

$$\frac{d\Delta i_{pfd}}{dt} = \frac{-\omega_0 R_{pf}}{L_{pf}}\Delta i_{pfd} + \omega_0\left(\Delta i_{pfq} + i_{pfq0}\Delta\omega\right) - \frac{\omega_0 \Delta V_{cpd}}{L_{pf}} +$$

$$\frac{\omega_0}{L_{pf}}\left[m_{pv}\cos\left(\psi_{pv}+\theta\right)\Delta V_{dcpv} - m_{pv}V_{dcpv0}\sin\left(\psi_{pv}+\theta\right)\Delta\psi_{pv} +\right.$$

$$\left. V_{dcp0}\cos\left(\psi_{pv}+\theta\right)\Delta m_{pv}\right] - \frac{\omega_0 R_{pdr}}{L_{pf}}\left(\Delta i_{pfd} - \Delta i_{pd}\right) \tag{3.48}$$

$$\frac{d\Delta i_{pfq}}{dt} = \frac{-\omega_0 R_{pf}}{L_{pf}}\Delta i_{pfq} - \omega_0\left(\Delta i_{pfd} + i_{pfd0}\Delta\omega\right) - \frac{\omega_0 \Delta V_{cpq}}{L_{pf}} +$$

$$\frac{\omega_0 \Delta V_{cpq}}{L_{pf}} + \frac{\omega_0}{L_{pf}}\left[m_{pv}\sin\left(\psi_{pv}+\theta\right)\Delta V_{dcpv} + m_{pv}V_{dcpv0}\cos\left(\psi_{pv}+\theta\right)\Delta\psi_{pv}\right.$$

$$\left. +V_{dcp0}\sin\left(\psi_{pv}+\theta\right)\Delta m_{pv}\right] - \frac{\omega_0 R_{pdr}}{L_{pf}}\left(\Delta i_{pfq} - \Delta i_{pq}\right) \tag{3.49}$$

The d-q components of the current linearized output through the coupling inductance is obtained by perturbing the equations as,

$$\frac{d\Delta i_{pd}}{dt} = \frac{-\omega_0 R_p}{L_p}\Delta i_{pd} + \omega_0\left(\Delta i_{pq} + i_{pq0}\Delta\omega\right) + \frac{\omega_0}{L_p}\left(\Delta V_{cpd} - \Delta V_{sd}\right) + \frac{\omega_0 R_{pdr}}{L_p}\left(\Delta i_{pfd} - \Delta i_{pd}\right) \tag{3.50}$$

$$\frac{d\Delta i_{pq}}{dt} = \frac{-\omega_0 R_p}{L_p}\Delta i_{pq} + \omega_0\left(\Delta i_{pd} + i_{pd0}\Delta\omega\right) + \frac{\omega_0}{L_p}\left(\Delta V_{cpq} - \Delta V_{sq}\right) + \frac{\omega_0 R_{pdr}}{L_p}\left(\Delta i_{pfq} - \Delta i_{pq}\right) \tag{3.51}$$

Dynamic relation for the voltage across filter capacitance is given by

$$\frac{d\Delta V_{cpd}}{dt} = \omega_0\left(\Delta V_{cpq} + V_{cpq0}\Delta\omega\right) + \frac{\omega_0}{C_{pf}}\left(\Delta i_{pfd} - \Delta i_{pd}\right) \tag{3.52}$$

$$\frac{d\Delta V_{cpq}}{dt} = -\omega_0\left(\Delta V_{cpd} + V_{cpd0}\Delta\omega\right) + \frac{\omega_0}{C_{pf}}\left(\Delta i_{pfq} - \Delta i_{pq}\right) \tag{3.53}$$

Thus, the linearized small-signal state space vector for the PV generation unit consists of the following,

$$\Delta X_{PV} = \left[\Delta i_{pv}, \Delta V_{dcpv}, \Delta i_{pfd}, \Delta i_{pfq}, \Delta i_{pd}, \Delta i_{pq}, \Delta V_{cpd}, \Delta V_{cpq}\right]$$

3.4 Composite Model of Microgrid

In this section, a composite configuration of a microgrid is modeled. At first micro-alternator and STATCOM are considered as a first system, later micro-alternator along with STATCOM and PV system is considered as a second system and further model for micro-alternator with STATCOM and wind system is modeled. All the system were connected to grid as well as Load. The non-linear model is obtained and is perturbed around an operating point to get the small perturbed model. Once the perturbed model is obtained, then a necessary control can be applied to make the system stable.

3.4.1 Micro-Alternator and STATCOM Model

Figure 3. 12 shows a microgrid system with a combination of micro-alternator and STATCOM integrated with a load connected to the utility grid. Where the point of common coupling or a common bus is termed as V_s. In earlier sections detail modeling of individual DG sources is expressed. The overall model for this setup can be seen by taking KCL at a common bus terminal.

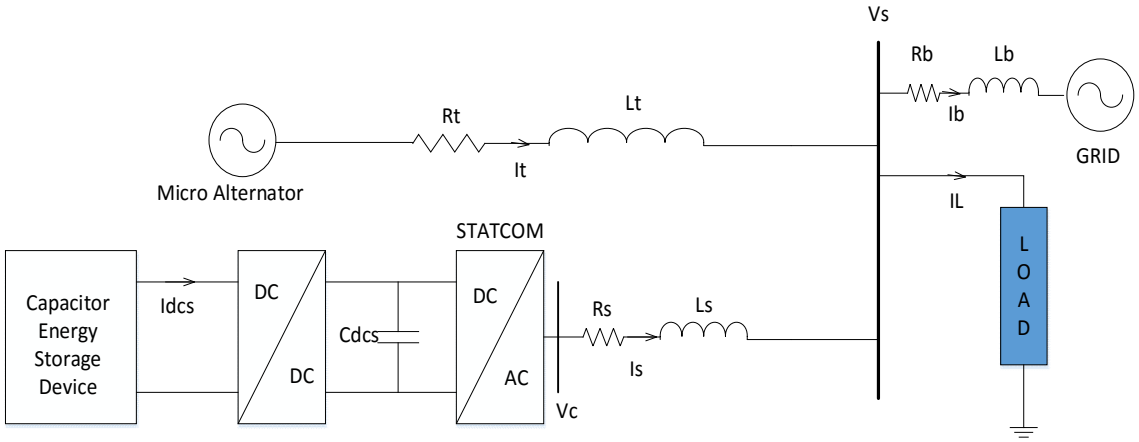

Figure 3. 12 Micro-alternator and STATCOM

The KCL at node V_s is given as

$$i_t + i_s = i_b + i_L$$

Where i_t , i_s , i_b , i_L are output currents of micro alternator, STATCOM , power grid and load current respectively.

Taking d-q components for above equation gives the following equations

$$i_{td} + i_{sd} = i_{bd} + i_{Ld}$$

$$i_{tq} + i_{sq} = i_{bq} + i_{Lq}$$

Now there is a need to express these currents as a function of V_{sd} and V_{sq}.

Load Current:

Let us consider load as admittance, $Y = g - j\ b$

Load current can be written as $I_L = V_s\ Y$

$$i_{Ld} + j\ i_{Lq} = \left(V_{sd} + j\ V_{sq}\right) * (g - j\ b)$$

Separating imaginary and real parts we get

$$i_{Ld} = g\ V_{sd} + b\ V_{sq}$$

$$i_{Lq} = g\ V_{sq} + b\ V_{sd}$$

Grid Current:

From the Figure 3. 12 , the grid current is expressed as

$$i_b = \frac{V_s - V_b}{R_b + jX_b}$$

$$i_{bd} + ji_{bq} = \frac{V_{sd} + jV_{sq} - (V_b sin\delta + jV_b cos\delta)}{R_b + jX_b}$$

Now equating the real and imaginary parts in the above equation, the d-q current components are obtained as shown,

$$i_{bd} = \frac{(V_{sq} - V_b sin\delta)R_b + (V_{sq} - V_b cos\delta)X_b}{{R_b}^2 + {X_b}^2}$$

$$i_{bq} = \frac{(V_{sq} - V_b cos\delta)R_b + (V_{sq} - V_b sin\delta)X_b}{{R_b}^2 + {X_b}^2}$$

On substituting grid currents and load currents in the KCL equation obtained above it is possible to get V_{sd} and V_{sq} in terms of state variables.

$$V_{sq} = D(i_{sd}) + E{e_q}' + \mathrm{F}\,(i_{sq}) + GV_b \tag{3.54}$$

$$V_{sd} = \frac{1}{A}[Z_b Z_1(i_{sd}) + Z_b X_2 {e_q}' + V_b Z_1(R_b \sin\delta + X_b \cos\delta) - \mathrm{B}V_{sq}] \tag{3.55}$$

By substituting V_{sd} and V_{sq} in the nonlinear differential equation of the components model we get the closed form as

$$\frac{dX}{dt} = f(X, u) \tag{3.56}$$

Where state vector is given as

$$X = \left[\delta, \omega, e_q', E_{fd}, i_{sd}, i_{sq}, V_{dcs}\right]^T$$

$$U = [m_{st}, \psi_{st}]$$

3.4.2 Linearized Model of Micro-Alternator and STATCOM

Repeating the same procedure for evolving linearized component of the DG's connected to the grid. As the previous sections have given us small signal model hence there is only need of V_s in terms of state variables. The following are d-q components of bus voltage.

$$\Delta V_{sq} = D(\Delta i_{sd}) + E\Delta {e_q}' + \mathrm{F}\,(\Delta i_{sq}) + G_1 \Delta\delta$$

$$\Delta V_{sd} = [\mathrm{A}_1(\Delta i_{sd}) + B_1(\Delta i_{sq}) + C_1 \Delta {e_q}' + \mathrm{D}_1 \Delta\delta]$$

By substituting V_{sd} and V_{sq} in the linear differential equation of the components model we get the non-linear closed form as

$$[\Delta \dot{X}_{GS}] = [A_{gen-stat}]_{7X7}[\Delta X_{GS}] + [B_{st}]_{7X2}[\Delta U_{st}]$$

$$\Delta X = \left[\Delta\delta, \Delta\omega, \Delta e'_q, \Delta E_{fd}, \Delta i_{sd}, \Delta i_{sq}, \Delta V_{dcs}\right]^T$$

The state matrix for this linear matrix is given by $A_{gen-stat}$

$$A_{gen-stat} = \begin{bmatrix} \left(A_{GG}\right)_{4x4} & \left(A_{GS}\right)_{4x3} \\ \left(A_{SG}\right)_{3x4} & \left(A_{SS}\right)_{3x3} \end{bmatrix}_{7x7} \qquad \Delta U = \left[\Delta m_{st}, \Delta \psi_{st}\right]$$

The sub-matrix A_{GG} represents system matrix of only micro-alternator while A_{SS} represents system matrix for STATCOM

$$A_{GG} = \begin{bmatrix} 0 & \omega_0 & 0 & 0 \\ P_{e4} & 0 & P_{e3} & 0 \\ E_{q4} & 0 & Eq3 & E_{q5} \\ V_{t4} & 0 & V_{t3} & \dfrac{-1}{T_A} \end{bmatrix} \qquad A_{SS} = \begin{bmatrix} S_{d5} & S_{d6} & S_{d7} \\ S_{q5} & S_{q6} & S_{q7} \\ S_{V5} & S_{V6} & 0 \end{bmatrix}$$

The other sub-matrices can be written as

$$A_{GS} = \begin{bmatrix} 0 & 0 & 0 \\ P_{e2} & P_{e2} & 0 \\ E_{q1} & E_{q2} & 0 \\ V_{t1} & V_{t2} & 0 \end{bmatrix} \qquad A_{SG} = \begin{bmatrix} S_{d1} & S_{d2} & S_{d3} & 0 \\ S_{q1} & S_{q2} & S_{q3} & 0 \\ 0 & 0 & 0 & 0 \end{bmatrix} \qquad B = \begin{bmatrix} 0 & 0 \\ 0 & 0 \\ 0 & 0 \\ 0 & 0 \\ B_{5a} & B_{5b} \\ B_{6a} & B_{6b} \\ B_{7a} & B_{7b} \end{bmatrix}$$

3.4.3 Micro-Alternator, STATCOM and PV Model

Figure 3. 13 shows a microgrid system with a combination of micro-alternator, STATCOM and PV system integrated with a load connected to the utility grid. Where the point of common coupling or a common bus is termed asV_s. In earlier sections detail modeling of individual DG sources is expressed. The overall model for this setup can be realized by taking KCL at a common bus terminal.

The KCL at node V_s is given as

$$i_t + i_s + i_p = i_b + i_L$$

Where i_t , i_s , i_b , i_L i_p are output currents of micro alternator, STATCOM , power grid, load and PV system current respectively.

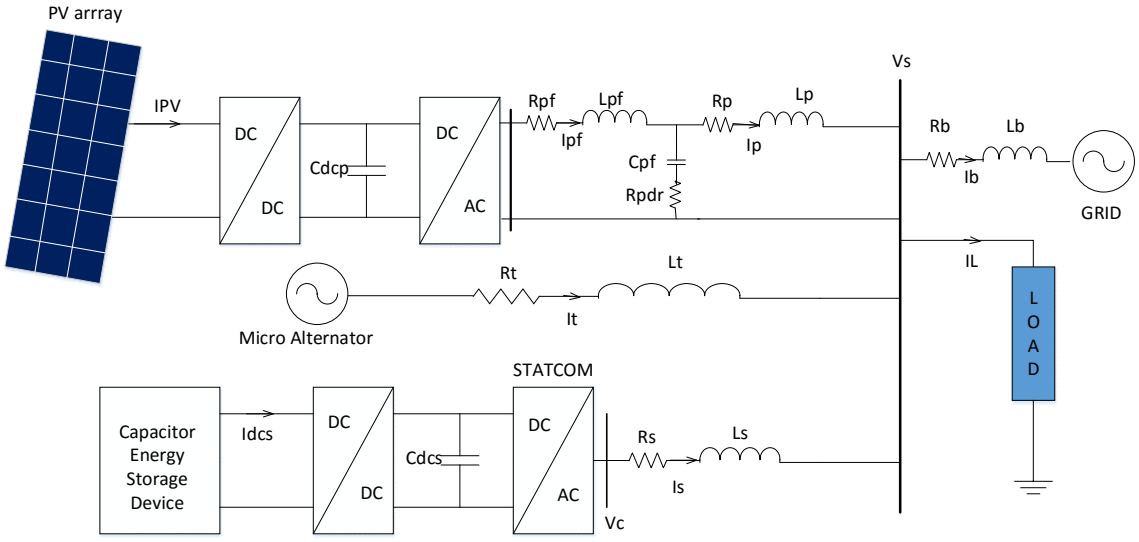

Figure 3. 13 Composite model of generator, STATCOM and PV

Taking d-q components for above equation gives the following equations

$$i_{td} + i_{sd} + i_{pd} = i_{bd} + i_{Ld}$$

$$i_{tq} + i_{sq} + i_{pq} = i_{bq} + i_{Lq}$$

Now there is a need to express these currents as a function of V_{sd} and V_{sq}. Recalling grid currents and load currents from previous section, it is possible to get bus voltage $V_s$in terms of state variables.

On substituting grid currents and load currents in the KCL equation obtained above we are able to get V_{sd} and V_{sq} in terms of state variables.

$$V_{sq} = D\left(i_{sd} + i_{pd}\right) + Ee_q{}' + \text{F}\,(i_{sq} + i\_pd\,) + \; + GV_b \tag{3.57}$$

$$V_{sd} = [Z_b Z_1(i_{sd}) + Z_b X_2 e_q{}' + V_b Z_1(R_b \sin\delta + X_b \cos\delta) - \text{B}V_{sq}] \tag{3.58}$$

By substituting V_{sd} and V_{sq} in the nonlinear differential equation of the components model we get the closed form as

$$\frac{dX}{dt} = f(X, u) \tag{3.59}$$

The state vector for this system is given as

$$X = \left[\delta, \omega, e_q', E_{fd}, i_{sd}, i_{sq}, V_{dcs}, i_{pv}\,, V_{dcp}, I_{pfd}, I_{pfq}\,, I_{pd}\,, I_{pq}\,, V_{opd}\,, V_{opq}\right]^T$$

$$U = \left[m_{st}, \psi_{st}, m_{pv}, \psi_{pv}\right]$$

These variables m_{st}, ψ_{st} are modulation index and phase angle for inverter connect near STATCOM, similarly m_{pv}, ψ_{pv} are modulation index and phase angle for inverter connect near PV system.

3.4.4 Linearized Model of Micro-Alternator, STATCOM and PV System

Repeating the same procedure for evolving linearized component of the DG's connected to the grid. As the previous sections have given us small signal model hence there is only need of V_s in terms of state variables. The following are d-q components of bus voltage.

$$\Delta V_{sq} = D\left(\Delta i_{sd} + i_{pd}\right) + E\Delta e_q{}' + \text{F}\,(\Delta i_{sq}\_i_{pq}) + G_1\Delta\delta$$

$$\Delta V_{sd} = [\mathrm{A}_1(\Delta i_{sd} + i_{pd}) + B_1(\Delta i_{sq} + i_{pq}) + C_1 \Delta e_q{}' + \mathrm{D}_1 \Delta\delta$$

By substituting V_{sd} and V_{sq} in the linear differential equation of the components model we get the non-linear closed form as

$$[\Delta \dot{X}_{GSP}] = [A_{gen-stat-P}\ ]_{15X1}\ [\Delta X_{GSP}] + [B_{stPv}]_{15X4}[\Delta U_{st}, \Delta U_{pv}]$$

$$\Delta X = [\Delta X_G, \Delta X_S, \Delta X_P]^T$$

State elements for micro-alternator is ΔX_G, while state elements for STATCOM is ΔX_S and State elements for PV system given by ΔX_P

$$\Delta X_G = [\Delta\delta, \Delta\omega, \Delta e'_q, \Delta E_{fd}] \qquad \Delta X_S = [\Delta i_{sd}, \Delta i_{sq}, \Delta V_{dcs}]$$

$$\Delta X_P = [\Delta i_{pv}\ , \Delta V_{dcp}, \Delta I_{pfd}, \Delta I_{pfq}\ , \Delta I_{pd}\ , \Delta I_{pq}\ , \Delta V_{opd}\ , \Delta V_{opq}]$$

The state matrix for this linear matrix is given by $A_{gen-stat-PV}$

$$A_{gen-stat-pv} = \begin{bmatrix} (A_{GG})_{4x4} & (A_{GS})_{4x3} & (A_{GP})_{4x8} \\ (A_{SG})_{3x4} & (A_{SS})_{3x3} & (A_{SP})_{3x8} \\ (A_{PG})_{8x4} & (A_{PS})_{8x3} & (A_{PP})_{8x8} \end{bmatrix}_{15x15}$$

$$A_{GP} = \begin{bmatrix} 0 & 0 & 0 & 0 & 0 & 0 & 0 & 0 \\ 0 & 0 & P_{e1} & P_{e2} & 0 & 0 & 0 & 0 \\ 0 & 0 & E_{q1} & E_{q2} & 0 & 0 & 0 & 0 \\ 0 & 0 & V_{t1} & V_{t2} & 0 & 0 & 0 & 0 \end{bmatrix} \quad A_{GP} = \begin{bmatrix} 0 & 0 & S_{d9} & S_{d10} & 0 & 0 & 0 & 0 \\ 0 & 0 & S_{q9} & S_{q10} & 0 & 0 & 0 & 0 \\ 0 & 0 & 0 & 0 & 0 & 0 & 0 & 0 \end{bmatrix}$$

$$A_{PG} = \begin{bmatrix} 0 & \omega_0 i_{pfq0} & 0 & 0 \\ 0 & -\omega_0 i_{pfd0} & 0 & 0 \\ -k_p D_1 & \omega_0 i_{pq0} & -k_p C_1 & 0 \\ -k_p G & -\omega_0 i_{pd0} & -k_p E & 0 \\ 0 & \omega_0 V_{cpq0} & 0 & 0 \\ 0 & -\omega_0 V_{cpd0} & 0 & 0 \\ 0 & 0 & 0 & 0 \\ 0 & 0 & 0 & 0 \end{bmatrix} \qquad A_{GP} = \begin{bmatrix} 0 & 0 & 0 \\ 0 & 0 & 0 \\ K_{9a} & K_{9b} & 0 \\ K_{10a} & K_{10b} & 0 \\ 0 & 0 & 0 \\ 0 & 0 & 0 \\ 0 & 0 & 0 \\ 0 & 0 & 0 \end{bmatrix}$$

$$A_{PP}=\begin{bmatrix} -K_{pf}R_{eq} & \omega_0 & K_{pf}R_d & 0 & -K_{pf} & 0 & 0 & K_{pf1} \\ -\omega_0 & -K_{pf}R_{eq} & 0 & K_{pf}R_d & 0 & -K_{pf} & 0 & K_{pf2} \\ K_pR_d & 0 & K_{9c} & \omega_0+K_{9b} & K_p & 0 & 0 & 0 \\ 0 & K_pR_d & -\omega_0+K_{10a} & K_{10c} & 0 & K_p & 0 & 0 \\ \frac{\omega_0}{C_{pf}} & 0 & -\frac{\omega_0}{C_{pf}} & 0 & 0 & \omega_0 & 0 & 0 \\ 0 & \frac{\omega_0}{C_{pf}} & 0 & -\frac{\omega_0}{C_{pf}} & -\omega_0 & 0 & 0 & 0 \\ 0 & 0 & 0 & 0 & 0 & 0 & \frac{ap}{L_{dc}} & K_{pv1} \\ K_{pd1}m_p & K_{pd2}m_p & 0 & 0 & 0 & 0 & K_{pv2} & 0 \end{bmatrix}$$

The state matrices for only generator and STATCOM A_{GG}, A_{SS}, A_{GS} and A_{SG} are expressed in earlier section. The Control matrix B_{stpv} obtained as

$$B_{stpv}=\begin{bmatrix} (0)_{4x1} & (0)_{4x1} & (0)_{4x1} & (0)_{4x1} \\ B_{5a} & B_{5b} & 0 & 0 \\ B_{6a} & B_{6b} & 0 & 0 \\ B_{7a} & B_{7b} & 0 & 0 \\ 0 & 0 & B_{8a} & B_{8b} \\ 0 & 0 & B_{9a} & B_{9b} \\ (0)_{5x1} & (0)_{5x1} & (0)_{5x1} & (0)_{5x1} \\ 0 & 0 & B_{15a} & B_{15b} \end{bmatrix}$$

3.4.5 Micro-Alternator, STATCOM and Wind Energy Model

Figure 3. 14 shows a microgrid system with a combination of micro-alternator, STATCOM and PV system integrated with a load connected to the utility grid. Where the point of common coupling or a common bus is termed asV_s. In earlier sections detail modeling of

individual DG sources is expressed. The overall model for this setup can be realized by taking KCL at a common bus terminal.

The KCL at node V_s is given as

$$i_t + i_s + i_w = i_b + i_L$$

Where i_t , i_s , i_b , i_L i_w are output currents of micro alternator, STATCOM , power grid, load and wind energy system current respectively.

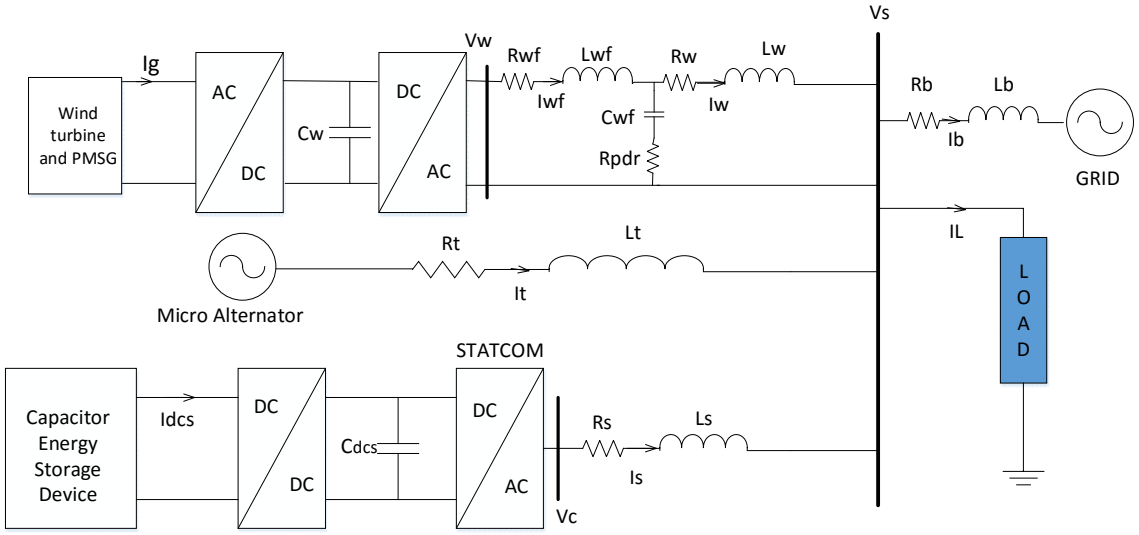

Figure 3. 14 Composite model of generator, STATCOM and Wind

Taking d-q components for above equation gives the following equations

$$i_{td} + i_{sd} + i_{wd} = i_{bd} + i_{Ld}$$

$$i_{tq} + i_{sq} + i_{wq} = i_{bq} + i_{Lq}$$

Now there is a need to express these currents as a function of V_{sd} and V_{sq}. Recalling grid currents and load currents from previous section, it is possible to get bus voltage $V_s$in terms of state variables.

On substituting grid currents and load currents in the KCL equation obtained above we are able to get V_{sd} and V_{sq} in terms of state variables

$$V_{sd} = [Z_b Z_1(i_{sd} + \mathrm{i_{wd}}) + Z_b X_2 e_q{}' + V_b Z_1(R_b \sin\delta + X_b \cos\delta) - \mathrm{B}V_{sq}]$$

$$V_{sq} = D(i_{sd} + i_{wd}) + E e_q{}' + \ \mathrm{F}\ (i_{sq} + i_{\mathrm{pq}}) + \ \ + GV_b$$

By substituting V_{sd} and V_{sq} in the nonlinear differential equation of the components model we get the closed form as

$$\frac{dX}{dt} = f(X, u)$$

The state vector for this system is given as

$$X_{GSW} = \left[X_G, \quad X_S, \quad X_W\right]^T$$

$$U = \left[m_{st}, \psi_{st}, m_{wr}, \ m_{wi}, \psi_{wi}\right]$$

$$X_{\mathrm{G}} = \left[\delta, \omega, e'_q, E_{fd}\right] \quad X_S = [i_{sd}, i_{sq}, V_{dcs}]$$

$$X_W = [\theta_s, \omega_t, \delta_w, \omega_w, i_{gd}, i_{gq}, V_{dcw}, i_{wfd}, i_{wfq}, i_{wd}, i_{wq}, V_{cwd}, V_{cwq}]$$

These variables m_{st}, ψ_{st} are modulation index and phase angle for inverter connect near STATCOM, similarly m_{wr} is the modulation index of the PMSG side converter system and m_{wi}, ψ_{wi} are modulation index and phase angle of grid side converter.

CHAPTER 4

CONTROLLER DESIGN & RESULTS

Designing the best controller for a complex system have always been a challenging task. Various traditional controllers such as P, PI, PID serves for this purpose. But any change in system dynamics results in a change in controller gains or parameters which are to be regularly updated. As a results, a robust controller shall be designed which controls the system robustly. For this purpose, robust controllers are needed such as loop shaping controller or $H_2\ and\ H_\infty$ control technique. The performance of a feedback system can be quantified in terms of the closed loop gain from the disturbance inputs to the reference outputs. This chapter presents the design of robust STATCOM controller. Designing a controller for a complex dynamic system is going to be a challenging task in the real application.

4.1 Loop Shaping Controller

This section gives a brief idea for designing loop shaping controller based on the theory of uncertainty modeling, robust stability criteria, and a graphical design technique 'loop shaping' for designing controller. For designing a stabilizing controller for the nonlinear system, one way is to linearize the given system around an operating point and then the controller is designed for such a linear system. If the designed controller is robust enough to perform well for a particular operating point even for the nonlinear model, then it can be said that our design objectives are met. Details procedure for designing loop shape controller can be expressed in the following sections

4.1.1 Uncertainty Modeling

The process of designing a controller starts by getting a nominal plant transfer function *P,* and considering perturbed plant transfer function $\hat{P}$, and so the relation between then can be expressed as

$$\frac{\hat{P}}{P} - 1 = \Delta W_2 \tag{4.1}$$

Where,

$\hat{P}$= Perturbed plant transfer function

Δ = A variable stable transfer function satisfying $\| \Delta \|_\infty \leq 1$

W_2 = fixed weight (stable transfer function)

Infinity norm of a function is the least upper bound of its absolute value, $\|\Delta\|_\infty = \sup_\omega |\Delta(j\omega)|$ is the highest value of gain on magnitude bode plot [24]. An assumption is made that unstable or imaginary axis poles of $P(s)$ are not cancelled in the formation of $\hat{P}(s)$.Thus $P(s)$ and $\hat{P}(s)$ will have same unstable poles. The plant dynamics can be expressed as

$$\Delta\dot{X} = A\Delta X + B\Delta U \text{ and } \Delta Y = C\Delta X$$

The transfer function of the plant is obtained as $P = C[sI - A]^{-1} B$. The given plant is perturbed to get $\hat{P}$, where the perturbation of plant is performed at various operating points. Thus the size of unstructured uncertainties is represented by the size of the envelope containing P and found to increase with increasing frequency. From the Figure 4. 1 the upper edge of the envelope confirms the plot of $(1 + |W_2(j\omega)||P(j\omega)|$, while the lower edge of envelope corresponds to the plot of $(1 - |W_2(j\omega)||P(j\omega)|$ and the envelope of actual plant correspond to plot of $|P(j\omega)|$.

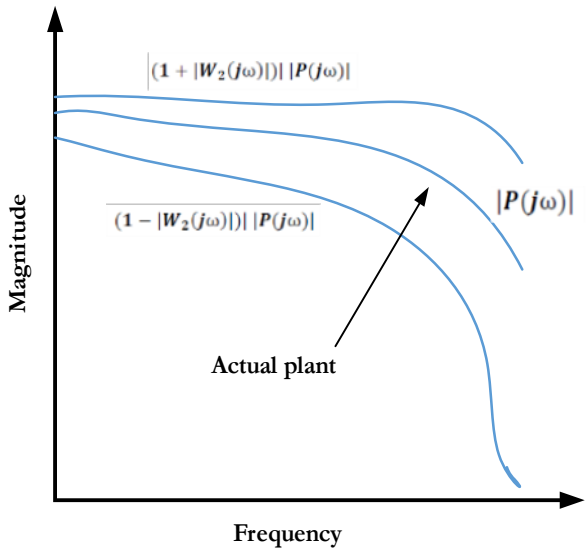

Figure 4. 1 Bode plot interpretation of multiplicative uncertainty

In the multiplicative uncertainty model Eq. (4.1), ΔW_2 is the normalized plant perturbation away from 1. If $\| \Delta \|_\infty \leq 1$, then

$$\left|\frac{\hat{P}(j\omega)}{P(j\omega)}\right| - 1 \leq |W_2(j\omega)| \tag{4.2}$$

Where $|W_2(j\omega)|$ provides the uncertainty profile and is roughly increasing function of ω. Hence uncertainty increases with increasing frequency.

4.1.2 Robust Stability

Assuming that the plant transfer function P belong to a set þ. Considering some general characteristics of a feedback system that the plant is internally stable. A controller C is robust with respect to this characteristics if this characteristic holds for every plant in þ. In the same manner, controller C provides robust stability if it provides internal stability for every plant in þ.

A multi-input control system is given in Figure 4. 2 if the controller provides internal stability for every plant in the uncertainty set þ. .Hence, a test for robust stability involves the controller and uncertainty set. The open loop transfer function is denoted as $L = PC$. S is the sensitivity function expressed as in equation (4.3) and input output transfer function or complementary sensitivity function (T) is expressed as equation (4.4)

$$S = \frac{1}{1+L} \tag{4.3}$$

$$T = 1 - S = \frac{PC}{1+PC} \tag{4.4}$$

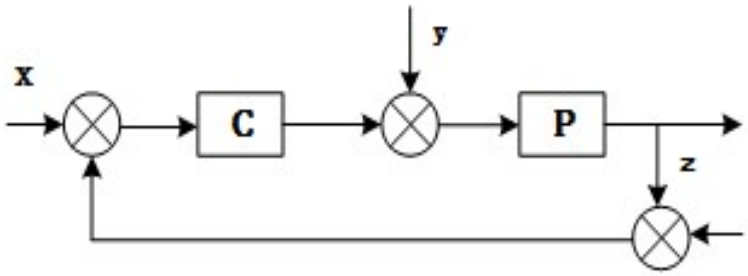

Figure 4. 2 Unity feedback plant with controller

Robust stability conditions are met for a multiplicative perturbation model if and only if $\left||W_2T|\right|_\infty < 1$ [47]. This results in obtaining an expression (4.5).Hence the stability condition can be generalized as

$$\left||W_2T|\right|_\infty \leq 1 \Leftrightarrow \left|\frac{W_2(j\omega)L(j\omega)}{1+L(j\omega)}\right| < 1, for\ all\ \omega$$

$$|W_2(j\omega)L(j\omega)| < |1+L(j\omega)|, for\ all\ \omega \tag{4.5}$$

$$\Leftrightarrow |\Delta(j\omega)W_2(j\omega)L(j\omega)| < |1+L(j\omega)|, for\ all\ \omega, \qquad \left||\Delta_\infty|\right| \leq 1$$

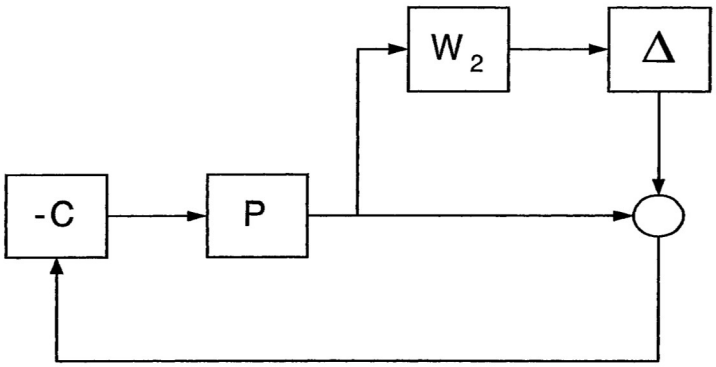

Figure 4. 3 Perturbed feedback system

A typical block diagram of a perturbed system, ignoring inputs as shown in Figure 4. 3. The transfer function to the output Δ to the inputs of Δ equals $-W_2T$. The maximum loop gain $\left||-\Delta W_2T|\right|_\infty$ is less than 1 for all allowable Δ if and only if the small gain condition $\left||W_2T|\right|_\infty < 1$ holds.

4.1.3 Robust Performance

The robust stability condition for an internally stable, nominal feedback system is $\left||W_2T|\right|_\infty < 1$. The nominal performance condition for an internally stable system is given as $\left||W_2S|\right|_\infty < 1$, where W_1 is a real-rational, stable, minimum phase transfer function, also called a weighting function such that

$$\left||W_2S|\right|_\infty < 1, \Leftrightarrow \left|\frac{W_1(j\omega)}{1+L(j\omega)}\right| < 1, \ \forall\ \omega$$

$$|W_1(j\omega)| < |1+L(j\omega)|, \ , \ \forall\ \omega$$

If P is perturbed to $\hat{P} = (1+\Delta W_2)P, S$ is perturbed to

$$\hat{S} = \frac{1}{1+\hat{P}C} = \frac{1}{1+(1+\Delta W_2)L} = \frac{S}{1+\Delta W_2T}$$

Also, the performance condition would be

$$\left|\left|W_2T\right|\right| < 1, and \left|\left|\frac{W_1S}{1+\Delta W_2T}\right|\right| < 1, \forall \left|\left|\Delta\right|\right| < 1$$

As a result $\left|\left|-\Delta W_2T\right|\right| \leq \left|\left|W_2T\right|\right|$. Thus $1+\left|\left|W_2T\right|\right| \geq 1-\left|\left|W_2T\right|\right|$ for a fixed frequency we can imply that

$$\left|\left|\frac{W_1S}{1+\Delta W_2T}\right|\right|_\infty \leq \left|\left|\frac{W_1S}{1+\Delta W_2T}\right|\right|_\infty \leq 1$$

From all the above equations robust stability and performance condition is given as [47]

$$\left|\left|W_1S\right|\right| + \left|\left|W_2T\right|\right|_\infty < 1 \tag{4.6}$$

4.2 Loop-Shaping Design

A graphical approach for designing a robust controller is loop shaping technique. The designed controller C shall satisfy the robust stability and performance criteria. The general idea for is to obtain a loop transfer function L satisfying the robust performance criteria. The underlying constraints are internal stability of nominal feedback system and properness of C, so that L is not freely assignable. In case if P or P^{-1} is not stable, then L must contains $P's$ unstable poles and zeros. Then the relationship of controller is given as $C = L/P$. L shall be designed in such a way that PC should not have any pole zero cancellation. Either $|W_1|$ or $|W_2|$ should be less than 1, is a necessary condition for robustness. W_1 is selected as a monotonically decreasing function. In this work third order Butterworth filter is selected as W_1. W_2 can be obtained from perturbed transfer function of plant.

$$W_1(s) = \frac{k_d f_c^2}{s^3 + 2s^2 f_c + 2s f_c^2 + f_c^3}$$

Depending on above two weights the open loop shape transfer function L should satisfy equation (6.9) & (6.10).

$$|L| > \frac{|W_1|}{1 - |W_2|} \quad \forall \quad \text{low frequency} \tag{4.7}$$

$$|L| < \frac{1 - |W_1|}{|W_2|} \approx \frac{1}{|W_2|} \quad \forall \quad \text{high frequency} \tag{4.8}$$

So the procedure for loop-shaping designs begins with plotting of two curves on a log-log scale, magnitude and frequency equation (4.7) over a range of low frequencies and second graph is the plot satisfying equation (4.8) over the range of high frequencies. On this plot fit another curve which is going to be the graph of $|L|$, such that at low frequency let it lie above the first curve and for high frequency let it lie below the second curve. For ensuring properness of *C,* $|L|$ should roll off as quickly as $|P|$. The gain at low frequency for open loop transfer function should be large enough, $|L|$ should not drop off to quickly near crossover frequency which results in internal instability [47].

4.2.1 Loop-Shaping Algorithm

The general algorithm shall follow for designing loop shaping controller function C.

1. Plot bode diagram for both nominal plant as well as perturb plant transfer functions.
2. Obtain W_2 satisfying the equation (4.2)
3. W_1 is selected as monotonically decreasing function, which is real, stable and rational function.
4. Select L such that equation (4.7) & (4.8) are satisfied the slope for L at crossover frequency should not be steeper than -20dB/decade and angle at crossover frequency is greater than 180^o.
5. Check whether robust stability and performance condition is satisfied given in equation (4.6).
6. The controller transfer function can be designed from relation $C = L/P$
7. Simulation is carried on closed loop transfer function for pre-selected disturbance and test for internal stability of the system.
8. If the satisfactory controller is not designed the repeat, the steps 4-6 again.

4.3 Results

In this section in order to test the effectiveness of controller, nonlinear time domain simulations have been carried out. From the previous section it is now possible to design the controller based on the procedure described earlier. The designing process starts with modeling of a nonlinear system of the microgrid. For the sake of designing controller, the given system is linearized about an operating point. If the designed controller performs well for this linear system for the specified operating points in the vicinity, then it is possible to say that the design objectives are met. This section gives detail response or behavior of the system when the system is subjected to any disturbance such as torque input disturbance for micro-alternator or three-phase fault at the grid bus. This section also gives the detail design procedure for a particular system and the performance of the controller when the controller designed is implemented. Based on the modeling of a microgrid, this research focuses on two different systems of the microgrid.

1. Microgrid formed by integrating micro-alternator with STATCOM.
2. Microgrid formed by integrating micro-alternator with PV and STATCOM.
3. Microgrid formed by integrating micro-alternator with wind and STATCOM.

4.3.1 Micro alternator with STATCOM Model

A fourth order micro-alternator is modeled along with STATCOM model which is connected to the point of common coupling along with acting load and utility power grid. As a result for this combined model, we obtain seven non-linear differential equations. In order to get control input from the controller, STATCOM serves two inputs namely modulation index of inverter (m_{st}) and phase angle of inverter(Ψ_{st}). The operating point for micro alternators electrical output power P_e=0.6 p.u while load for the system is considered as S_{load}=1+0.15i p.u. The designed system is subjected to 20% torque input

disturbance at 1 second for a duration of 100ms. The micro alternator speed, rotor angle and Bus voltage response can be shown in Figure (4.4 - 4.6).

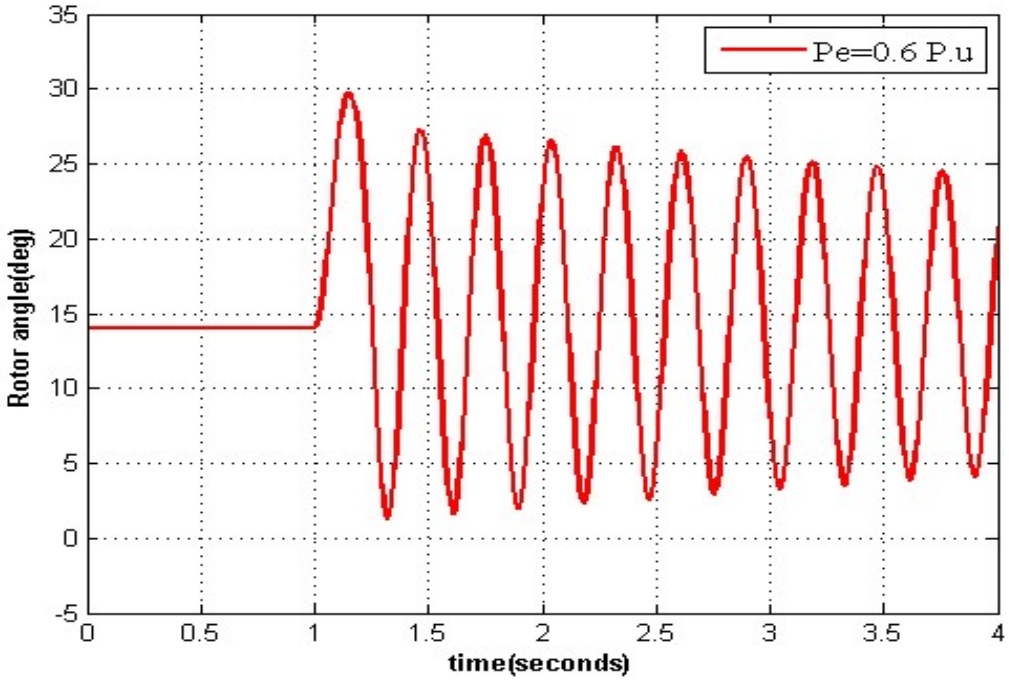

Figure 4. 4 Response of micro- alternator's rotor angle subjected to disturbance at 1 second

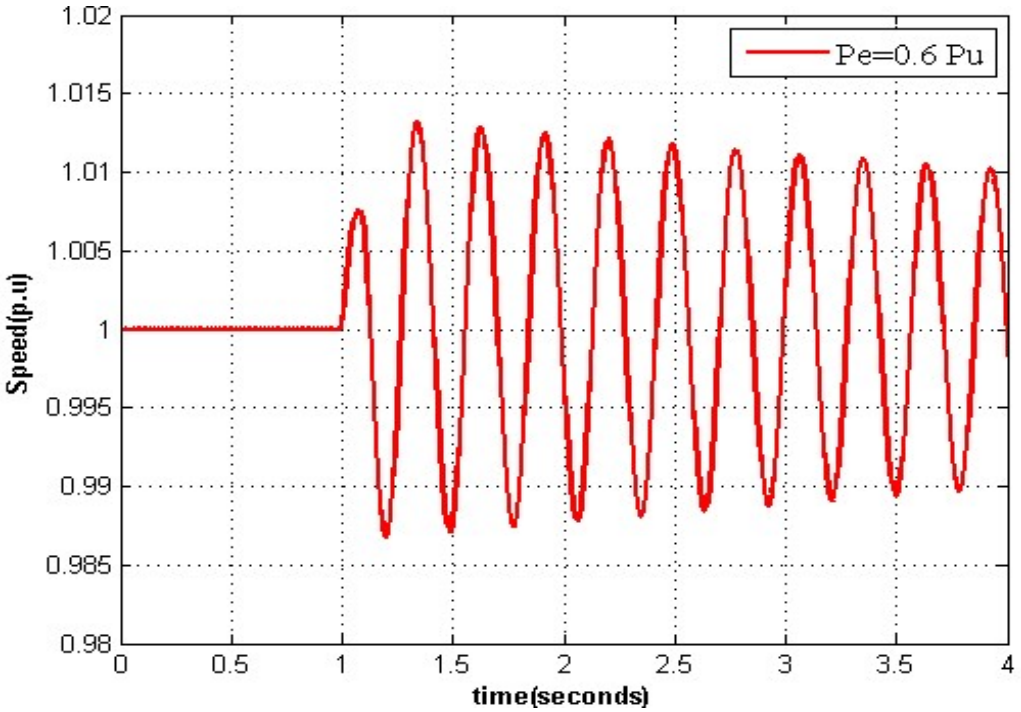

Figure 4. 5 Response of micro- alternator's speed when subjected to disturbance at 1 second

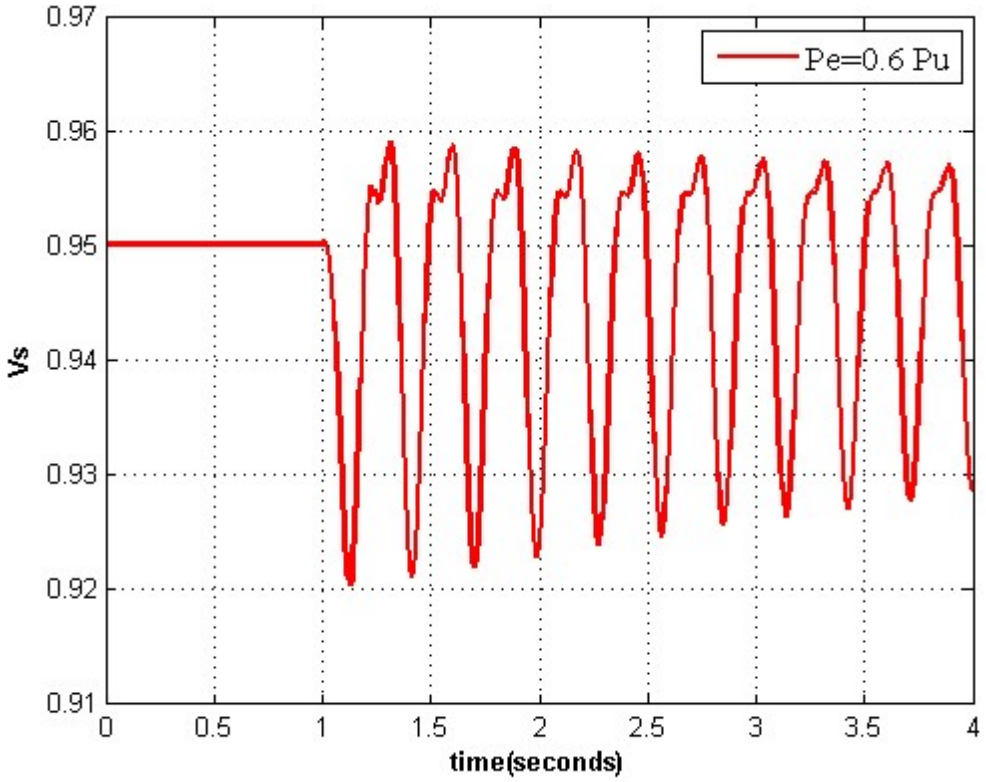

Figure 4. 6 Response of Bus voltage at common Bus with disturbance at 1 second

The nonlinear simulation result for the uncontrolled system is shown above. Now for the purpose of designing loop shaping controller, there is a need to estimate the linear model for this system. As the procedure of designing loop shape starts with transfer function analysis. Considering speed as the output from the plant and phase angle of inverter of STATCOM (Ψ_{st}) as input to the system we are able to get the transfer function of the system by the expression $C(sI - A^{-1})B$. Transfer function of this system can be given as

$$P = \frac{197.48 * s(s + 785.11)(s + 99.160)(s + 1.4918)(s + 0.7566)}{(s^2 + 434.481s + 234213.51)(s + 99.17)(s^2 + 0.401s + 167.7)(s^2 + 2.043 + 1.1745)}$$

After analyzing the plant transfer function, now there is a need of getting perturbed transfer function based on the equation $|\hat{P}(j\omega))/P(j\omega)| - 1$ for each perturbed plant. The dB magnitude of perturbed plant is plotted on semi log scale as shown in Figure 4. 7

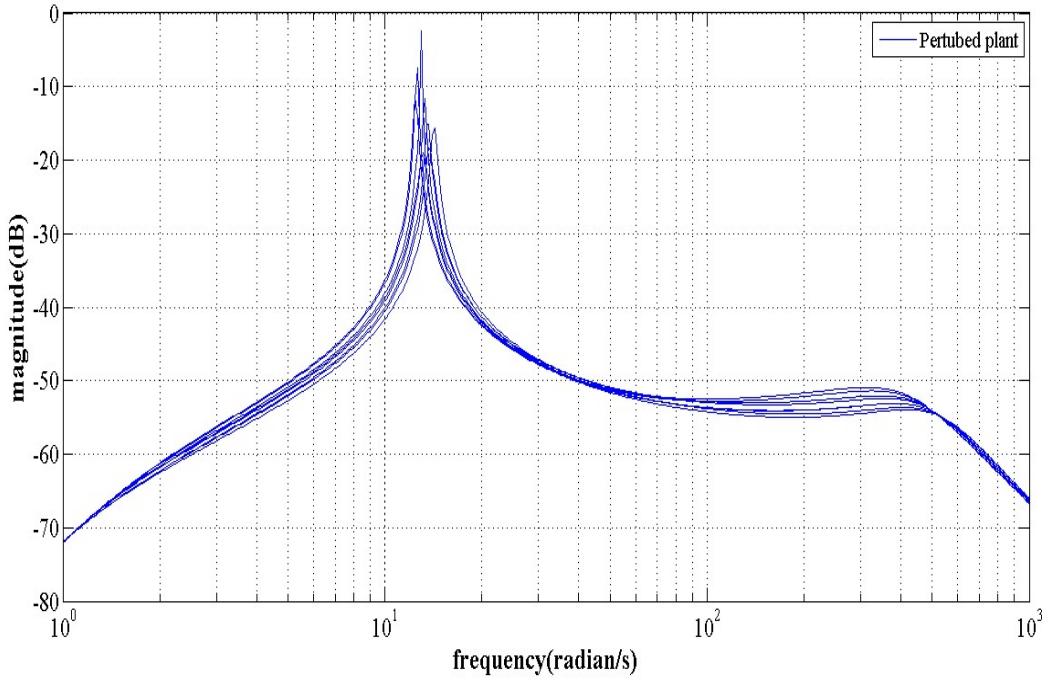

Figure 4. 7 Perturbed Bode plot of plant

The uncertainty profile is fitted to a function W_2 as

$$W_2 = \frac{0.3s^2 + 4.1s + 14.4}{s^2 + 1.68s + 144}$$

Whereas W_1 is estimated as a third order Butterworth filter, K_d=0.00001 and f_c=1, can be written as

$$W_1(s) = \frac{k_d f_c^2}{s^3 + 2s^2 f_c + 2s f_c^2 + f_c^3}$$

As W_2 is based on uncertainty modeling, the obtained W_2 can be plotted to on log-log scale as shown Figure 4. 8

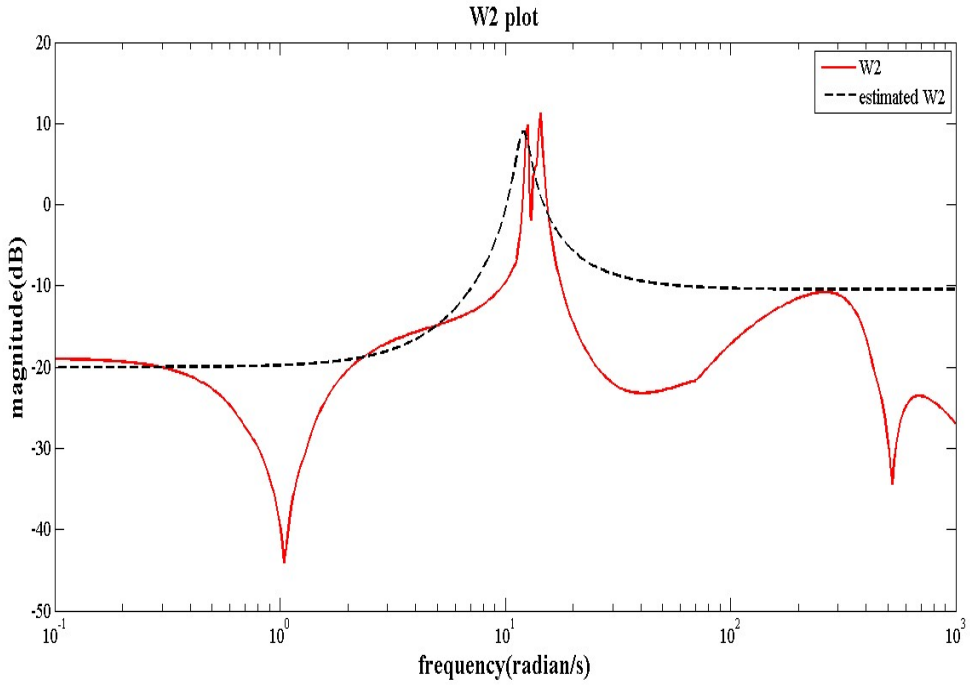

Figure 4. 8 Estimation of W2

For the selected W_1 and W_2, open loop transfer function L can be estimated by keeping L above the relation satisfying $|L| > (|W_1|)/(1 - |W_2|)$ for low frequency and for high frequency $|L| > 1/|W_2|$. The given L should also satisfy to the robust stability criteria $\left||W_1 S|\right| + \left||W_2 T|\right|_\infty < 1$ and nominal performance criteria $\left||W_1 S|\right| < 1$. As a result based on this observation we can get the, desired loop shape as

$$L = \frac{70 * (s + 1.5)(s + 1.4)(s + 0.756)}{(s + 99.18)(s + 30)(s + 10)(s^2 + 0.401s + 167.47)}$$

The plots for desired loop shape can be shown in Figure 4. 9 and the plots for robust stability criteria and nominal performance is given in Figure 4. 10. Such that the curve for robust stability $\left||W_1 S|\right| + \left||W_2 T|\right|_\infty$ is always less than 0 dB.

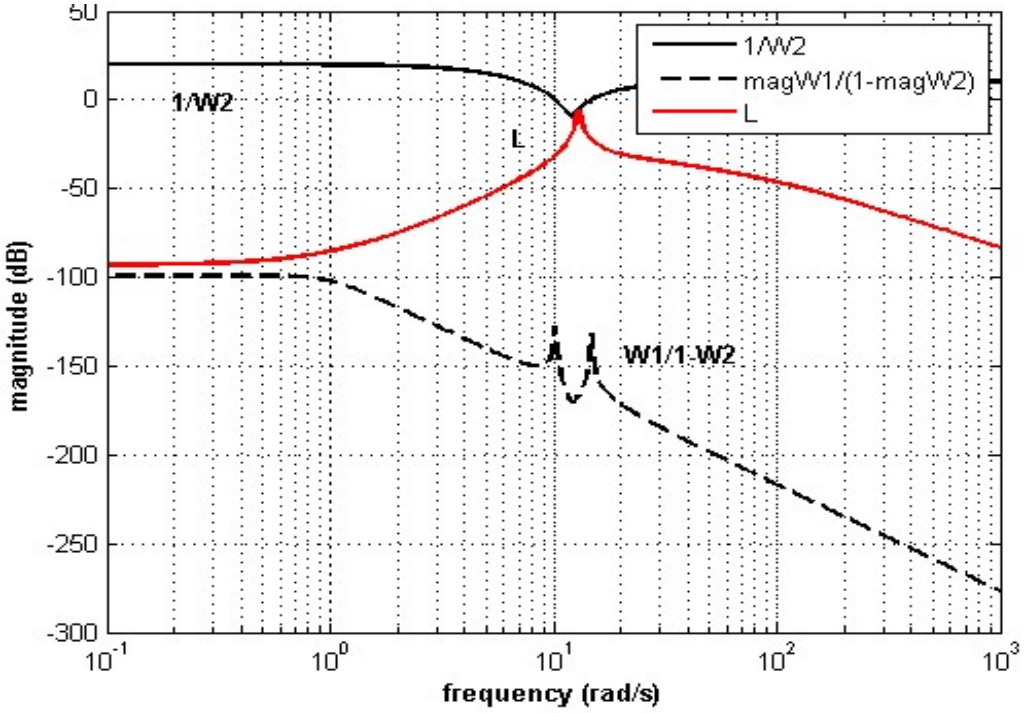

Figure 4. 9 Loop shape design

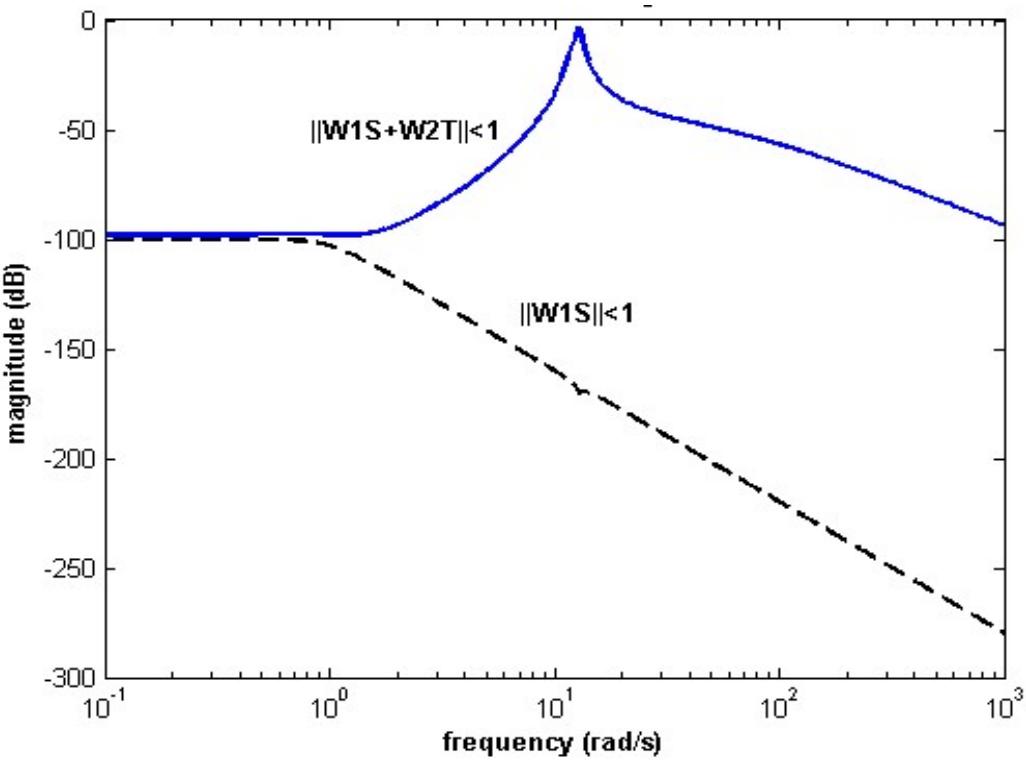

Figure 4. 10 Plot for Performance and stability criteria

From the above open loop transfer function, the controller function was obtained from the relation

$$C = \frac{L(s)}{P(s)}$$

The function is obtained as

$$C = \frac{0.358 * (s + 1.4)(s^2 + 434.48s + 234213.5)(s^2 + 2.043s + 1.1745)}{s(s + 30)(s + 30)(s + 99.16)(s + 785.11)}$$

4.3.1.1 Torque Disturbance

The designed robust STATCOM controller was tested was tested under 20% torque input disturbance for a duration of 100ms at operating point P_e=0.6 p.u for this linear system. Then the same controller was even tested for nonlinear system and simulation is carried on ODE routines. Figure 4. 11 to Figure 4. 13 shows the response of generator angle, angular speed and bus voltage respectively.

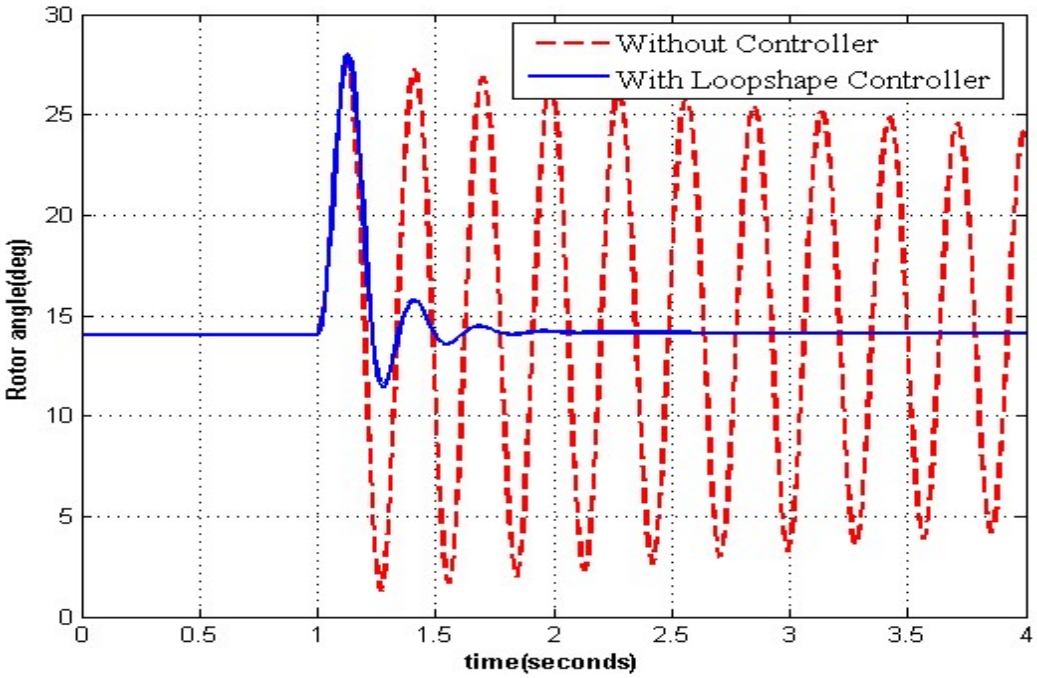

Figure 4. 11 Response of micro- alternator's rotor angle with Loop-shape controller

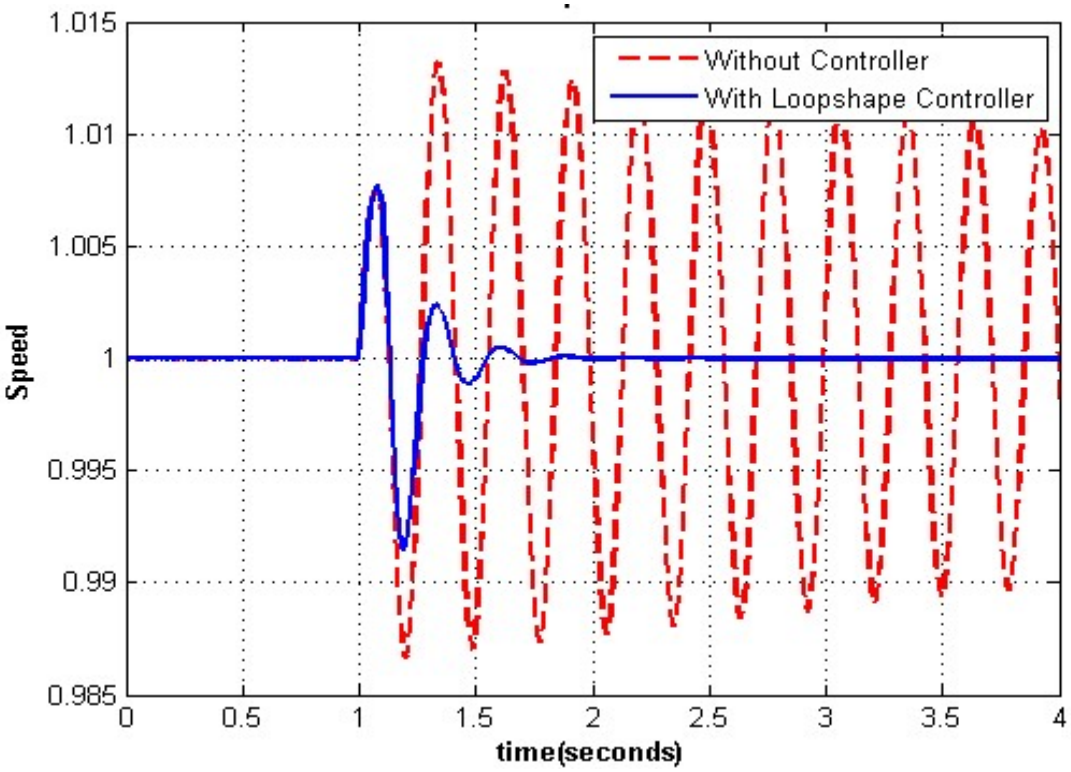

Figure 4. 12 Response of micro-alternator speed with Loop-shape controller

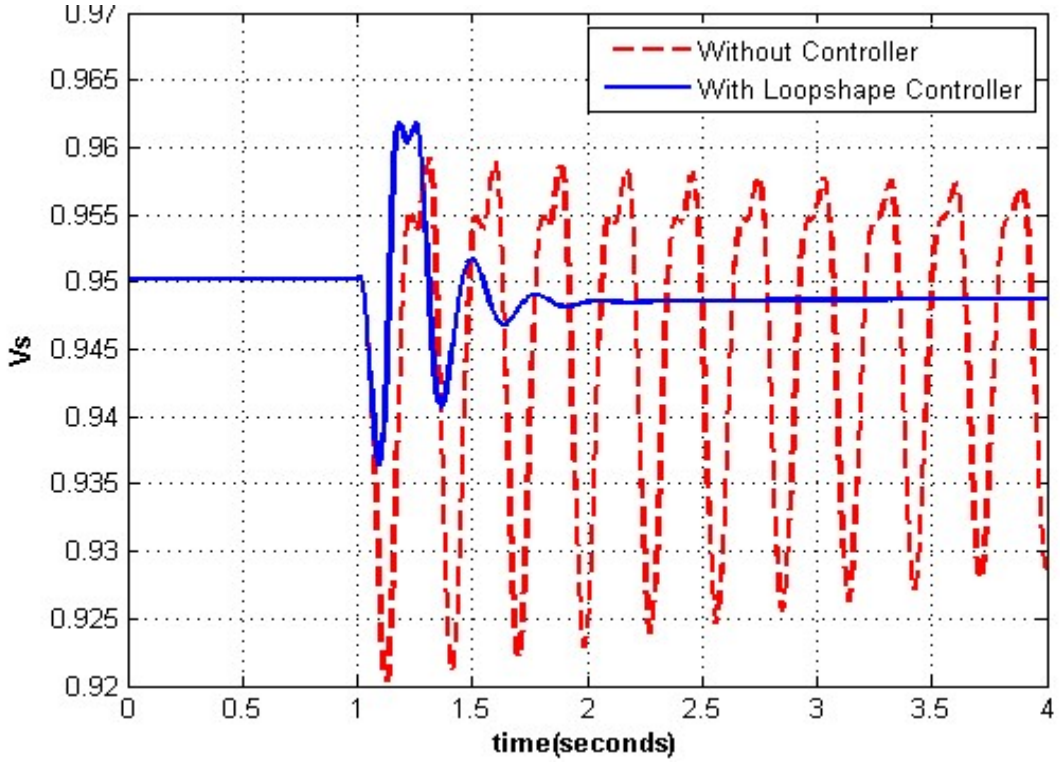

Figure 4. 13 Response of Bus voltage with Loop-shape controller

Comparison of results with different level of torque disturbance at various operating points:

The following controller was tested for various operating point $P_e = 0.6$ p.u, $P_e = 0.8$ p.u, $P_e = 1.0$ p.u. and also for different torque disturbances varying form 10 % to 50 %. The corresponding rotor angle variation as well as bus voltage variations and angular speed variation are shown in Figures (4.14 -4.16). Based on verification of the designed controller it is observed that the controller obtained is a robust controller that does not require any tuning of controller parameters even for various operating condition.

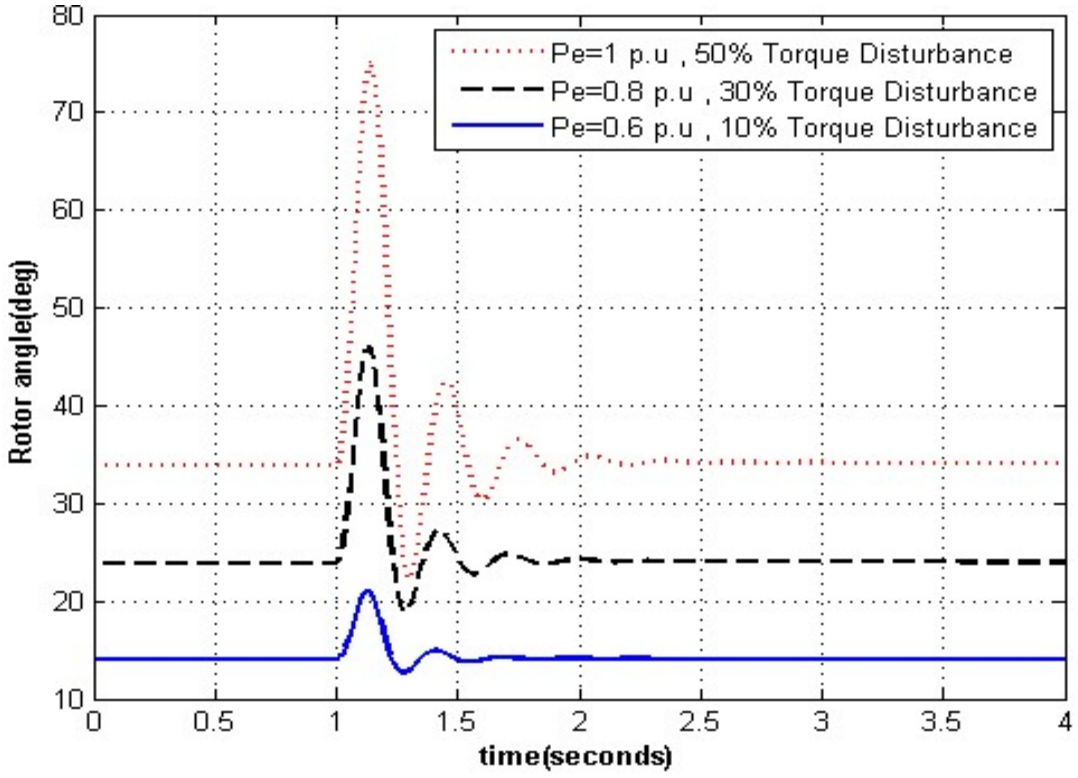

Figure 4. 14 Angle response Micro-alternator's with different torque disturbance for different operating points

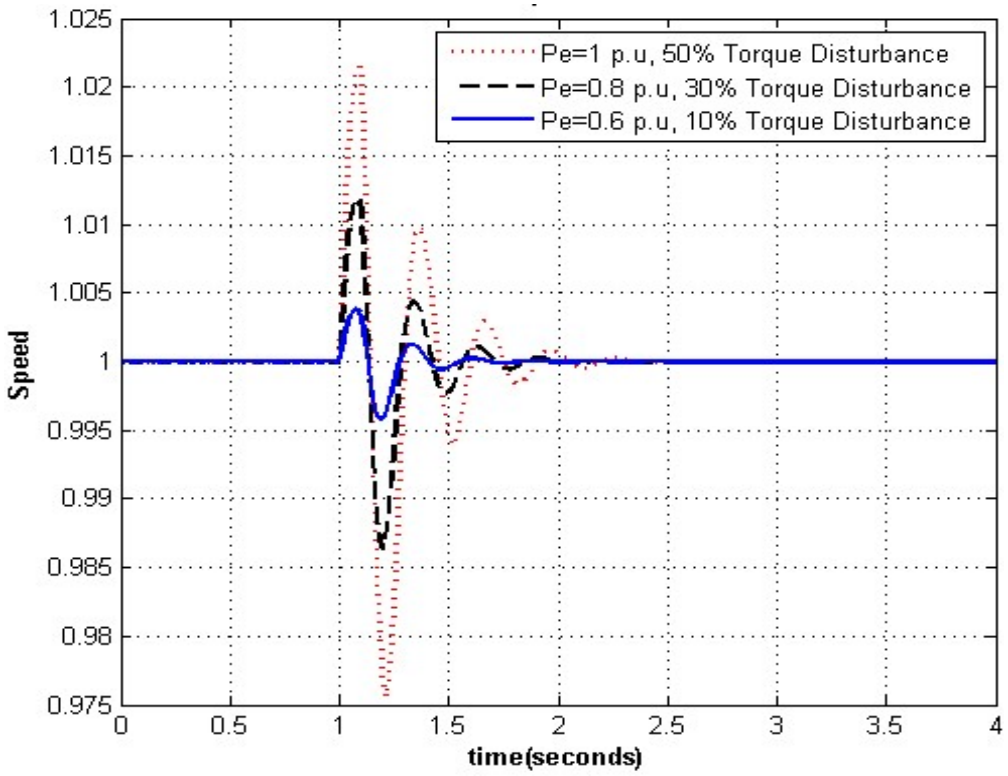

Figure 4. 15 Speed response of micro-alternator with different torque disturbance for different operating points

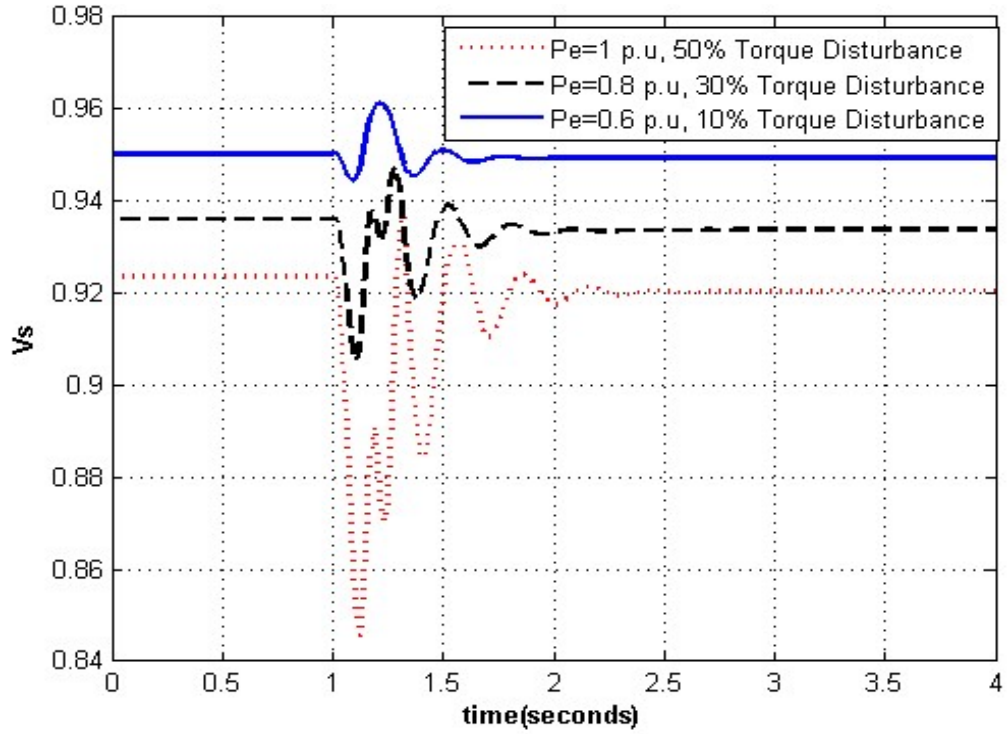

Figure 4. 16 Bus voltage response with different torque disturbance for different operating points

4.3.1.2 Three phase fault testing

The robust STATCOM loop-shape controller after being implemented for the system, now the system is bound to test for a severe three-phase fault at the common bus terminal (PCC). The fault duration considered in this study is for 100ms. This assumption is made keeping in mind that the fault obtained in the system shall be cleared within a duration of 100ms. The operating point considered as electrical power output for micro-alternator $P_e = 0.9$ p.u. The response for generator angle can be shown in Figure 4. 17

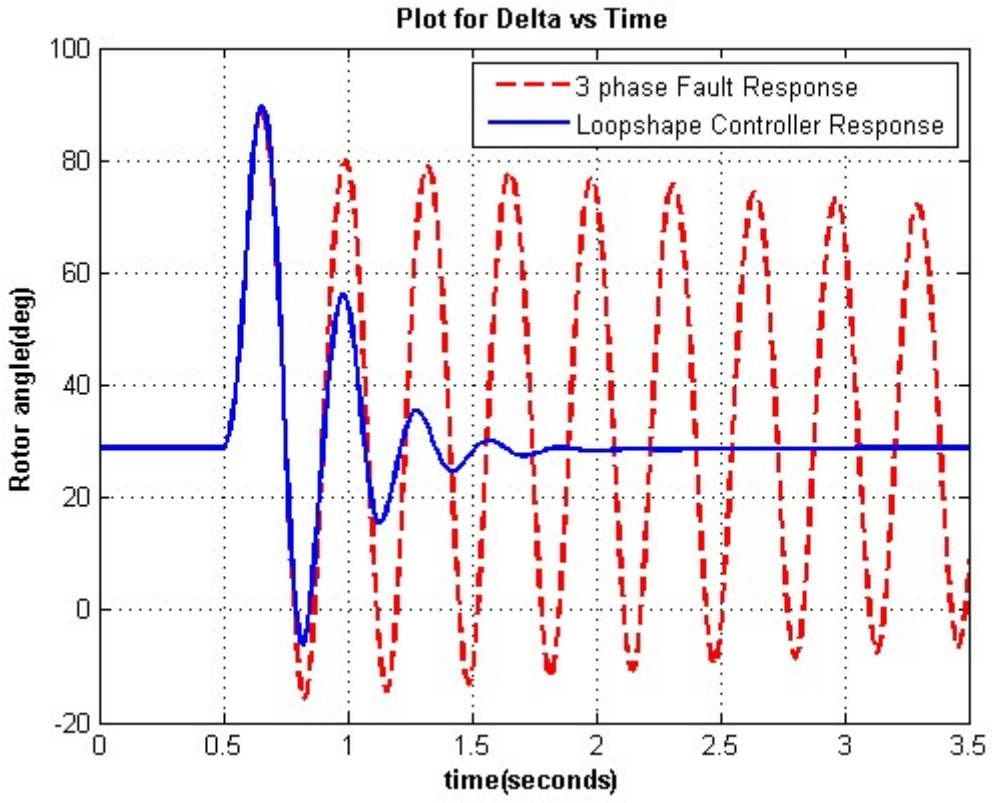

Figure 4. 17 Response of Rotor angle due to three phase fault at Common Bus Vs

4.3.2 Micro alternator, PV system and STATCOM Model

This type of system is formed by integrating micro-alternator, PV system, and STATCOM along with load which is connected to power grid. The combined model is found to be very complex of about 15th order. From the previous chapters, we are able to get the nonlinear model of microgrid system. For this system, we are able to extract four control input, (m_{st}) modulation index for inverter connected towards STATCOM, (Ψ_{st}) phase angle for inverter connected towards STATCOM, (m_{pv}) and (Ψ_{pv}) are modulation index and phase angle for the inverter connected towards PV system respectively. For this system we require a central STATCOM controller which should be able to stabilize the system when subjected to various disturbances. As there are two DG sources in current system, it is extremely important in considering the power sharing for alternator as well as PV system. The operating points for alternator power P_e=0.8 p.u and PV power of P_{pv}=0.2 p.u while a constant load for the system is considered as S_{load}=1.5+0.15i p.u. The nonlinear simulations have been carried on ODE routines. The micro alternator speed, rotor angle and Bus voltage response when subjected to 10% torque disturbance for 200ms can be shown in Figure (4.18-4.20).

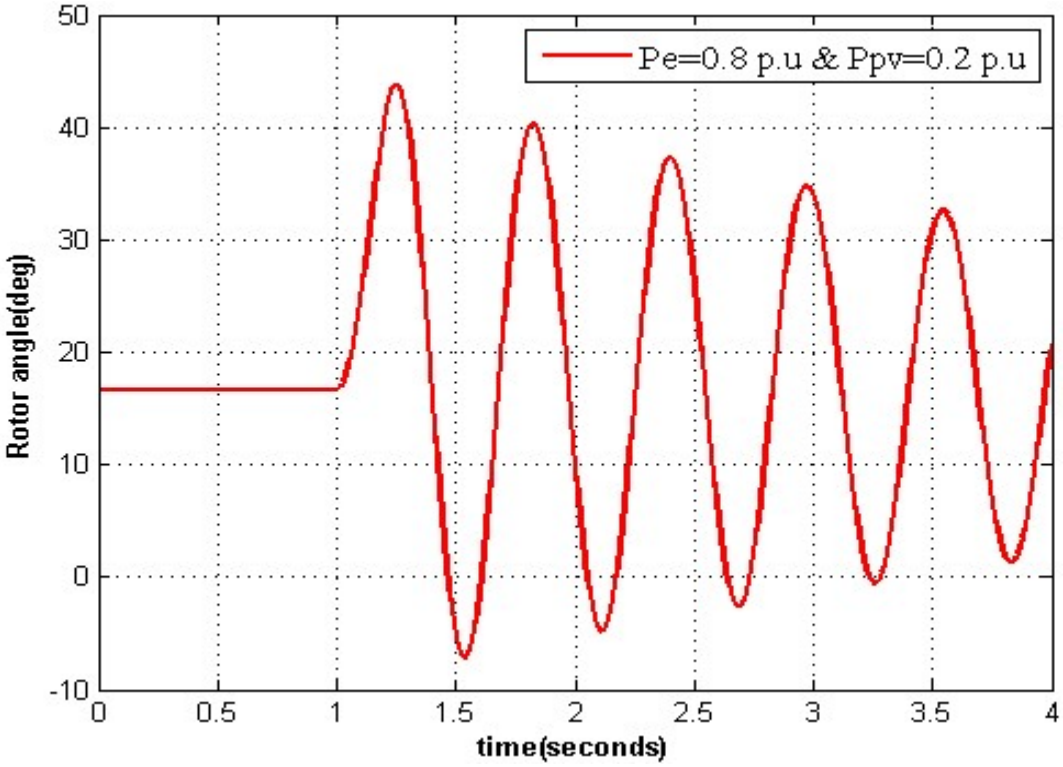

Figure 4. 18 Response of Micro-alternator's rotor angle subjected to disturbance

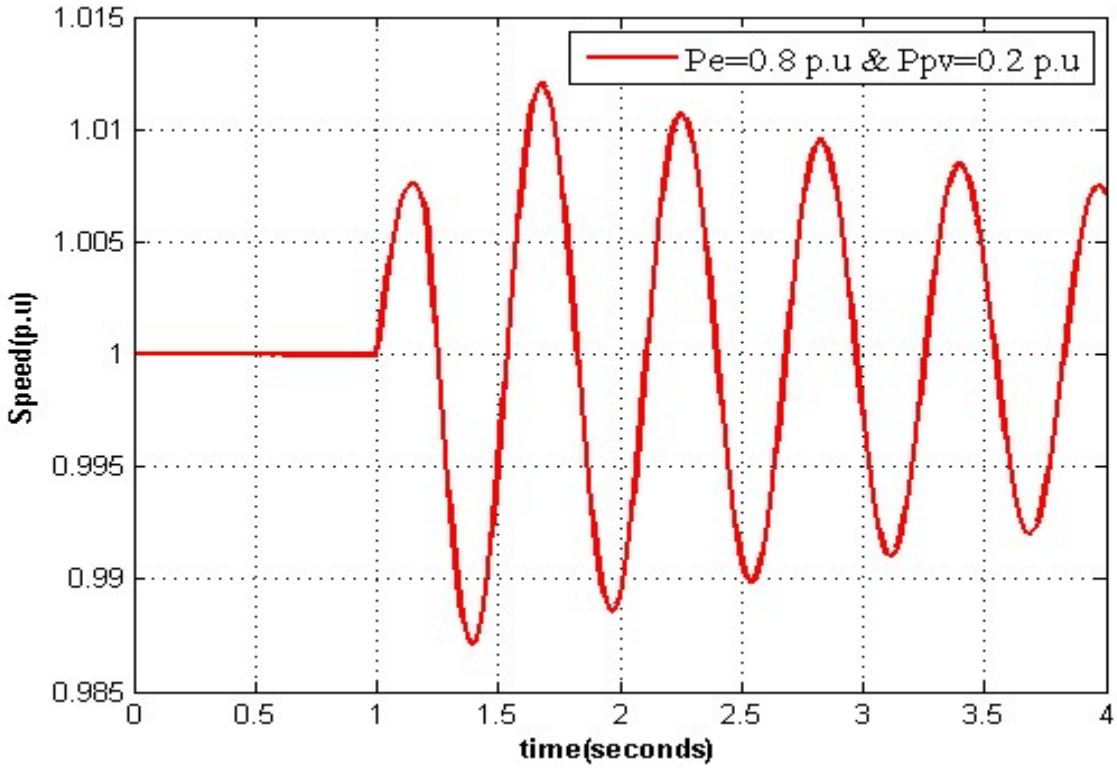

Figure 4. 19 Response of micro-alternator speed subjected to disturbance

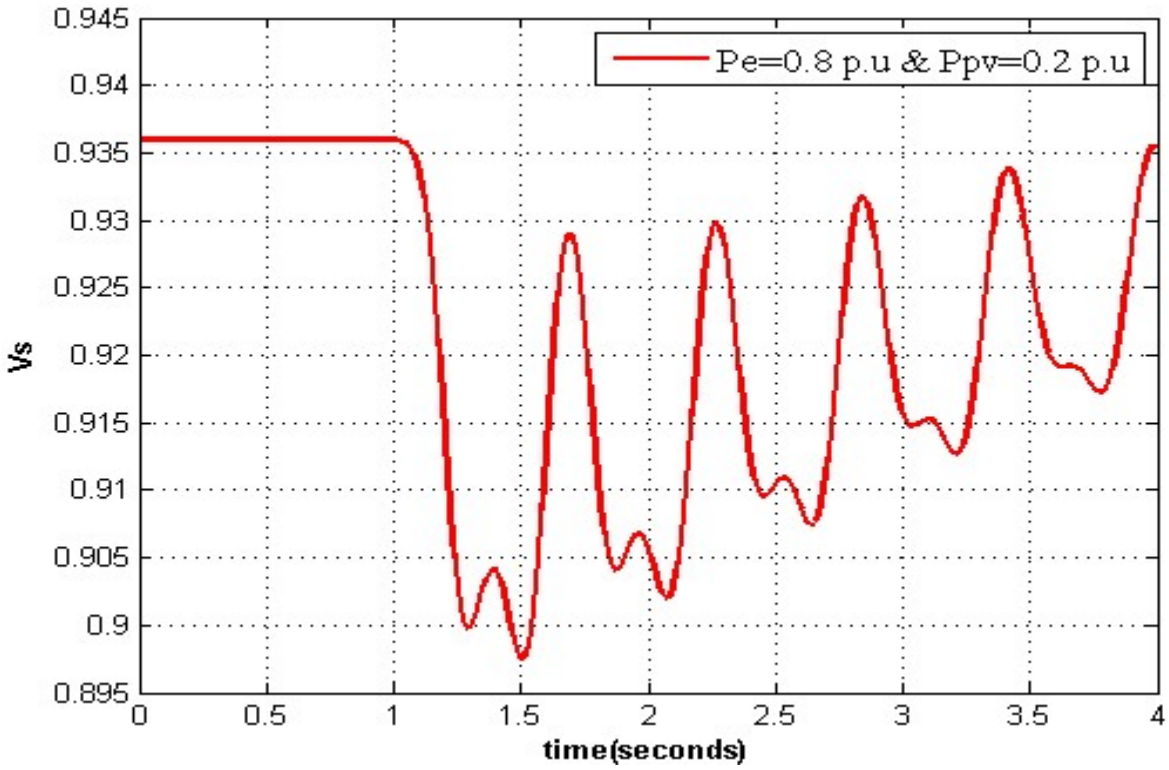

Figure 4. 20 Response of voltage at common bus subjected to disturbance

In order to select desired loop-shape controller, the linear model is obtained about a certain operating point. Variation of speed of micro-alternator is selected as the output of the system and Ψ_{st} is selected as input to the plant. A 15th order transfer function of this system is estimated and can be given as *P*. After getting the plant transfer function, now there is a need of estimating perturbed transfer function based on the equation $|\hat{P}(j\omega))/P(j\omega)| - 1$ for each perturbed plant. The dB magnitude of perturbed plant is plotted on semi log scale as shown in Figure 4. 21

$$P = \frac{143.43X(s^2 + 175.49s + 10100)(s + 2.1)(s^2 + 0.869s + 3.24)(s + 0.7)(s + 1380.3)}{(s^2 + 581.6s + 9.7x10^6)(s^2 + 495.6s + 4.9x10^5)(s^2 + 487.9s + 5.04x10^5)(s + 99.2)}\text{X}$$

$$\frac{s(s + 99.1)(s^2 + 597.05s + 8.8\text{x}10^6)(s^2 + 646.84s + 10^5)}{(s^2 + 143s + 74351)(s^2 + 0.9s + 3.2)(s^2 + 2.76s + 2.5)(s^2 + 0.0285s + 156.25)}$$

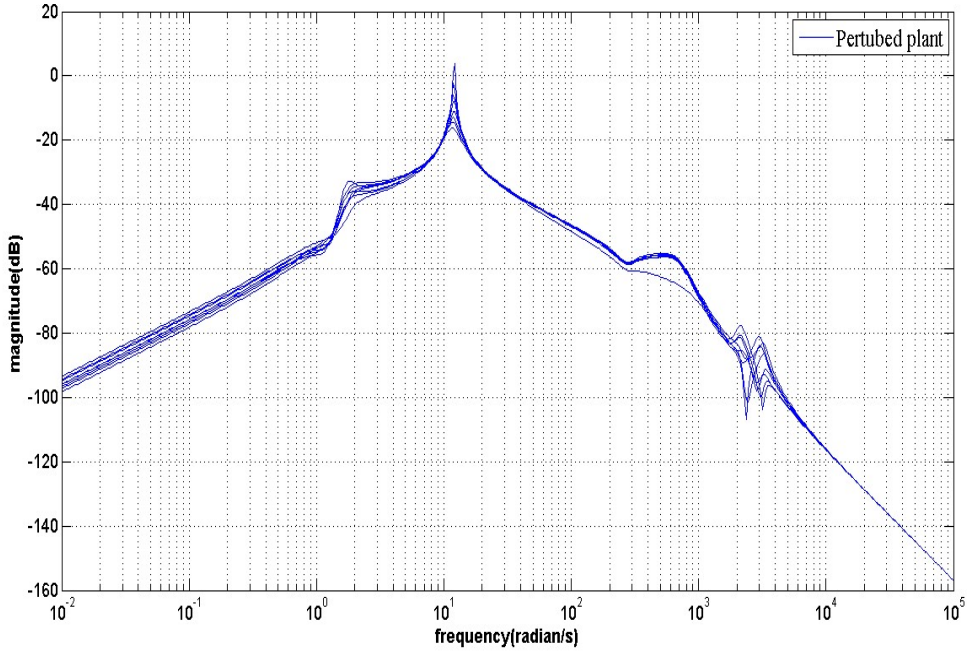

Figure 4. 21 Perturbed Bode plot of plant

The uncertainty profile is fitted to a function W_2 as

$$W_2 = \frac{0.15s^2 + 0.06s + 14.7}{s^2 + 42s + 49}$$

Whereas W_1 is estimated as a third order Butterworth filter, K_d=0.00001 and f_c=1, can be written as

$$W_1(s) = \frac{k_d f_c^2}{s^3 + 2s^2 f_c + 2s f_c^2 + f_c^3}$$

As W_2 is based on uncertainty modeling, the obtained W_2 can be plotted to on log-log scale as shown in Figure 4. 22

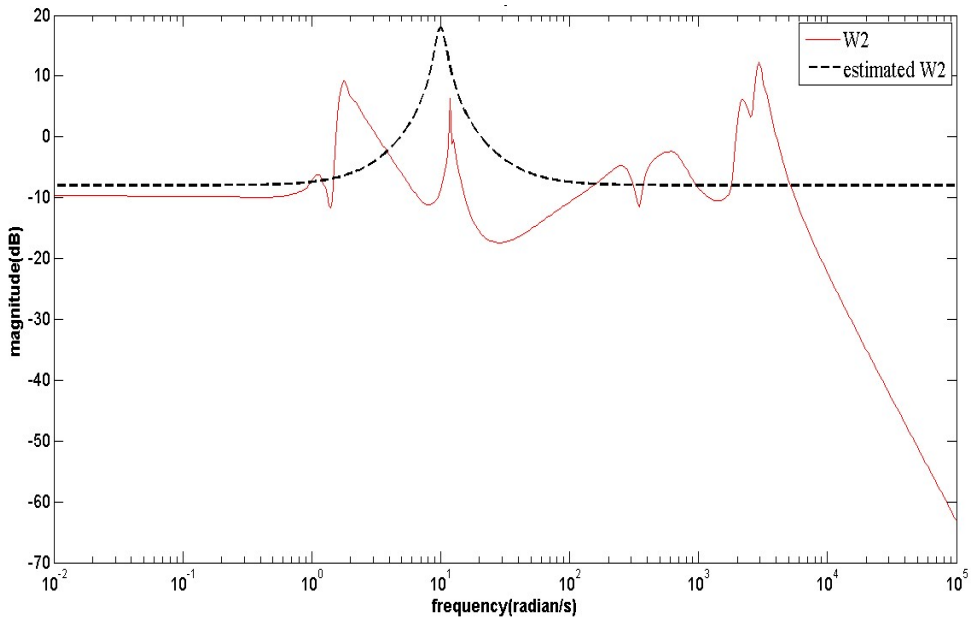

Figure 4. 22 Estimation of W2

Considering the conditions, selecting open loop transfer function which satisfies the performance and stability criteria. The obtained loop-shape is given as

$$L = \frac{400\ \mathrm{X}\ (s^2 + 0.869s + 3.24)(s + 99.1)(s + 2.1)}{(s^2 + 0.9s + 3.2)(s^2 + 2.76s + 2.5)(s^2 + 0.0285s + 156.25)}\mathrm{X}$$

$$\frac{(s + 0.7)(s + 0.1)(s + 0.01)}{(s + 100)(s + 150)(s + 200)}$$

The open loop shape transfer function satisfies the criteria of performance and stability. The figures clearly show the plots of the open loop transfer function, and plots of performance and stability criteria found to be less than 0 dB. Based on the selection of open loop transfer function, the controller function was obtained from the relation

$$C = \frac{L(s)}{P(s)}$$

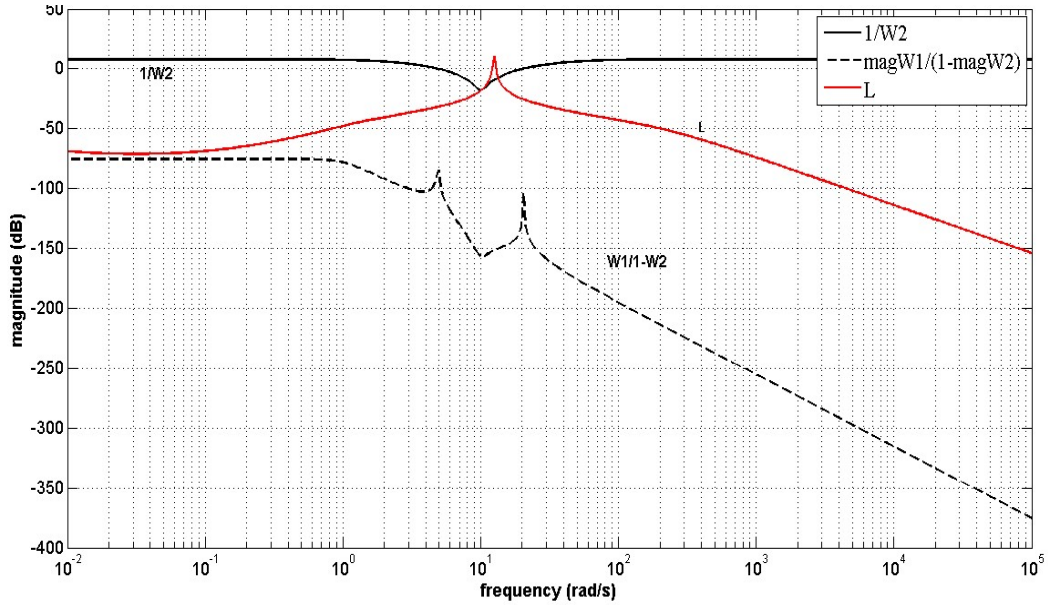

Figure 4. 23 Loop shape design

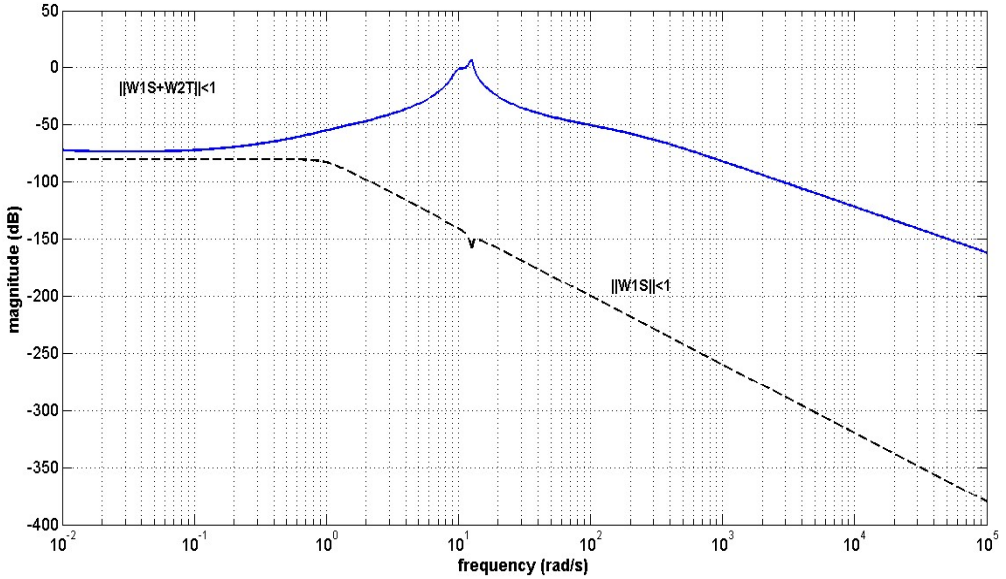

Figure 4. 24 Plot for Performance and stability criteria

The controller function can be written as

$$C = \frac{1.7\text{X}(s^2 + 581.6s + 9.7x10^6)(s^2 + 495.6s + 4.9x10^5)(s^2 + 487.9s + 5.04x10^5)}{(s^2 + 597.05s + 8.8\text{x}10^6)(s^2 + 646.84s + 10^5)(s^2 + 175.49s + 10100)}$$

$$\frac{(s^2 + 143s + 74351)(s + 99.2)(s + 0.1)(s + 0.01)}{s(s + 1380.3)(s + 100)(s + 150)(s + 200)}$$

4.3.2.1 Torque Disturbance

Now for the system with controller obtained was subjected to 10 percent torque disturbance for a duration of 200ms. The operating point for the plant was considered as electrical power output of micro-alternator P_e=0.6 p.u and electrical power output for PV system alone P_{pv}=0.4 p.u, with a constant load of S_{load}=1.5+0.15i p.u. The nonlinear simulations were carried on by implementing the controller. Finally the response for rotor angle, speed and bus voltage can be shown in Figure 4. 25 - Figure 4. 27

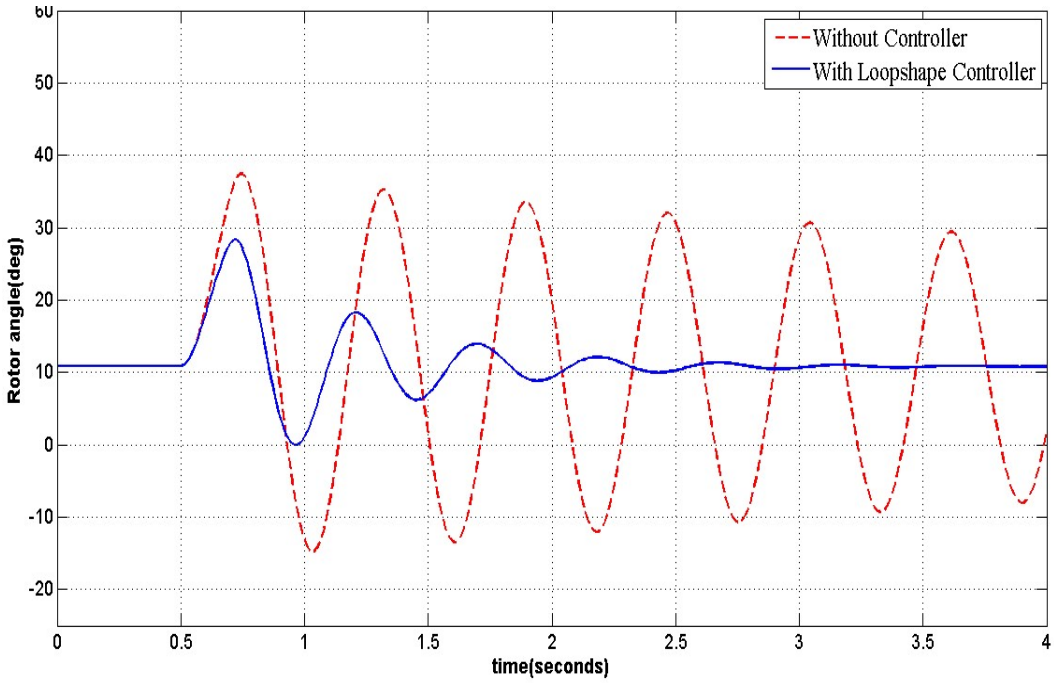

Figure 4. 25 Response of micro-alternator rotor angle with loop-shape controller with 10% torque disturbance for 200ms

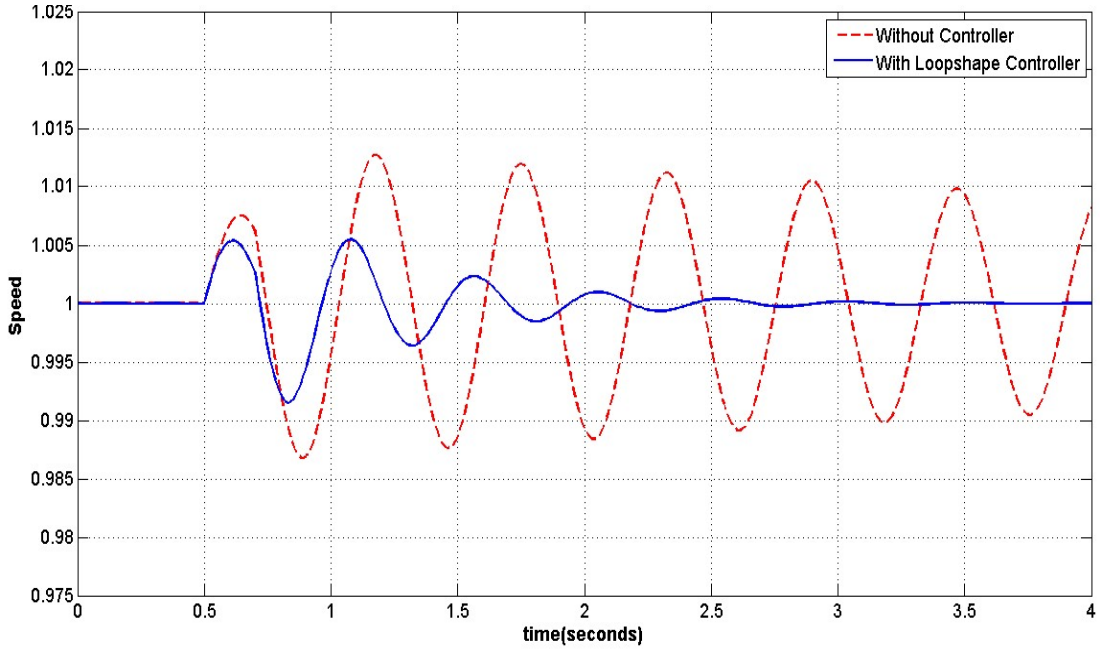

Figure 4. 26 Response of micro-alternator rotor speed with loop-shape controller with 10% torque disturbance for 200ms

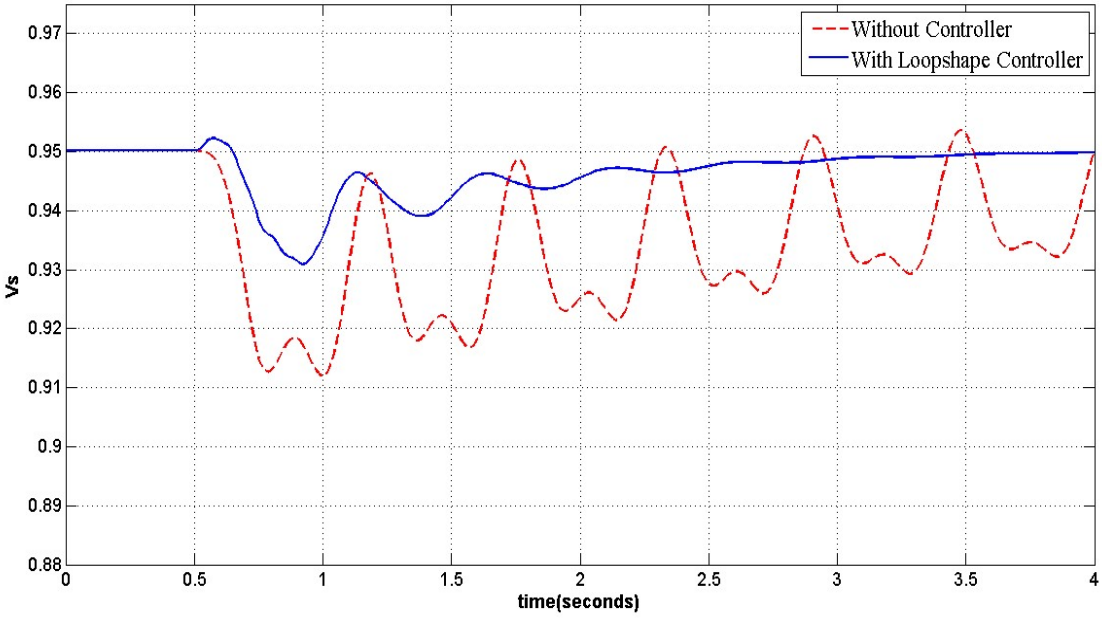

Figure 4. 27 Response of Bus voltage with loop-shape controller with 10% torque disturbance for 200ms

Comparison of results with different level of torque disturbance at various operating points:

The following controller was tested for various operating point where electrical Power output of micro-alternator is considered as $P_e = 0.5$ p.u, $P_e = 0.7$ p.u, and electrical power for PV system as $P_{PV} = 0.5$ p.u, $P_{PV} = 0.3$ p.u also for different torque disturbances varying form 20 % and 50 % respectively. The corresponding rotor angle variation as well as bus voltage variations and angular speed variation are shown in Figures (4.28 -4.30). Based on verification of the designed controller it is observed that the controller obtained is a robust controller that does not require any tuning of controller parameters even for various operating condition.

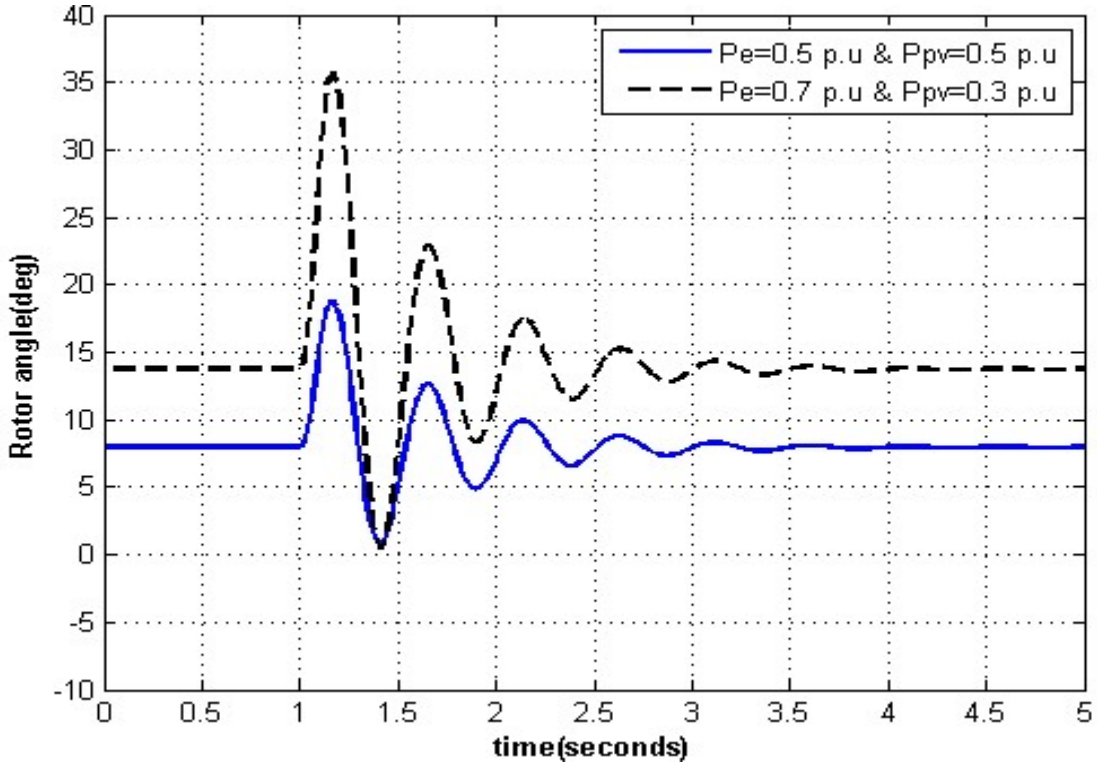

Figure 4. 28 : Angle response for different torque disturbance for different operating points

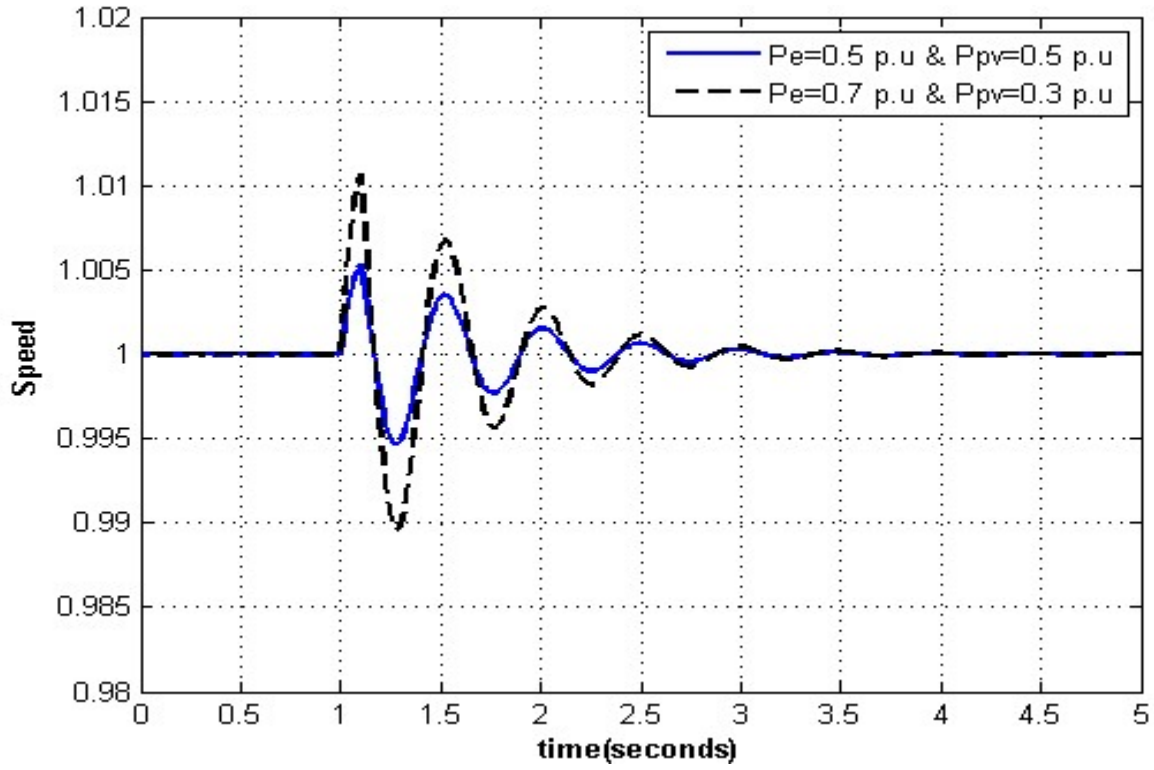

Figure 4. 29: Speed response for different torque disturbance for different operating points

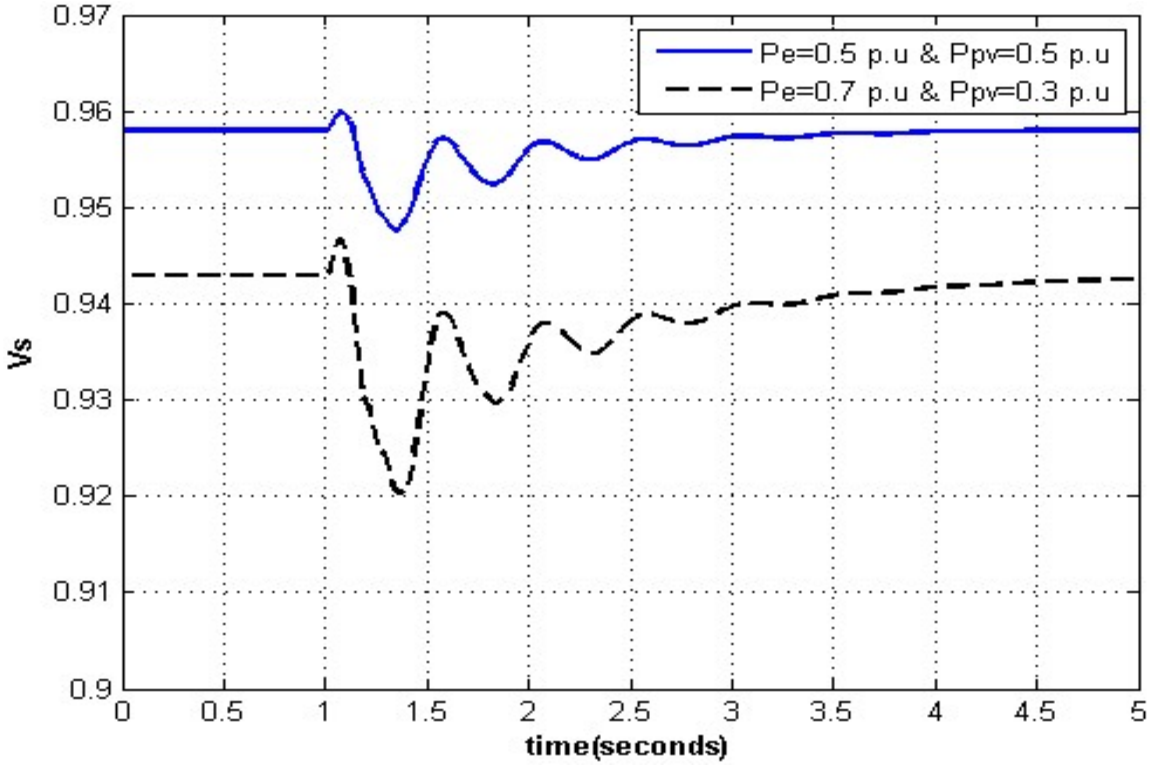

Figure 4. 30: Bus voltage response for different torque disturbance for different operating points

4.3.2.2 Three phase fault testing

The robust STATCOM loop-shape controller after being implemented for the system, now the system is bound to test for a severe three-phase fault at the common bus terminal (PCC). The fault duration considered in this study is for 100ms. This assumption is made keeping in mind that the fault obtained in the system shall be cleared within a duration of 100ms. The operating point considered as electrical power output for micro-alternator $P_e = 0.7$ p.u and electrical power output for PV system $P_{pv} = 0.3$ p.u. The response for generator angle and generator speed can be shown in Figure 4. 31 and Figure 4. 32 respectively.

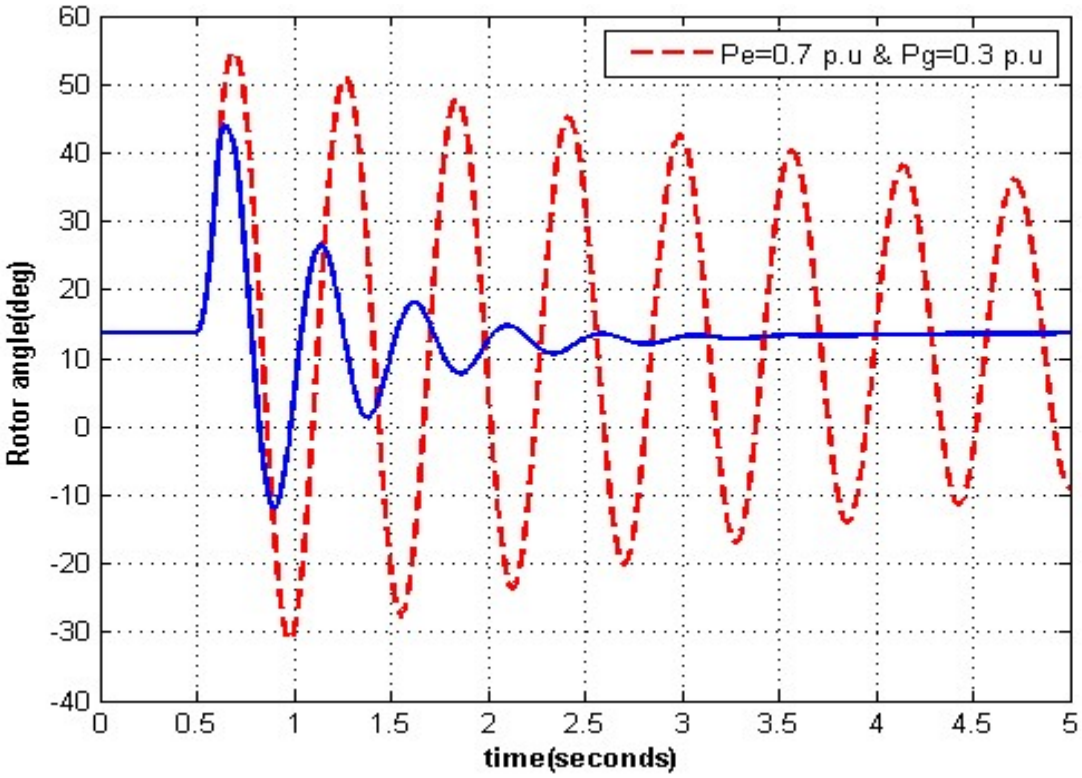

Figure 4. 31 Rotor angle response for three phase fault at common bus

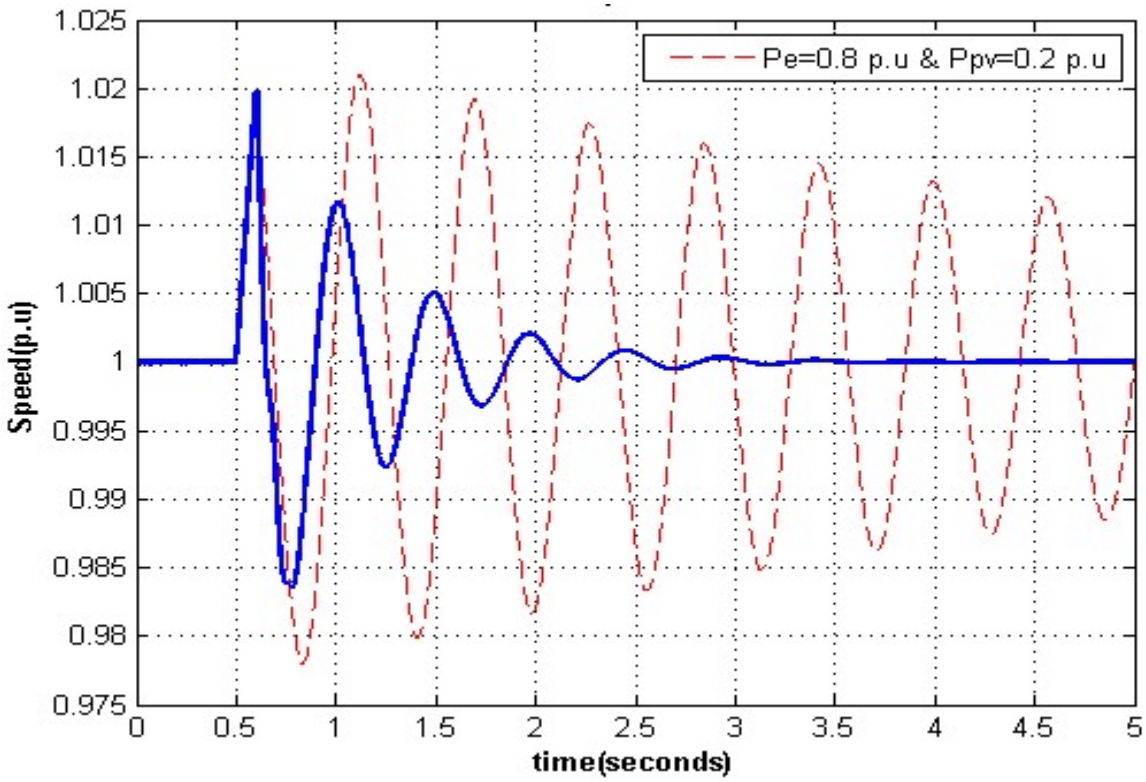

Figure 4. 32 Speed Response for three phase fault at common bus

4.3.3 Micro alternator, Wind system and STATCOM model

This section gives the implementation of the loop-shape controller on a microgrid system formed by integrating micro-alternator, STATCOM along with wind system. The detail nonlinear modeling of a wind system and its integration with micro-alternator is given in the previous chapter. Thus, the model obtained by the integrated system was found to be of 20th order. It is possible to extract five control inputs from this system. Two control inputs from STATCOM namely modulation index(m_{st}) of inverter and phase angle of inverter(Ψ_{st}). Similarly three control inputs are estimated from wind system namely modulation index of rectifier(m_{wr}), modulation index of inverter (m_{wi}) and phase angle of inverter (Ψ_{wi}). In this system, proper sharing of all the DG's associated with microgrid is considered, as increasing the power output from the wind system with respect to the

power output of micro alternator takes a system to slightly unstable environment. Clear idea can be obtained from the direct simulations carried out for nonlinear system. The operating points were considered, where electrical power output for micro alternator as P_e=0.8 p.u, electrical power output for wind system as P_g=0.3 p.u and subjecting the system to 10% torque disturbance for 200ms.The nominal load conditions were considered as S_{load}=1.5+0.15i p.u. The Figure 4. 33 - Figure 4. 35 shows the response of micro alternator's angular frequency, rotor angle and voltage at common bus terminal.

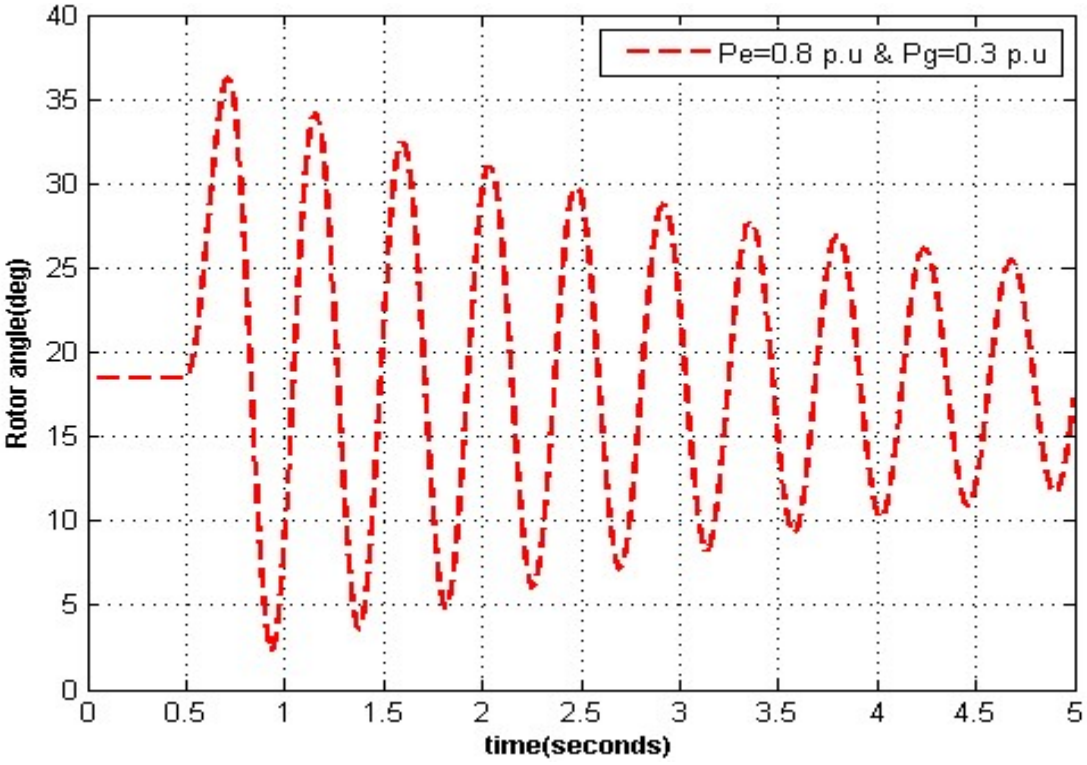

Figure 4. 33 Uncontrolled response of rotor angle of generator

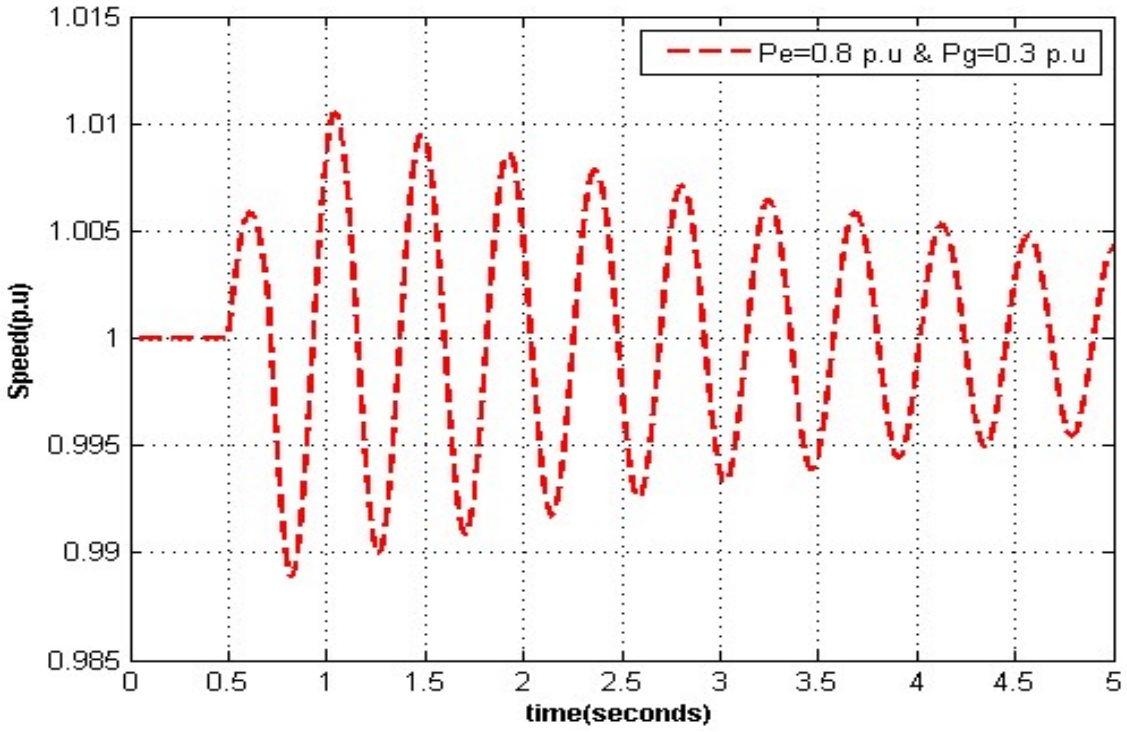

Figure 4. 34 Uncontrolled response of angular speed of generator with different operating points

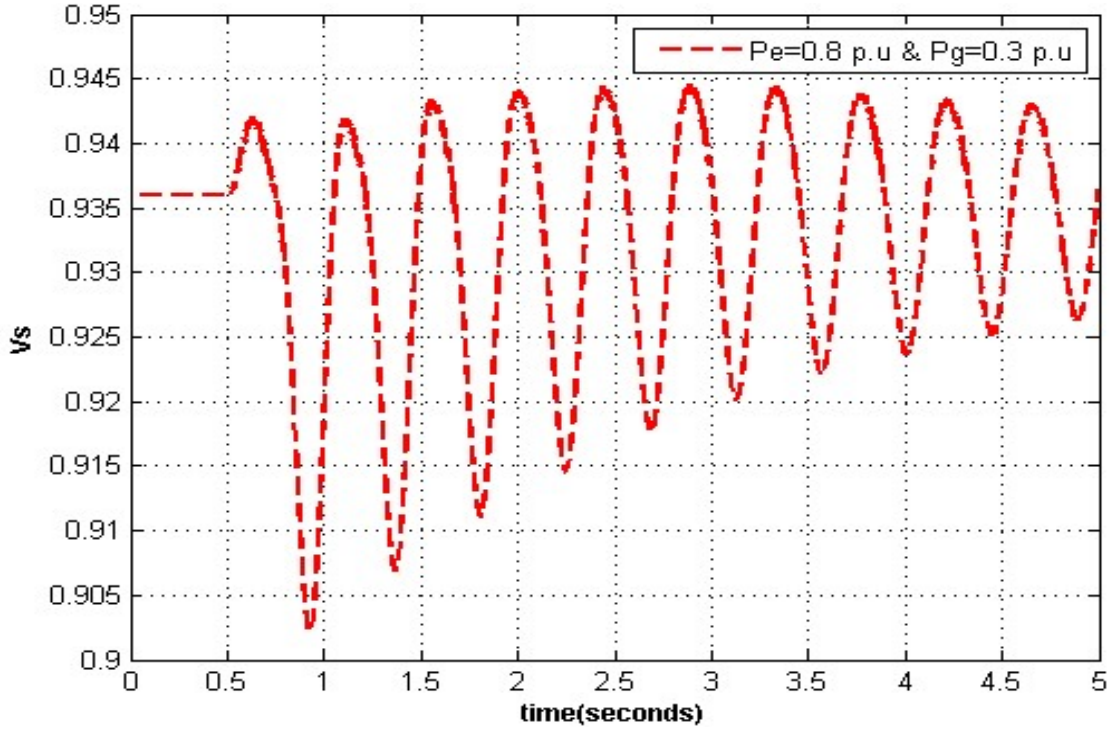

Figure 4. 35 Uncontrolled response of Bus voltage with different operating points

The process of designing loop-shape controller starts with estimating a transfer function from obtained linear model of microgrid system. Linearization was carried out by considering the nominal operating conditions. The output of the plant which is to be fed back to the controller 'C' was considered to be generators angular speed variation $\Delta\omega$. The 20th order transfer function can be expressed as P. After getting the plant transfer function, now there is a need of getting perturbed transfer function based on the equation $|\hat{P}(j\omega))/P(j\omega)| - 1$ for each perturbed plant. These perturbations were executed for various operating points for micro alternator varying from P_e=0.2-0.8 p.u and for wind system P_g=0.2-0.8 p.u. The dB magnitude of perturbed plant is plotted on semi log scale as shown in Figure 4. 36

$$P = \frac{273.92 \text{ X s } (s^2 + 288.6s + 9.1x10^6)(s + 296.8s + 5.1x10^6)(s^2 + 9.294s + 1.4x10^5)}{(s^2 + 301.38s + 9.7x10^6)(s^2 + 229.15s + 4.9x10^6)(s^2 + 646.9s + 5.68x10^5)}\text{X}$$

$$\frac{(s^2 + 192.89s + 1.03\text{x}10^5)(s^2 + 0.864s + 1.12x10^3)(s + 837.1)(s + 2.5)}{(s^2 + 9.2s + 1.4x10^5)(s^2 + 150s + 7.2x10^4)(s^2 + 0.86s + 1.1x10^3)(s + 99.2)}X$$

$$\frac{(s^2 + 0.15s + 16.82)(s^2 + 1.46s + 0.63)(s + 98.8)}{(s^2 + 0.5s + 130)(s^2 + 0.15s + 16.8)(s^2 + 2s + 1.7)(s + 1.4)}$$

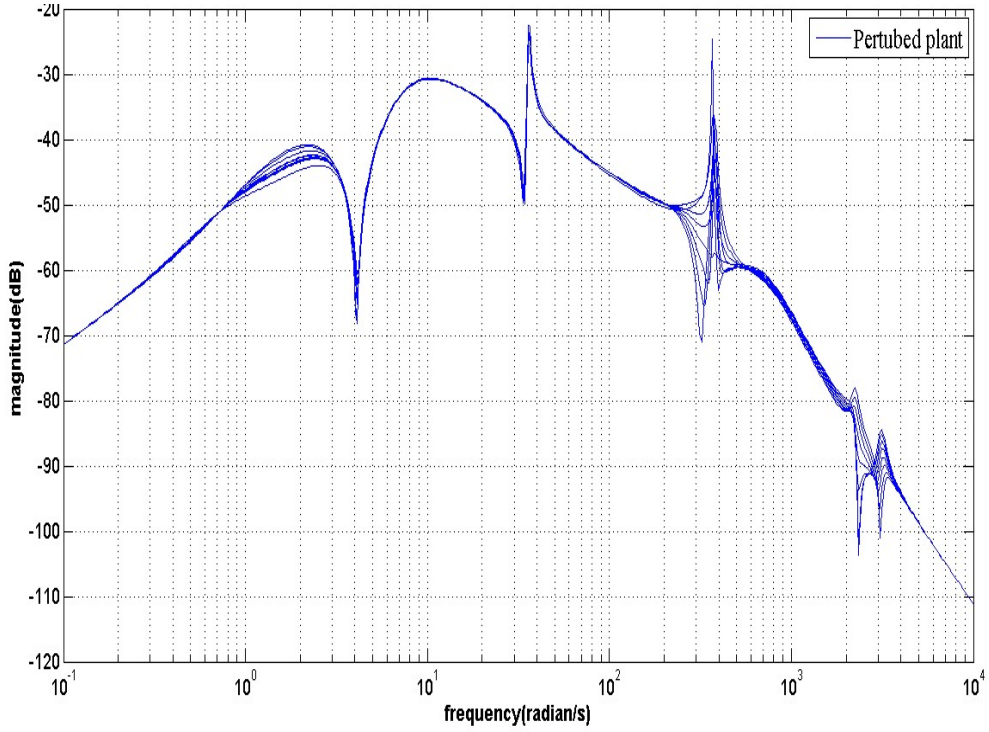

Figure 4. 36 Perturbation of Plant

The uncertainty profile is fitted to a function W_2 as

$$W_2 = \frac{s^2 + 15s + 0.1}{s^2 + 5s + 50}$$

Whereas W_1 is estimated as a third order Butterworth filter, K_d=0.00001 and f_c=0.1, can be written as

$$W_1(s) = \frac{k_d f_c^2}{s^3 + 2s^2 f_c + 2s f_c^2 + f_c^3}$$

As W_2 is based on uncertainty modeling, the obtained W_2 can be plotted to on log-log scale as shown in

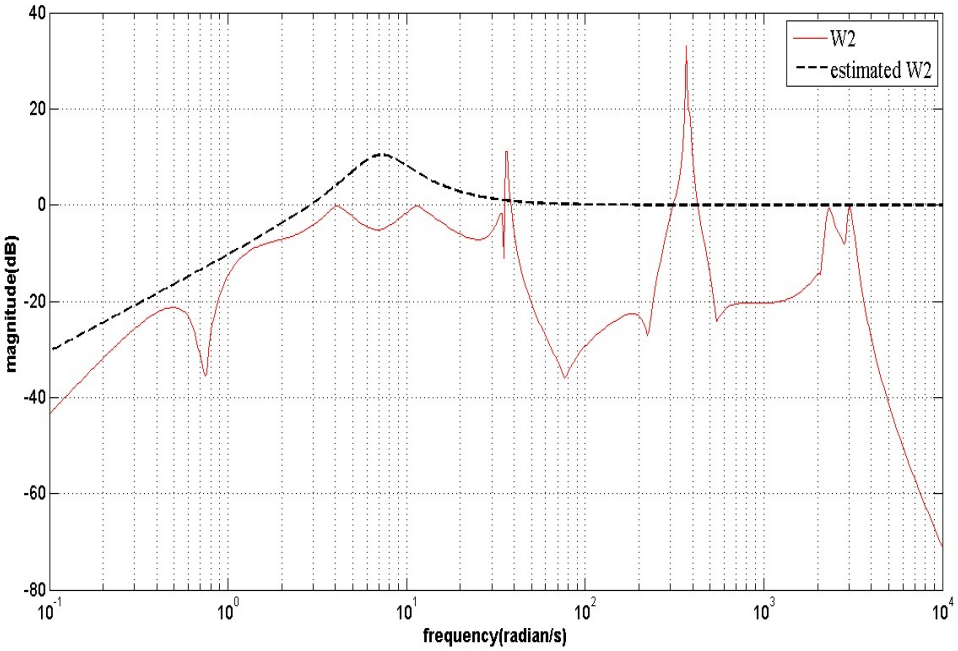

Figure 4. 37 Estimation of W2

Open loop transfer function is selected such that this function satisfies the performance and stability criteria. The open loop transfer function is given by 'L'.

$$L = \frac{200 \text{ X } (s^2 + 288.6s + 9.1x10^6)(s + 296.8s + 5.1x10^6))}{(s^2 + 301.38s + 9.7x10^6)(s^2 + 229.15s + 4.9x10^6)(s^2 + 0.5s + 130)} \text{X}$$

$$\frac{(s^2 + 1.46s + 0.63)(s + 0.1)(s + 2)(s + 1)}{(s + 99.2)(s^2 + 2s + 1.7)(s + 100)(s + 0.001)}$$

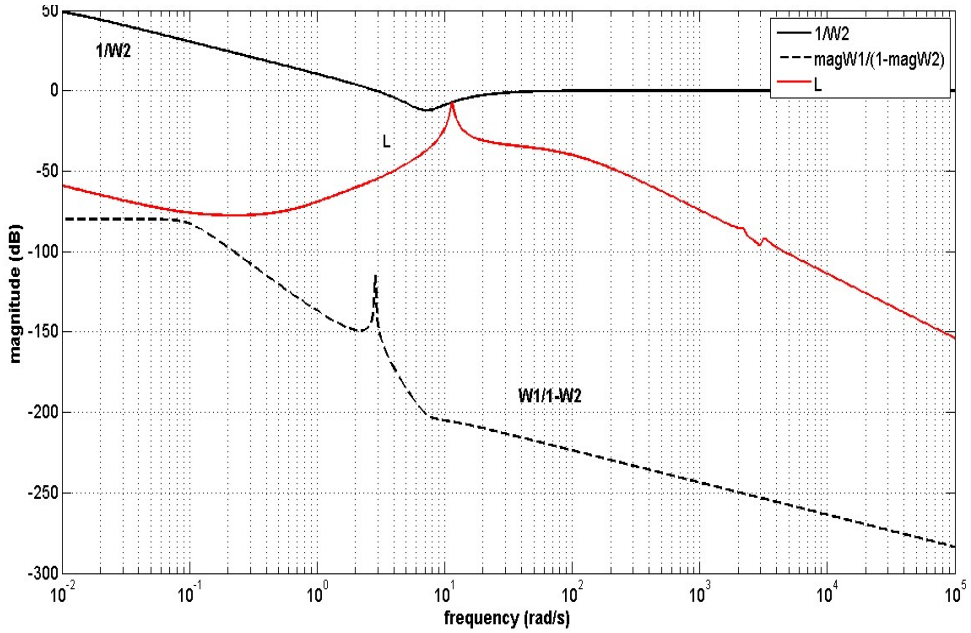

Figure 4. 38 Loop-shape Design

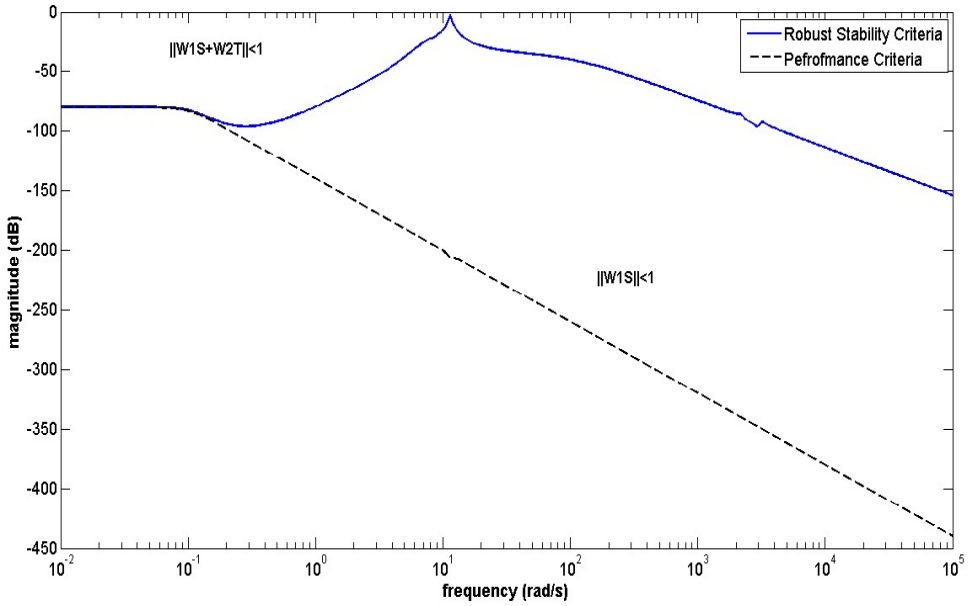

Figure 4. 39 Performance and stability criteria

A graphical representation of loop-shape plot is obtained by adopting loop-shape algorithm and is represented as shown in Figure 4. 38. The open loop shape transfer function satisfies the criteria of performance and stability. The figures clearly show the plots of the open loop transfer function, and plots of performance and stability criteria were found to be less than 0 dB. Based on the selection of open loop transfer function, the controller function was generated from the relation,

$$C = \frac{L(s)}{P(s)}$$

$$C = \frac{0.730\text{X}\,(s^2 + 646.9s + 5.68x10^5)(s^2 + 9.2s + 1.4x10^5)(s^2 + 150s + 7.2x10^4)}{s(s^2 + 9.294s + 1.4x10^5)(s^2 + 192.89s + 1.03\text{x}10^5)(s^2 + 0.864s + 1.12x10^3)}\text{X}$$

$$\frac{(s^2 + 0.86s + 1.1x10^3)(s^2 + 0.15s + 16.8)(s + 1.4)(s + 0.1)(s + 1)}{(s^2 + 0.15s + 16.82)(s + 837.1)(s + 98.8)(s + 100)(s + 0.001)}$$

4.3.3.1 Torque Disturbance

The designed controller is implemented on the nonlinear system of microgrid integrated with wind system. A torque disturbance of 10% is injected for a duration of 200ms. The operating point for electrical power output of micro-alternator P_e=0.8 p.u and electrical power output for wind system P_W=0.2 p.u were assumed, with a constant load of S_{load}=1.5+0.15i p.u. The nonlinear simulations were carried on by implementing the controller. Finally the response for rotor angle, speed and voltage at PCC can be recorded as shown in Figure 4. 40 - Figure 4. 42.

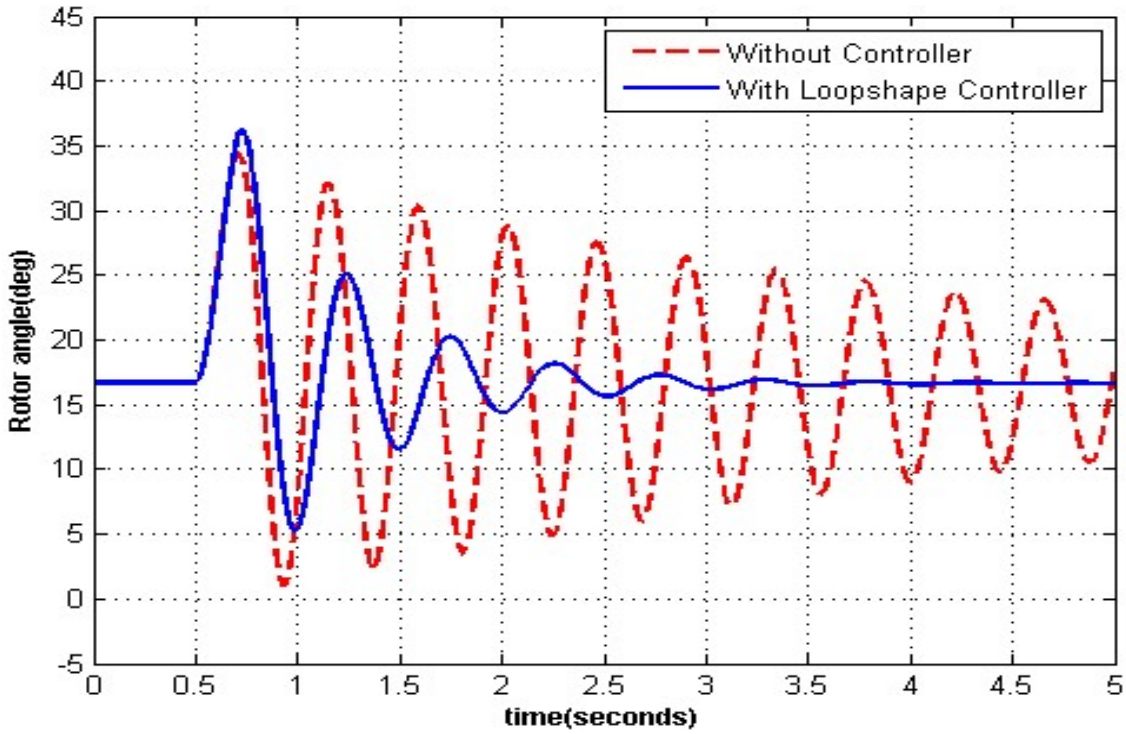

Figure 4. 40 Response of loop-shape controller for rotor angle

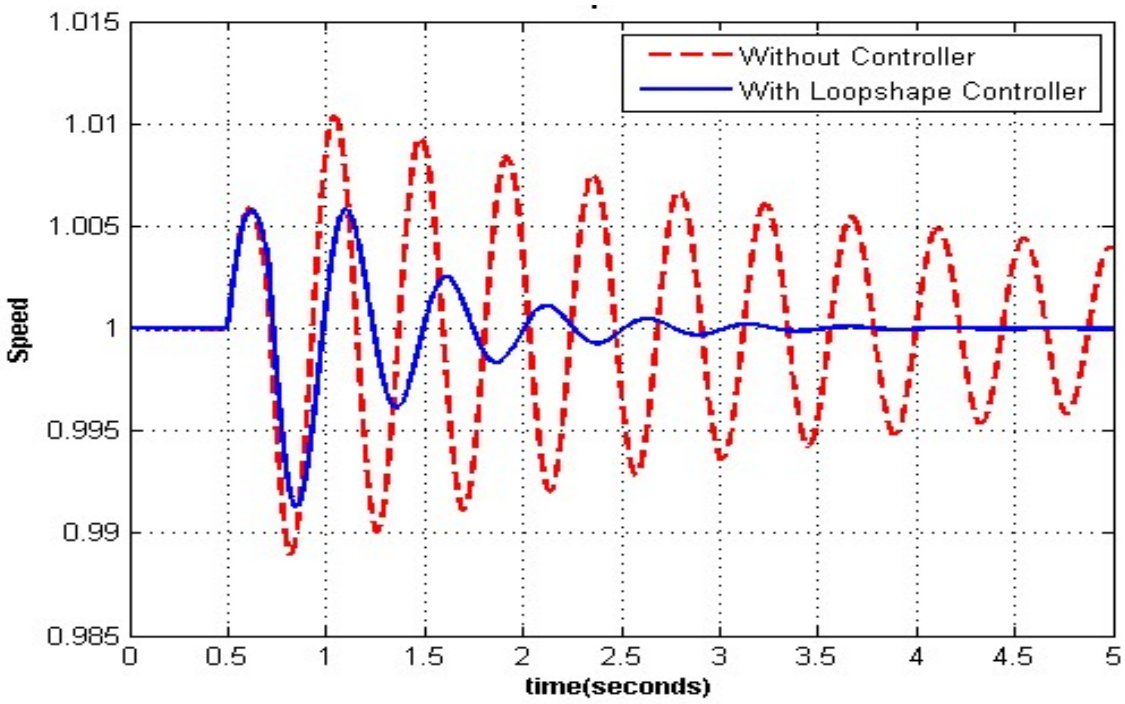

Figure 4. 41 Response of loop-shape controller for rotor speed

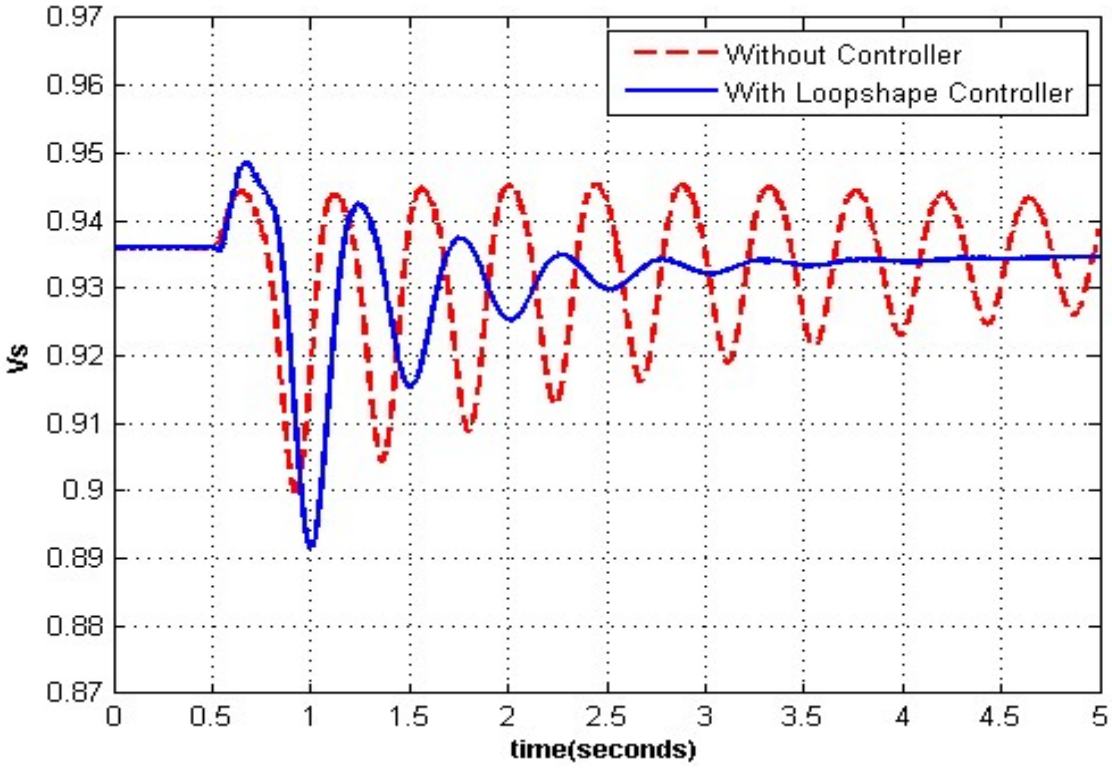

Figure 4. 42 Response of loop-shape controller for common bus voltage

Comparison of results with different level of torque disturbance at various operating points:

In order to test the performance of the designed loop-shape controller, nonlinear simulations were carried out for different operating conditions as well as the various level of torque disturbance. A 10% torque disturbance is applied to the system operating with electrical power output of micro-alternator P_e=0.6 p.u and electrical power output for wind system P_w=0.4 p.u. On another instance a 20% torque disturbance was applied with P_e=0.7 p.u and P_w=0.3 p.u. The figure shows the response of micro alternator's rotor angle, speed, also the response of Common bus voltage are shown in Figure 4. 43 - Figure 4. 45 respectively.

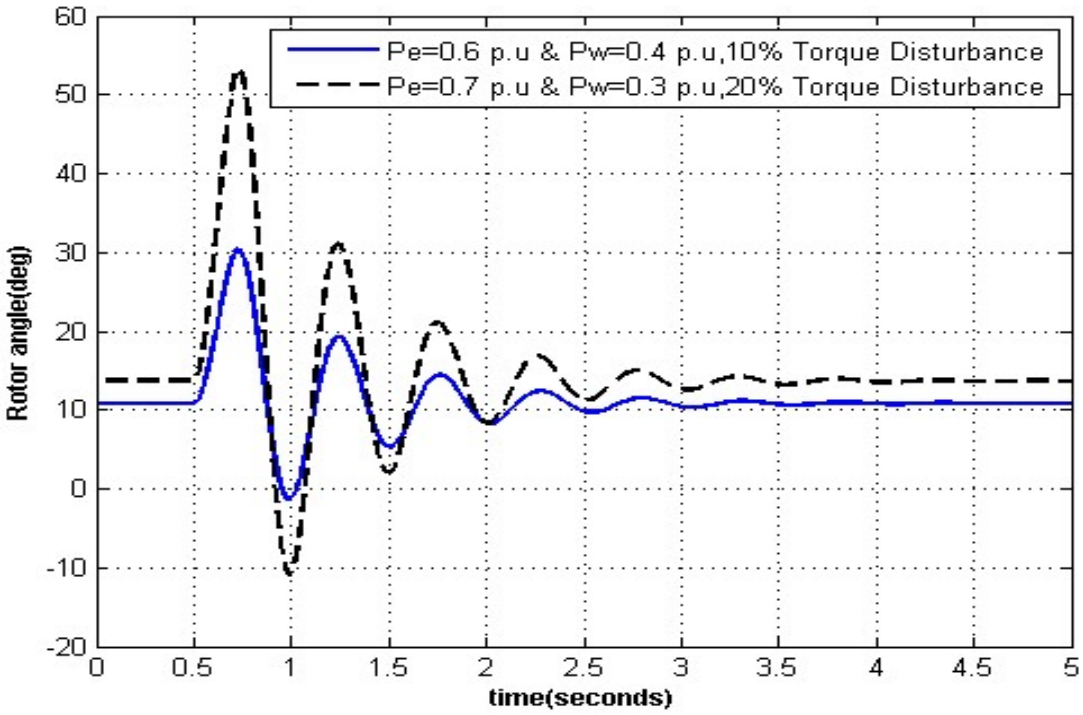

Figure 4. 43 Response of micro-alternator's rotor angle subjected to different torque disturbance and operating conditions

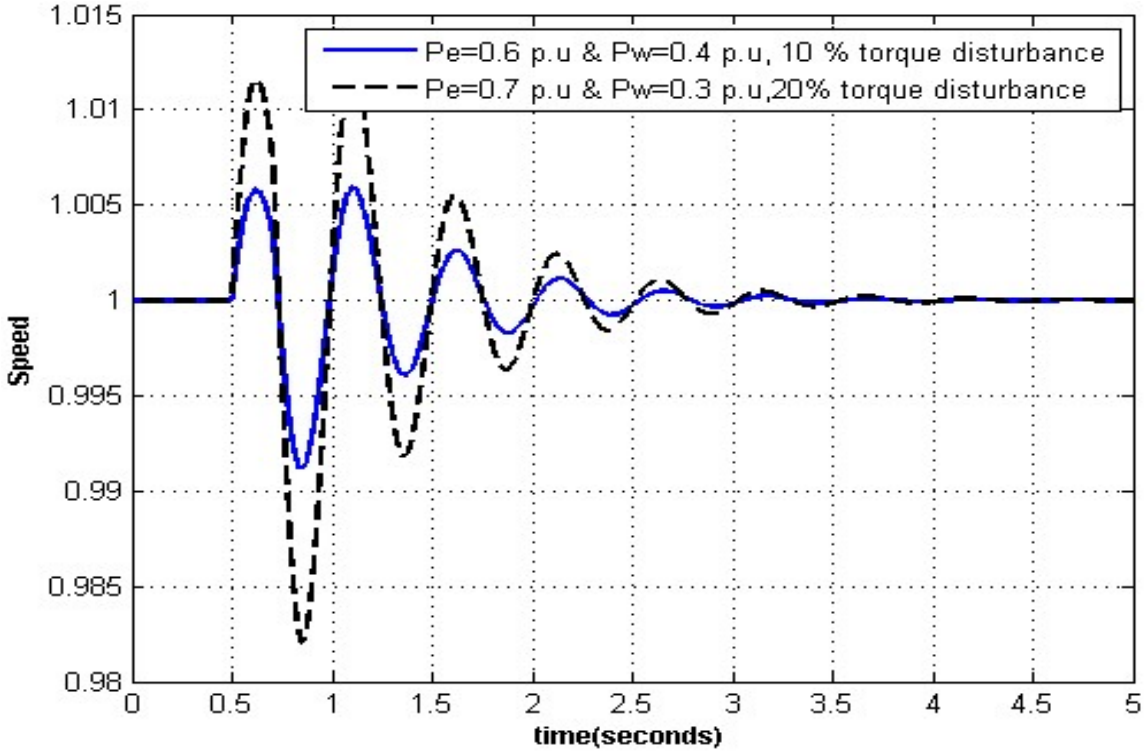

Figure 4. 44 Response of micro- alternator's speed subjected to different torque disturbance and operating conditions

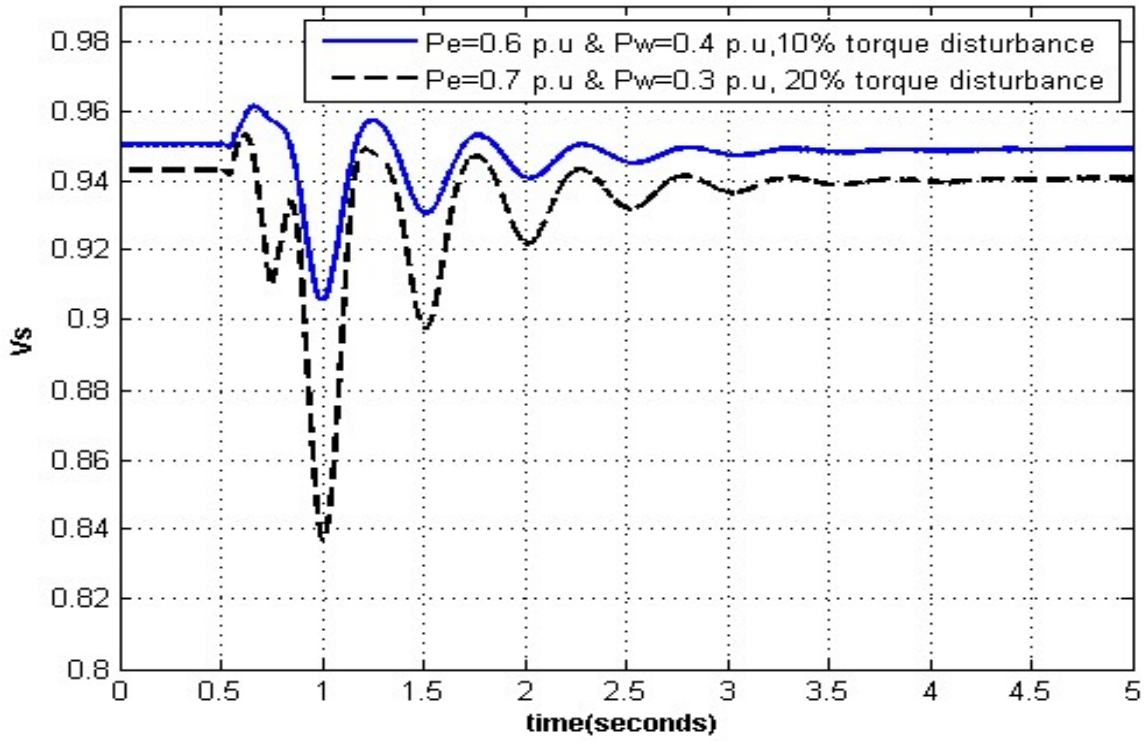

Figure 4. 45 Response of Bus voltage subjected to different torque disturbance and operating conditions

4.3.3.2 Three Phase Fault Testing

The robust loop-shape controller was implemented on the microgrid system. The system is bound to test for a three-phase fault at the common bus terminal (PCC) which is considered to be most severe fault in power system study. The fault duration considered in this research is for 100ms. This assumption is made keeping in mind that the fault obtained in the system shall be cleared within a duration of 100ms. The operating point considered for micro-alternator as P_e=0.6 p.u and for wind power as P_w=0.4 p.u. The response for generator's angle and speed can be shown in Figure 4. 46 and Figure 4. 47.

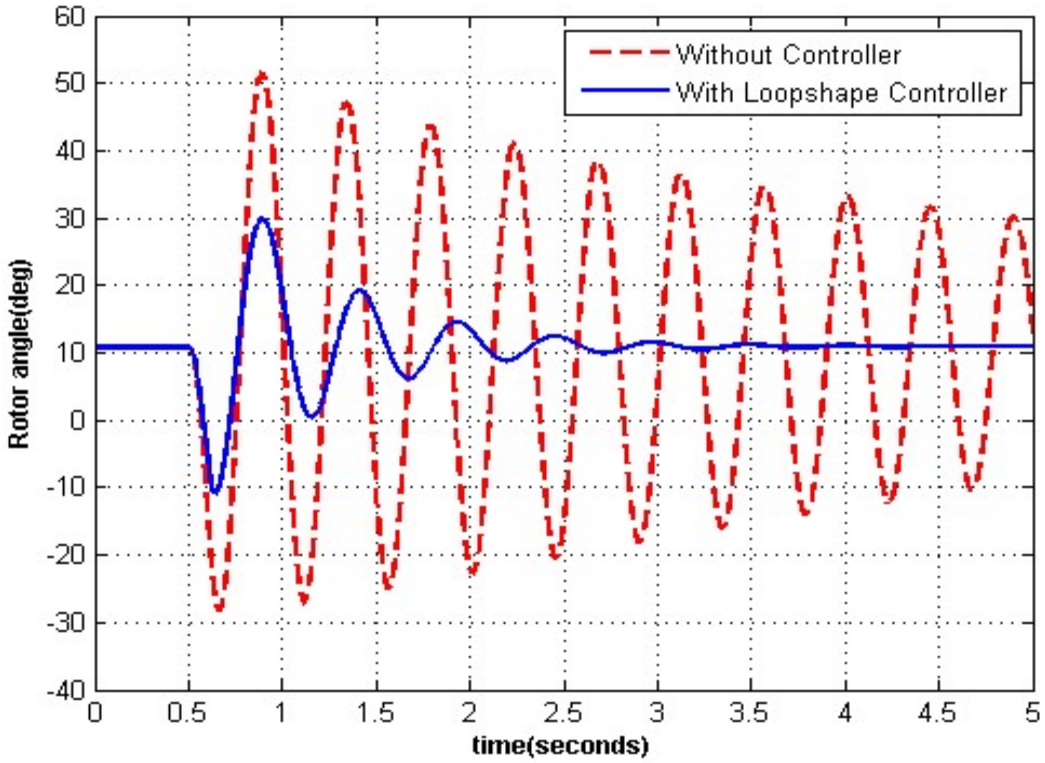

Figure 4. 46 Response of micro- alternator's rotor angle subjected to three phase fault at common bus

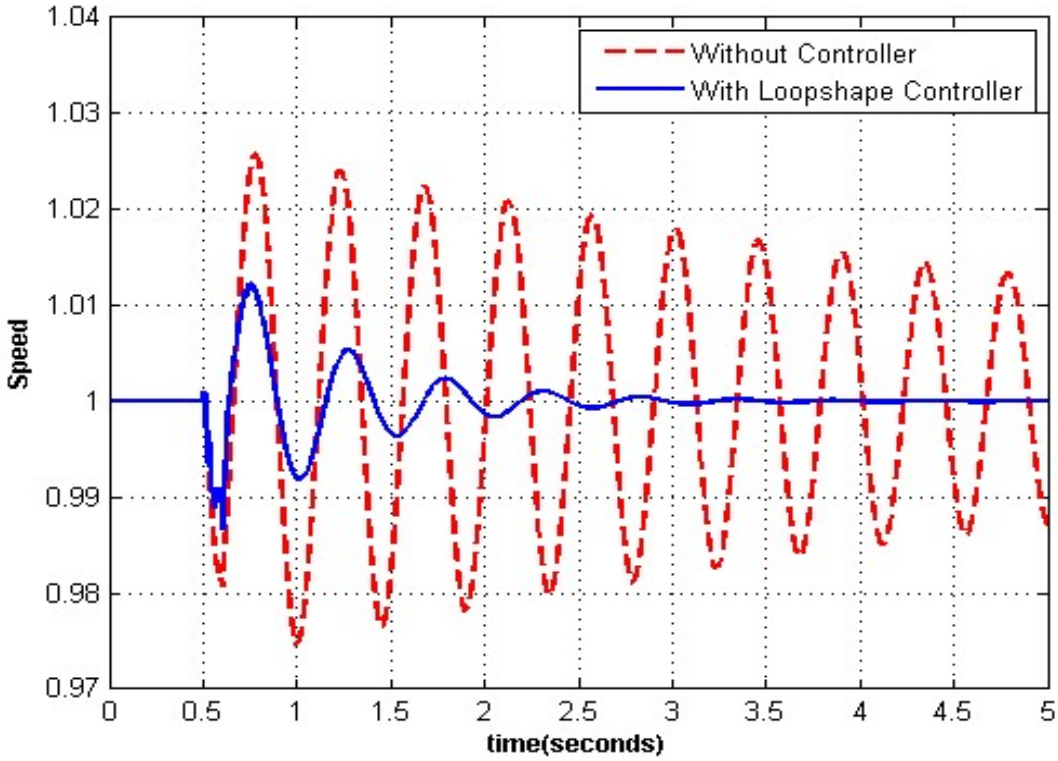

Figure 4. 47 Response of micro- alternator's speed subjected to three phase fault at common bus

4.3.3.3 Comparison of Loop-Shape Controller with PID Controller

In order to test the robustness of the designed Loop-shape controller, this section highlights the comparison o developed controller with PID technique. The PID gains we calculated and the controller was implemented on the microgrid system. With K_p=5, K_I=2, $K_D = 1$ controller was implemented and the performance were compared with Loop-shape. The operating conditions were set to P_e=0.7 p.u for generator, P_w=0.3 p.u for wind system. The system was subjected to 10% torque disturbance for 100ms on both the designed controllers. Fine tuning was carried in order to get better results for PID controller. On the other hand, no tuning was performed on loop-shape controller parameters. The performance of the two controllers can be verified from the Figure 4. 48 - Figure 4. 50 which shows the response of generator's angle, speed and voltage at common bus terminal. It is evident from the responses that loop-shape controller stabilizes the system in less than 3 sec, while PID controller requires 5 seconds to stabilize the system. Comparing response of rotor angle it is evident that the overshoot in case of PID controller is 25% more when compared to loop-shape response. Also PID controller response for bus voltage does not settle on its initial value while loop-shape response does settles at initial value, thus indicating the robustness of loop-shape controller.

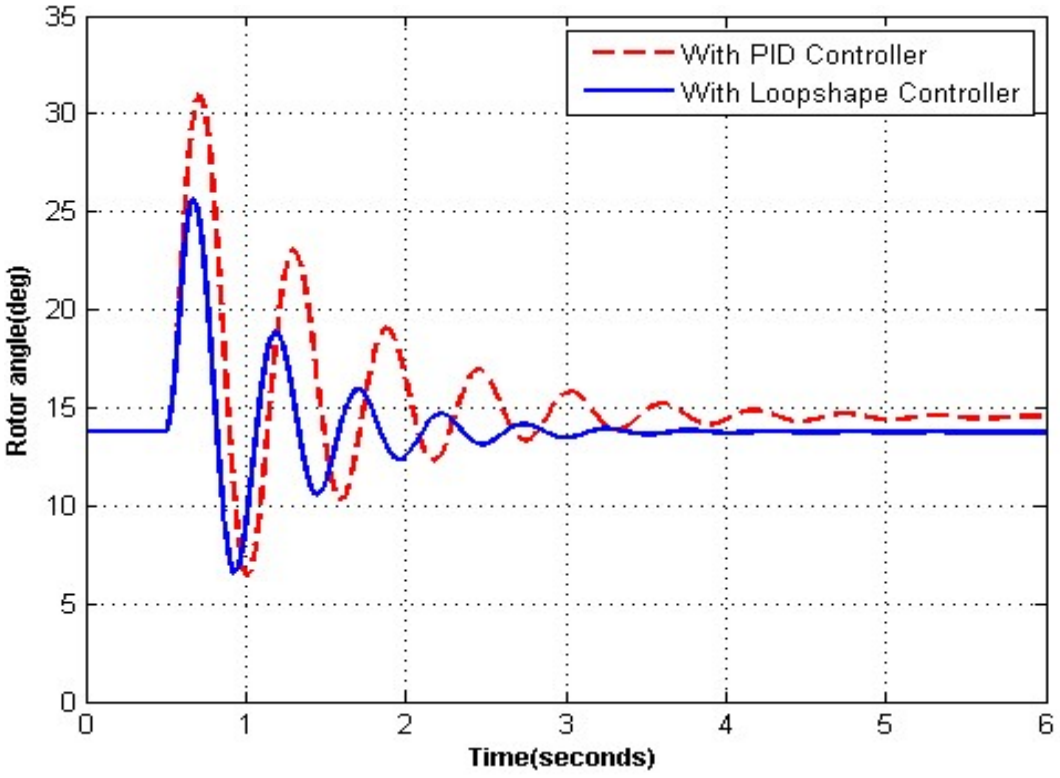

Figure 4. 48 Micro-alternator's angle response of loop-shape controller and PID controller

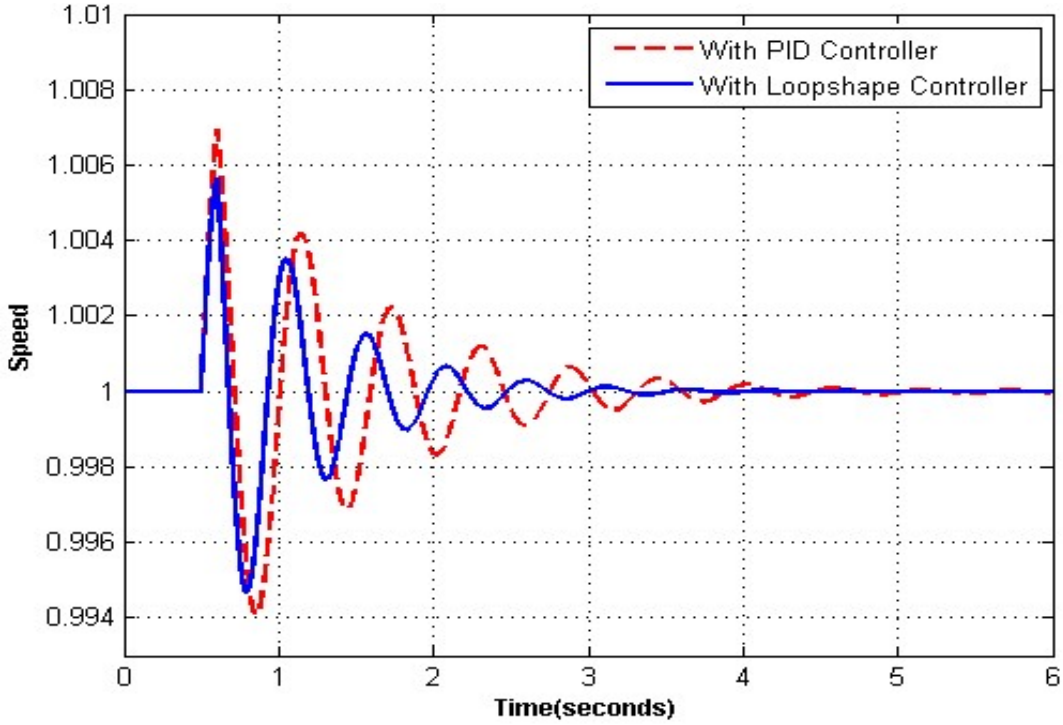

Figure 4. 49 Micro-alternator's speed response of loop-shape controller and PID controller

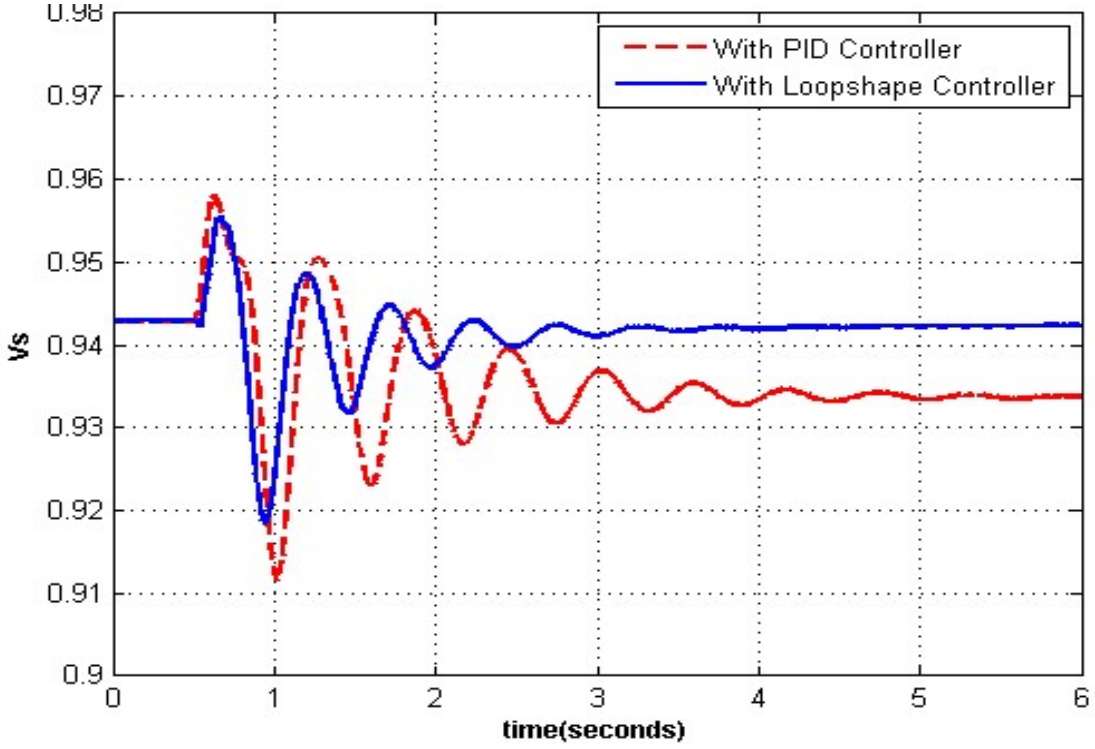

Figure 4. 50 Bus voltage response of loop-shape controller and PID controller

CHAPTER 5

CONCLUSION AND FUTURE WORK

5.1 Conclusion

This study presents robust controller designs for a microgrid using the loop-shape algorithm. The nonlinear dynamic model of a microgrid is formed by using non-conventional energy sources such as PV system. Because of the DC nature of PV system we are bound to use power electronic devices or converters in order to estimate a complete nonlinear model of PV system. A controller was designed for two different microgrid models. The first model was formed by integrating STATCOM with a simple micro-alternator system. The second system was modified version of first one, except that here the PV system is incorporated along with STATCOM and micro-alternator.

The nonlinear model was linearized at a certain operating point, and the behavior of DG interactions has been investigated through small-signal analysis. Two control inputs were identified for the first system, whereas for the second system four control inputs were identified. Since we are aiming to get a central supervisory controller for each model, we are considering the phase angle of the inverter connected in STATCOM configuration as a control input for both systems. It indicates that sudden large penetration of power from renewables can cause instability. Similarly, low power participation of micro-alternator could also lead to instabilities. Keeping these scenarios in mind the transfer function of the plant is estimated considering the speed of micro-alternator as output.

The graphical loop-shape controller was designed for the linear system. The given plant was perturbed for various operating points and based on this an open loop transfer function is estimated. The robust linear controller was obtained and was directly implemented on the nonlinear system. Now the system was subjected to torque disturbance, but the robust controller was able to stabilize the system in less than 3 seconds. The operating conditions were even changed, and the obtained controller was tested subjected to even 50% torque disturbance but, the robust controller was found to be effective in stabilizing the system. Finally, the system was subjected to asymmetrical 3ϕ fault at the point of common coupling (at common bus terminal), even under this circumstances the controller was able to perform excellently. At last loop-shape controller was designed for a microgrid system formed by integrating Wind system. The system was investigated by subjecting different disturbances and as well as three phase fault. Thus, it can be concluded that the graphical loop-shape controller design method is simple and straightforward.

5.2 Future Work

In the following are some recommendations for future research in the area

1. A loop-shape controller can even be designed for a higher order system formed by integrating PV system, wind system, and STATCOM along with micro-alternator.
2. The effect of battery storage in a microgrid can also be studied.
3. The performance of loop-shape controller can be compared with other robust control techniques such as H_2 or H_∞ control.
4. It will be interesting to observe the effect of this controller when the system is initially unstable.

REFERENCES

[1] F. Katiraei, M. R. Iravani, and P. W. Lehn, "Micro-grid autonomous operation during and subsequent to islanding process," *IEEE Trans. Power Deliv.*, vol. 20, no. 1, pp. 248–257, 2005.

[2] X. Yu, "Interplay of Smart Grids and Intelligent Systems and Control," *2011 Int. Conf. Power Eng. Energy Electr. Drives*, no. May, pp. 1–1, 2011.

[3] Z. Zhang, Y. Li, and W. Chen, "The research on micro-grid mode conversion," *2012 China Int. Conf. Electr. Distrib.*, no. Cited, pp. 1–7, 2012.

[4] B. Kroposki, R. Lasseter, T. Ise, S. Morozumi, S. Papathanassiou, and N. Hatziargyriou, "Making microgrids work," *IEEE Power Energy Mag.*, vol. 6, no. 3, pp. 40–53, 2008.

[5] T. C. Green and M. Prodanović, "Control of inverter-based micro-grids," *Electr. Power Syst. Res.*, vol. 77, no. 9, pp. 1204–1213, 2007.

[6] D. Jayaweera, S. Galloway, G. Burt, and J. R. McDonald, "A sampling approach for intentional islanding of distributed generation," *IEEE Trans. Power Syst.*, vol. 22, no. 2, pp. 514–521, 2007.

[7] S. Bose, Y. Liu, K. Bahei-Eldin, J. De Bedout, and M. Adamiak, "Tieline controls in microgrid applications," *2007 iREP Symp. Bulk Power Syst. Dyn. Control - VII, Revital. Oper. Reliab.*, pp. 33–40, 2007.

[8] W. Deng, X. Tang, and Z. Qi, "Research on dynamic stability of hybrid wind/PV system based on Micro-Grid," *Electr. Mach. Syst. 2008. ICEMS 2008. Int. Conf.*, pp. 2627–2632, 2008.

[9] R. H. Lasseter, "MicroGrids," *2002 IEEE Power Eng. Soc. Winter Meet. Conf. Proc. (Cat. No.02CH37309)*, vol. 1, pp. 4285–4290, 2002.

[10] P. Piagi and R. H. Lasseter, "Autonomous control of microgrids," *2006 IEEE Power Eng. Soc. Gen. Meet.*, p. 8 pp., 2006.

[11] H. Nikkhajoei and R. H. Lasseter, “Microgrid protection,” *2007 IEEE Power Eng. Soc. Gen. Meet. PES*, pp. 1–6, 2007.

[12] M. G. Villalva, J. R. Gazoli, and E. R. Filho, “Comprehensive Approach to Modeling and Simulation of Photovoltaic Arrays,” *Power Electron. IEEE Trans.*, vol. 24, no. 5, pp. 1198–1208, 2009.

[13] D. Verma, S. Nema, A. M. Shandilya, and S. K. Dash, “Maximum power point tracking (MPPT) techniques : Recapitulation in solar photovoltaic systems,” vol. 54, pp. 1018–1034, 2016.

[14] A. S. Oshaba, E. S. Ali, and S. M. Abd Elazim, “MPPT control design of PV system supplied SRM using BAT search algorithm,” *Sustain. Energy, Grids Networks*, vol. 2, pp. 51–60, 2015.

[15] S. Ozdemir, N. Altin, and I. Sefa, “Single stage three level grid interactive MPPT inverter for PV systems,” *Energy Convers. Manag.*, vol. 80, pp. 561–572, 2014.

[16] S. Achilles, S. Schramm, and J. Bebic, “Transmission system performance analysis for high-penetration photovoltaics,” *Renew. Energy Grid Integr. Tech. Perform. Requir.*, no. February, pp. 1–56, 2011.

[17] R. J. Bravo, R. Yinger, S. Robles, and W. Tamae, “Solar PV inverter testing for model validation,” *Power Energy Soc. Gen. Meet. 2011 IEEE*, pp. 1–7, 2011.

[18] W. Du, Q. Jiang, M. J. Erickson, and R. H. Lasseter, “Voltage-source control of PV inverter in a CERTS microgrid,” *IEEE Trans. Power Deliv.*, vol. 29, no. 4, pp. 1726–1734, 2014.

[19] G. Bayrak, E. Kabalci, and M. Cebeci, “Real time power flow monitoring in a PLL inverter based PV distributed generation system,” *2014 16th Int. Power Electron. Motion Control Conf. Expo.*, pp. 1035–1040, 2014.

[20] B. Li, X. Tian, and H. Zeng, “with Fluctuant Reactive Load,” pp. 786–790, 2011.

[21] S. J. Watson, L. Landberg, and J. A. Halliday, “Application of wind speed forecasting to the integration of wind energy into a large scale power system,” *IEE Proc. - Gener. Transm. Distrib.*, vol. 141, no. 4, pp. 357–362, 1994.

[22] T. Ackermann, *Wind Power in Power Systems*. .

[23] F. M. Gonzalez-longatt, O. Amaya, M. Cooz, and L. Duran, "Dynamic Behavior of Constant Speed WT based on Induction Generator Directly connect to Grid."

[24] J. Li, Y. Liu, C. Li, and L. Zhang, "Energy-based coordinated control of generator and static var compensator in power systems with nonlinear loads," *2009 IEEE Int. Conf. Intell. Comput. Intell. Syst.*, pp. 767–771, 2009.

[25] S. Li, L. Xu, and T. a. Haskew, "Control of VSC-based STATCOM using conventional and direct-current vector control strategies," *Int. J. Electr. Power Energy Syst.*, vol. 45, no. 1, pp. 175–186, 2013.

[26] Skandarama K., R. C. Mala, and N. Prabhu, "Control of Bifurcation in a VSC Based STATCOM," *Procedia Technol.*, vol. 21, pp. 187–195, 2015.

[27] N. Li, Y. Liu, J. Wang, Y. Ji, and B. Xie, "Dynamic allocation method of DC side power based on the SoC of battery for STATCOM/BESS," *Electr. Power Syst. Res.*, vol. 125, pp. 141–149, 2015.

[28] A. Agbedahunsi, M. Sumner, E. Christopher, A. Watson, A. Costabeber, and R. Parashar, "Frequency control improvement within a microgrid, using enhanced STATCOM with energy storage," *6th IET Int. Conf. Power Electron. Mach. Drives (PEMD 2012)*, no. c, pp. A23–A23, 2012.

[29] I. M. El-amin and M. A. Abido, "Stability Enhancement of a Power System with Wind Generation & STATCOM."

[30] M. Abdul-Malek and M. Abido, "STATCOM based controller design using Particle Swarm Optimization for power system stability enhancement," *Ind. Electron. 2009. ISIE …*, no. ISlE, pp. 1218–1223, 2009.

[31] I.-Y. Chung, W. Liu, D. A. Cartes, and K. Schoder, "Control parameter optimization for a microgrid system using particle swarm optimization," *2008 IEEE Int. Conf. Sustain. Energy Technol.*, pp. 837–842, 2008.

[32] I. J. Balaguer, U. Supatti, Q. Lei, N. S. Choi, and F. Z. Peng, "Intelligent control for intentional islanding operation of microgrids," *2008 IEEE Int. Conf. Sustain. Energy Technol. ICSET 2008*, pp. 898–903, 2008.

[33] J. M. Guerrero, J. C. Vasquez, J. Matas, L. G. De Vicuña, and M. Castilla, "Hierarchical control of droop-controlled AC and DC microgrids - A general approach toward standardization," *IEEE Trans. Ind. Electron.*, vol. 58, no. 1, pp. 158–172, 2011.

[34] A. Timbus, M. Liserre, R. Teodorescu, P. Rodriguez, and F. Blaabjerg, "Evaluation of Current Controllers for Distributed Power Generation Systems," *Power Electron. IEEE Trans.*, vol. 24, no. 3, pp. 654–664, 2009.

[35] Y. A. R. I. Mohamed and A. a. Radwan, "Hierarchical control system for robust microgrid operation and seamless mode transfer in active distribution systems," *IEEE Trans. Smart Grid*, vol. 2, no. 2, pp. 352–362, 2011.

[36] C. X. Dou, F. Zhao, X. B. Jia, and D. Le Liu, "H∞ robust control of DC-AC interfaced microsource in microgrids," *Int. J. Autom. Comput.*, vol. 10, no. 1, pp. 73–78, 2013.

[37] H. Nikkhajoei and R. H. Lasseter, "to the CERTS Microgrid," *Power*, vol. 24, no. 3, pp. 1598–1608, 2009.

[38] J. Kennedy and R. Eberhart, "Particle swarm optimization," *Neural Networks, 1995. Proceedings., IEEE Int. Conf.*, vol. 4, pp. 1942–1948 vol.4, 1995.

[39] M. Babazadeh and H. Karimi, "A robust two-degree-of-freedom control strategy for an islanded microgrid," *IEEE Trans. Power Deliv.*, vol. 28, no. 3, pp. 1339–1347, 2013.

[40] S. A. Taher and M. Zolfaghari, "Designing robust controller to improve current-sharing for parallel-connected inverter-based DGs considering line impedance impact in microgrid networks," *Int. J. Electr. Power Energy Syst.*, vol. 63, pp. 625–644, 2014.

[41] K. Berkoune, E. Ben Sedrine, L. Vido, and S. Le Ballois, "Robust control of hybrid excitation synchronous generator for wind applications," *Math. Comput. Simul.*, 2015.

[42] S. F. Faisal and A. H. M. A. Rahim, "A robust STATCOM damping controller for a multi-machine power system," *2005 Int. Power Eng. Conf.*, pp. 1–371, 2005.

[43] A. H. M. A. Rahim and M. F. Kandlawala, “Robust STATCOM voltage controller design using loop-shaping technique,” *Electr. Power Syst. Res.*, vol. 68, pp. 61–74, 2004.

[44] V. J. Fesharaki, M. Dehghani, J. J. Fesharaki, and H. Tavasoli, “The Effect of Temperature on Photovoltaic Cell Efficiency,” *Proceeding 1st Int. Conf. Emerg. Trends Energy Conserv.*, no. November, pp. 20–21, 2011.

[45] W. Kramer, S. Chakraborty, B. Kroposki, and H. Thomas, “Advanced Power Electronic Interfaces for Distributed Energy Systems Part 1 : Systems and Topologies Advanced Power Electronic Interfaces for Distributed Energy Systems Part 1 : Systems and Topologies,” no. March, p. 132, 2008.

[46] M. Mansour, M. N. Mansouri, and M. F. Mimouni, “Study of performance of a variable - speed wind turbine with pitch control based on a Permanent Magnet Synchronous Generator,” *Syst. Signals Devices (SSD), 2011 8th Int. Multi-Conference*, pp. 1–6, 2011.

[47] J. C. Doyle, *Feedback Control Theory*. 2003.

VITAE

Name	:Meer Abdul Mateen Khan
Nationality	:Indian
Date of Birth	:10/7/1990
Email	:meermateen2000@gmail.com
Address	:#210, AVALON, Mehdipatnam, Hyderabad, INDIA
Academic Background	:**MS (Electrical Engineering)** December 2015 King Fahd University of Petroleum and Minerals, Dhahran, SAUDI ARABIA. **B.E. (Electronics and Instrumentation Engineering)** June 2012 Osmania University, Hyderabad, INDIA.